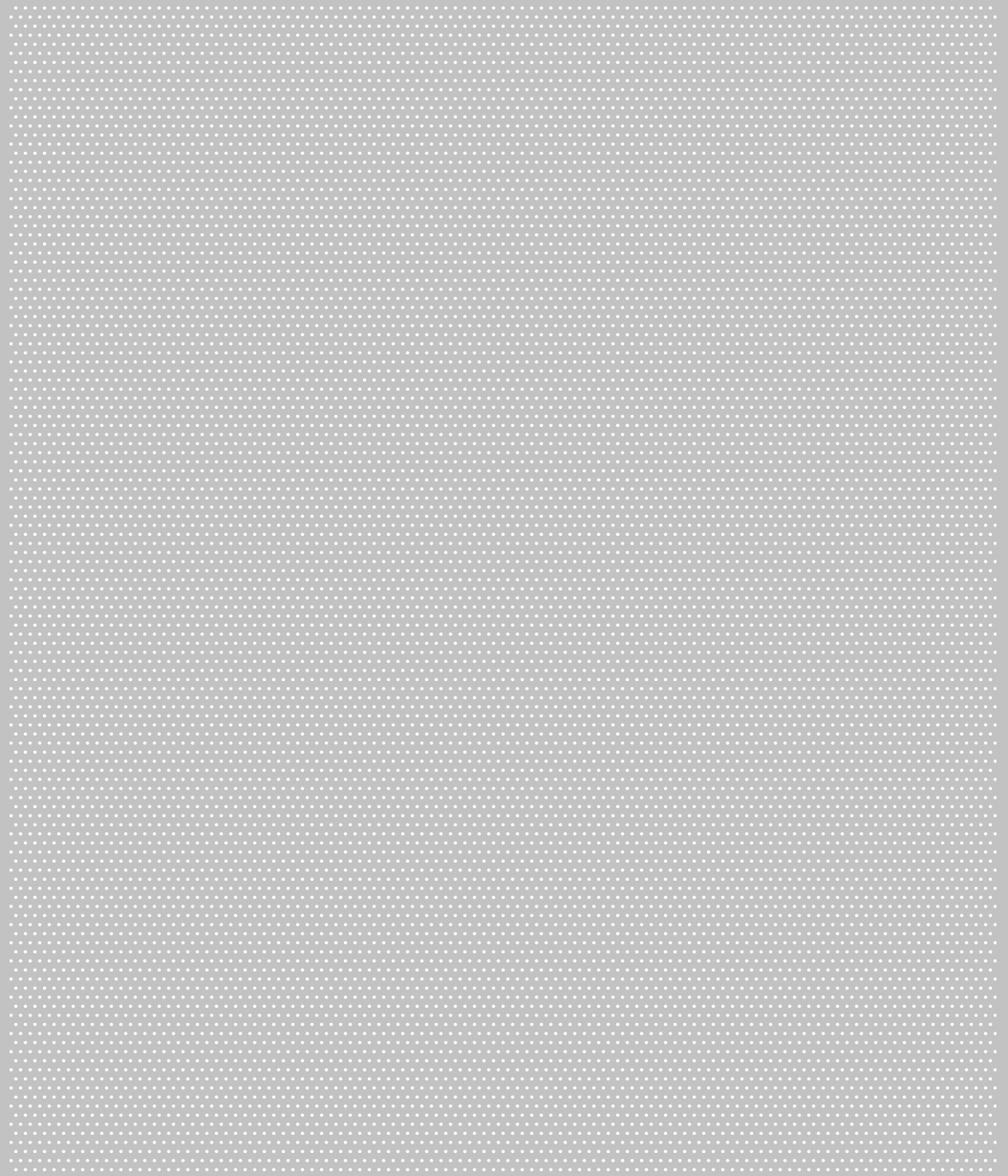


2/2009e

IFA Report

Electromagnetic fields at handheld spot-welding guns



Author: Fritz Börner

Institut für Arbeitsschutz der
Deutschen Gesetzlichen Unfallversicherung (IFA)
Alte Heerstraße 111
53757 Sankt Augustin
Germany
Telefon: +49 2241 231 02
Telefax: +49 2241 231 2234
Internet: www.dguv.de/ifa
E-mail: ifa@dguv.de

Published by: Deutsche Gesetzliche Unfallversicherung (DGUV)
Mittelstraße 51
10117 Berlin
Germany
Telefon: +49 30 288 76 38 00
Telefax: +49 30 288 76 38 08
Internet: www.dguv.de
E-mail: info@dguv.de
— Januar 2013 —

Typesetting
and Layout: Deutsche Gesetzliche Unfallversicherung

ISBN: 978-3-86423-060-8

ISSN: 2190-7994

Abstract

Electromagnetic fields at hand-held spot-welding guns

During welding with hand-held spot-welding guns, violation of the exposure limit values (permissible values to BGV B11) for the magnetic fields cannot be excluded. Whether violation of the permissible values presents a hazard to the welder's health, however, depends upon the effects of the fields within the exposed body. In the project described here, the exposure of welders during tasks involving hand-held spot-welding guns with separate 50 Hz AC power supplies was assessed for the first time with reference not only to results from workplace measurements, but also to calculated body current densities. For frequent work situations, body current densities were calculated and visualized in a three-dimensional field simulation in multiple layers of the body (genitals, torso, neck and head).

The results were compared with the basic limit values currently applicable for the central nervous system (spinal cord and brain), and evaluated. Violations of the limit values in various fat and muscle tissues and in the spinal fluid (liquor) were found here to be possible, depending upon the interval, position and orientation of the spot-welding gun with respect to the body model; the limit values were however found to be observed within the central nervous system (brain and spinal cord). In all work situations, a maximum of 10 to 20% (1 mA/m^2) of the basic limit value was exploited in the central nervous system; the magnetic flux densities lay above the derived limit values.

Kurzfassung

Elektromagnetische Felder an handgeführten Punktschweißzangen

Beim Schweißen mit handgeführten Punktschweißzangen kann eine Überschreitung der Expositionsgrenzwerte (zulässige Werte nach BGV B11) für die magnetischen Felder nicht ausgeschlossen werden. Ob eine Überschreitung der zulässigen Werte jedoch die Gesundheit der Schweißer gefährdet, hängt von den Wirkungen der Felder im exponierten Körper ab. Im hier beschriebenen Projekt wurde die Exposition von Schweißern bei Tätigkeiten mit handgeführten Punktschweißzangen mit separaten 50-Hz-Wechselstromquellen erstmals nicht nur anhand von Ergebnissen aus Arbeitsplatzmessungen, sondern auch mit berechneten Körperstromdichten beurteilt. Für häufige Arbeitssituationen wurden in einer dreidimensionalen Feldsimulation Körperstromdichten in mehreren Körperschichten (Genitalien, Rumpf, Hals und Kopf) berechnet und visualisiert.

Die Ergebnisse wurden mit den derzeit für das Zentralnervensystem (Rückenmark und Gehirn) geltenden Basisgrenzwerten verglichen und bewertet. Dabei zeigte sich, dass die Grenzwerte in verschiedenen Fett- und Muskelgeweben und in der Rückenmarksflüssigkeit (Liquor) je nach Abstand, Position und Lage der Punktschweißzange zum Körpermodell die Grenzwerte überschritten werden können, im Zentralnervensystem (Gehirn und Rückenmark) aber eingehalten werden. Bei allen Arbeitssituationen wurden im Zentralnervensystem maximal 10 bis 20 % (1 mA/m^2) des Basisgrenzwertes ausgeschöpft, wobei die magnetischen Flussdichten über den abgeleiteten Grenzwerten lagen.

Résumé

Champs électromagnétiques créés par des pinces à souder par points manuelles

Lors du soudage avec des pinces à souder par points manuelles, un dépassement des valeurs limites d'exposition (valeurs admissibles selon règlement de prévention BGV B11) aux champs magnétiques ne peut être exclu. La dangerosité d'un dépassement de valeurs admissibles pour la santé des soudeurs dépend cependant des effets des champs sur l'organisme. Dans le cadre du projet décrit, l'exposition de soudeurs travaillent avec des pinces à souder par points manuelles alimentées par des sources de courant alternatif 50 Hz externes a été évaluée, pour la première fois, non seulement à l'aide de résultats de mesures effectuées sur le poste de travail, mais aussi au moyen de densités de courant induit dans le corps humain calculées. Les densités de courant induit dans différentes parties du corps humain (parties génitales, tronc, cou et tête) ont été calculées et visualisées à l'aide d'une simulation tridimensionnelle de champ, pour des situations de travail rencontrées fréquemment.

Les résultats ont été comparés aux valeurs limites de base valables actuellement pour le système nerveux central (cerveau et moelle épinière) et évalués. Il s'est avéré que les valeurs limites peuvent être dépassées dans divers tissus adipeux et musculaires ainsi que dans le liquide céphalo-rachidien en fonction de la distance et de la position de la pince à souder par points par rapport au modèle corporel, mais elles sont respectées dans le système nerveux central (cerveau et moelle épinière). Dans toutes les situations de travail, les valeurs calculées n'excédaient pas 10 à 20 % (1 mA/m^2) de la valeur limite de base dans le système nerveux central, les densités de flux magnétique étant supérieures aux valeurs limites découlant de la valeur limite de base.

Resumen

Campos electromagnéticos en pinzas manuales de soldadura por puntos

Al soldar con las pinzas manuales de soldadura por puntos no se debe descartar que se excedan los valores límites de exposición (los valores permitidos según BGV B11) para los campos magnéticos. Sobrepasar los valores permitidos pone en peligro la salud del soldador en función de los efectos que ejercen los campos sobre el cuerpo expuesto. En el proyecto que se describe aquí se ha valorado la exposición a la que están sometidos los soldadores mientras trabajan con pinzas manuales de soldadura por puntos con fuentes separadas de alimentación de corriente alterna de 50 Hz, en un principio, no sólo basándose en los resultados extraídos de las mediciones del puesto de trabajo, sino también en las densidades de corriente apreciadas en el cuerpo. Para los entornos laborales más frecuentes se han calculado y visualizado las densidades de corriente en el cuerpo a través de una simulación tridimensional y sobre diversos niveles corporales (genitales, torso, cuello y cabeza).

Los resultados se compararon y se valoraron con los valores límites básicos válidos actualmente para el sistema nervioso central (médula espinal y cerebro). Ello demostró que los valores límite se pueden sobrepasar en diferentes tejidos musculares y adiposos, así como en el líquido cefalorraquídeo (liquor) dependiendo de la distancia, posición y estado de las pinzas de soldadura por puntos respecto al modelo corporal, aunque los valores límite se deben mantener en el sistema nervioso central (cerebro y médula espinal). En todos los entornos laborales se aprovechó como máximo del 10 al 20% (1 mA/m^2) del valor límite básico, quedando las densidades magnéticas de flujo por encima de los valores límite deducidos.

Table of contents

1	Objective of the project	9
2	Problem	11
3	Objects of the study	13
4	Studies performed in the course of the project	15
5	Project Step 1: studies and measurements performed at the user's site	17
5.1	Objective of the study	17
5.2	Measurements in Project Step 1	17
5.3	Instruments employed	17
5.4	Measurement results and permissible values	17
5.5	Evaluation of the measurement results	20
5.6	Analysis of the welders' working positions on the spot-welding guns studied at the user's site.....	21
5.6.1	Performance of the analysis	21
5.6.2	Results.....	25
5.7	Conclusions regarding the subsequent procedure	25
6	Project Step 2: studies in the laboratory.....	27
6.1	Objective of the studies performed in the laboratory	27
6.2	Studies in the laboratory.....	27
6.3	Results of the laboratory measurements	31
6.4	Permissible values	40
6.5	Assessment and evaluation of the results	40
7	Project Step 3: field simulation	41
7.1	General.....	41
7.2	Simulations	41
7.3	Objective of the field simulation.....	41
7.4	Calculation of the field distribution	41
7.5	Results of the field simulation.....	42
7.6	Conclusions	45
8	Project Step 4: calculation of the body-current densities	47
8.1	General.....	47
8.2	Exposure simulation	47

8.3	Simulation sections	49
8.4	Cable influences	50
8.5	Results	51
8.5.1	Spot-welding gun with small gun window	51
8.5.2	Spot-welding gun with small gun window, positioned horizontally	62
8.5.3	Spot-welding gun with small gun window, positioned vertically	62
8.5.4	Spot-welding gun with small gun window, positioned vertically rotated through 90°	62
8.5.5	Spot-welding gun with large gun window	62
8.5.6	Results concerning cable routing.....	69
8.5.6.1	Double conductor	69
8.5.6.2	Cable routing to prEN 50444.....	69
8.5.6.3	Cable routing to BGI 5011 Figure 22	70
8.5.7	Results for the genital region	71
9	Project Step 5: Assessment and evaluation of the results	73
9.1	Limit values	73
9.2	The central nervous system.....	73
9.2.1	Structure.....	73
9.2.2	The brain	73
9.2.3	The spinal cord	74
9.2.4	The CNS in the body model.....	75
9.3	Electrical tissue properties.....	76
9.4	Assessment	76
10	Summary and discussion	81
11	References.....	83

1 Objective of the project

In response to an initiative of the BG for the metalworking industry in Northern Germany (now the German Social Accident Insurance Institution for the metalworking industry), the Institute for Occupational Safety and Health of the German Social Accident Insurance (BGIA, now the IFA) has since February 2005 been studying the exposure of persons to magnetic fields on spot-welding guns (without integral transformer). The objective of the study is to determine the margin during assessment of exposure to magnetic fields on spot-welding guns which is created when the «basic values» (body current densities) of accident prevention regulation BGV B11 [1] are used instead of the limit values for the «derived values» (magnetic flux density). In addition, the exposure to magnetic fields in various parts of the human body is to be determined and evaluated by field calculations and field simulations.

2 Problem

During the use of spot-welding guns, strong pulsed magnetic fields occur in the immediate vicinity of the welding gun. These fields are generated by transient electric currents in the magnitude of several kiloamps. Since welders generally position and hold the spot-welding gun with their hands in front of the body as they work, a high level of exposure to magnetic fields must be anticipated. In the process, depending upon the magnitude of the welding current and the position of the welder in relation to the spot-welding gun, the permissible values for the magnetic flux density stated in Section 3 of the BGV B11 [1] accident prevention regulation and the permissible variation in the magnetic flux density over time may be exceeded. A hazard to welders' health presented by strong magnetic fields cannot be ruled out, since a high level of exposure of the human body may cause excitation of nerves and muscle cells. In a worst-case scenario, this may lead to ventricular fibrillation.

In order to permit assessment of whether a health hazard exists, the exposure must be evaluated. A number of limit values are set out in BGV B11 for this purpose. A distinction is drawn between «basic values», which describe the effect of an external electromagnetic field in the human body, and the «derived values», which are the measurable field quantities. Examples of basic values are the electric current density and the specific absorption rate. Examples of the derived values are the electric and magnetic field strengths.

Since up to now, measurement of the electric current density in the human body was either impossible or highly resource-intensive, evaluation of the exposure to magnetic fields has been based upon the result of a comparison between the measured magnetic flux density and the permissible derived values stated in BGV B11. Observance of these values assures that the basic values in accordance with BGV B11, in this case for the electric current density, are observed.

It does not follow however that should the permissible derived value be exceeded, the basic value is necessarily also exceeded. Consequently, when the permissible derived values are exceeded, observance of the basic values must be determined by additional examination/calculation/simulation. Owing to the difficulties associated with measurement of the basic values, only very simple mathematical models have been employed to date with reference to basic values for evaluation of the exposure. This has always led to the exposure being estimated conservatively. Improvements in body models and scope for performance of a field calculation and visualization of the results now enable the basic values in the human body to be calculated and presented with greater precision.

3 Objects of the study

The welding machines under examination are handheld 50 Hz AC spot-welding machines. They consist essentially of three discrete components: the welding power supply (welding transformer), the welding gun and a control unit. The welding power supply and the welding gun are connected by forward and return conductors (welding cables). The welding current is adjusted by means of a phase angle controller located on the mains side in the primary circuit of the welding power supply. The spot-welding guns studied differed in their size and geometry. A distinction was drawn between small and large spot-welding guns. Welding currents ($f = 50$ Hz) of up to 20 kA may flow during welding. A single welding cycle lasts approximately from 300 to 1,200 ms. Depending upon the workpiece, this time comprises one to three almost identical current durations.

4 Studies performed in the course of the project

The project involved five steps.

- In **Step 1**, pilot measurements of the field distribution were performed on eight spot-welding guns (without integral transformer) at the site of a user in the automotive industry. In addition, the welders' different working positions were analysed in terms of the distance between body and welding gun. The spot-welding guns are comparable to those studied in Step 2.
- In **Step 2**, the distribution of the magnetic flux density in the vicinity of the spot-welding guns was measured in the laboratory on two spot-welding guns (without integral transformer) as a function of the welding current in several sections and at different distances from the spot-welding gun.
- In **Step 3**, the magnetic field in the vicinity of the spot-welding guns was calculated by means of the EMPIRE field calculation program. The boundary conditions, such as the geometry of the spot-welding guns, welding current levels, measured values, etc., were the same as those in Steps 1 and 2.
- In **Step 4**, the body model of the EMPIRE simulation software was used to determine the basic values (body current densities) for the external magnetic field distributions in the proximity of the spot-welding guns which were calculated in Step 3.
- In **Step 5**, the results of measurement and simulation were evaluated.

5 Project Step 1: studies and measurements performed at the user's site

5.1 Objective of the study

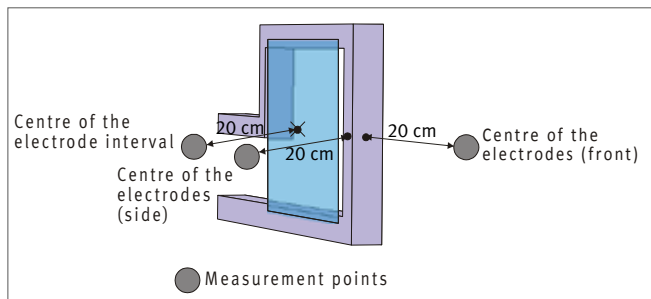
Pilot measurements were to be performed at the site of a user in the automotive industry in order to determine what exposures to magnetic fields may be expected during work with spot-welding guns. For this purpose, the peak values of the magnetic flux densities in the area occupied by the welders was determined at eight workplaces, and the different working positions of the welders during welding were analysed in terms of the distances between the body and the welding gun.

5.2 Measurements in Project Step 1

The magnetic flux density in the proximity of the gun window and on the welding cables was measured during production on eight different cable spot-welding guns. The measurements at the gun window were performed at a distance of 20 cm from the:

- Centre of the gun window
- Centre of the electrodes (front)
- Centre of the electrodes (side); see Figure 1

Figure 1: Measurement points on the welding equipment at the user's site



For measurement on the welding cables, the measurement probe was in contact with the surface of the cable.

The variations in welding current and magnetic flux density over time were measured and recorded. For a worst-case estimate, the cable guns were short-circuited during measurement, i.e. the electrodes were moved into contact with each other under pressure without the presence of a workpiece. This measure ensured that the maximum selected welding current actually occurred. The maximum peak value of the magnetic flux density was then determined for each measurement point from the time behaviour of the field and current, and the permissible values calculated in accordance with BGV B11, Appendix 1, Section 3, „Pulsed fields“.

The climatic conditions prevailing during the measurements at the sites of measurement were as follows:

- Temperature: 20.5 to 27.4 °C
- Relative humidity: 35.0 to 65.5%

5.3 Instruments employed

The following instruments were used for performance of the measurements:

• Electromagnetic field measurement system

Manufacturer:	Chauvin Arnoux
Type:	CA 42
H-field probe	
Manufacturer:	Chauvin Arnoux
Type:	M 400
Bandwidth:	10 Hz to 400 kHz
Directional pattern:	X, Y, Z
Measurement range:	10 nT to 25 mT
Uncertainty of measurement:	± 3% of the display

• Oscilloscope

Manufacturer:	Tektronix
Type:	TDS2012
Serial number:	C046119

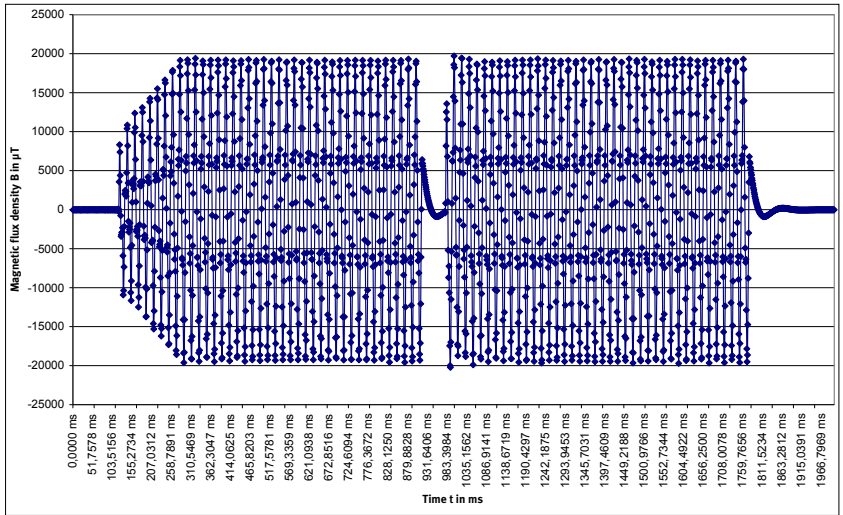
• Rogowski current wave transducer

Manufacturer:	Power Electronic Measurements Ltd.
Type:	IRF 150 D12
Serial number:	6394-1546
Peak current rating:	30 kA/5 kHz

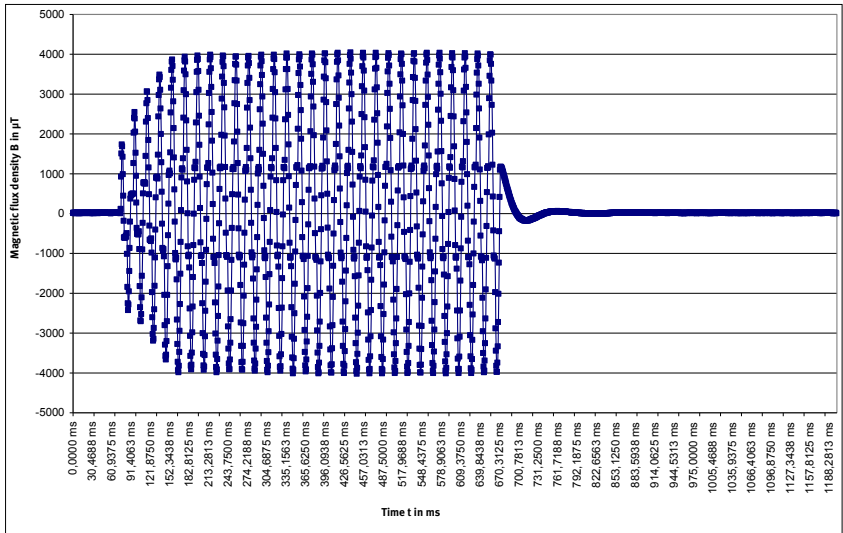
5.4 Measurement results and permissible values

The measurement results are shown in Figure 2 and Table 1 (see Page 18-20). Figure 2 shows the typical variations in the magnetic flux density over time on the spot-welding guns studied, measured in the proximity of the gun window. In the interests of clarity, the variation of the flux density B over time is shown for only one axis of measurement. Table 1 shows the peak values of the magnetic flux density B_{max} for the various measurement points, calculated over the time behaviour in the measurement axes X, Y and Z.

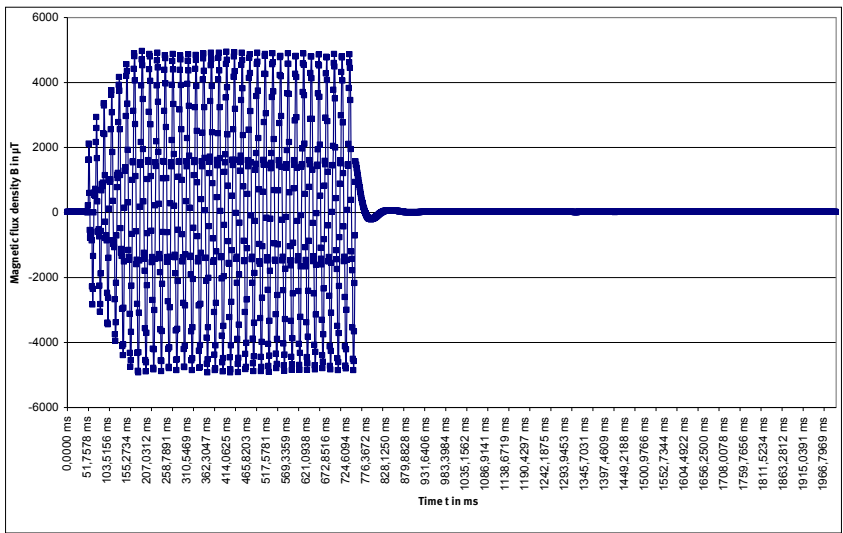
Figure 2:
Measured time behaviour of the magnetic flux density on different spot-welding guns



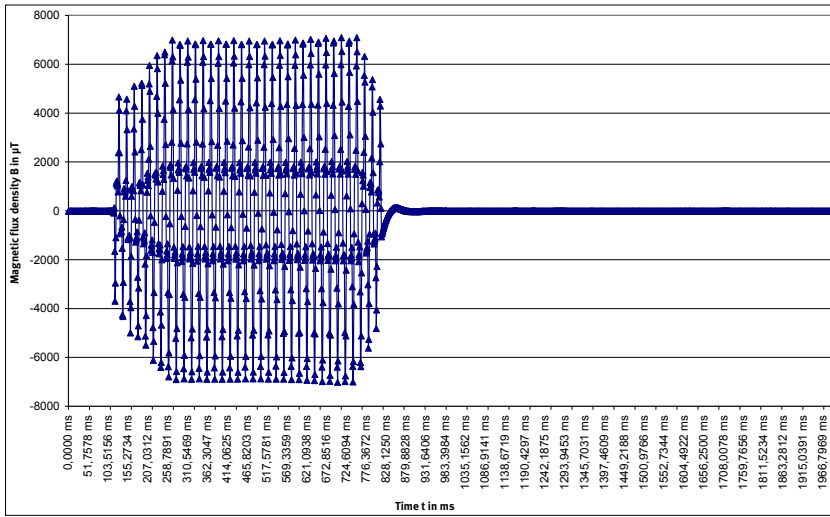
a)
Spot-welding gun No. 1 in the centre of the electrode, measured in sensor axis X at a distance of 20 cm



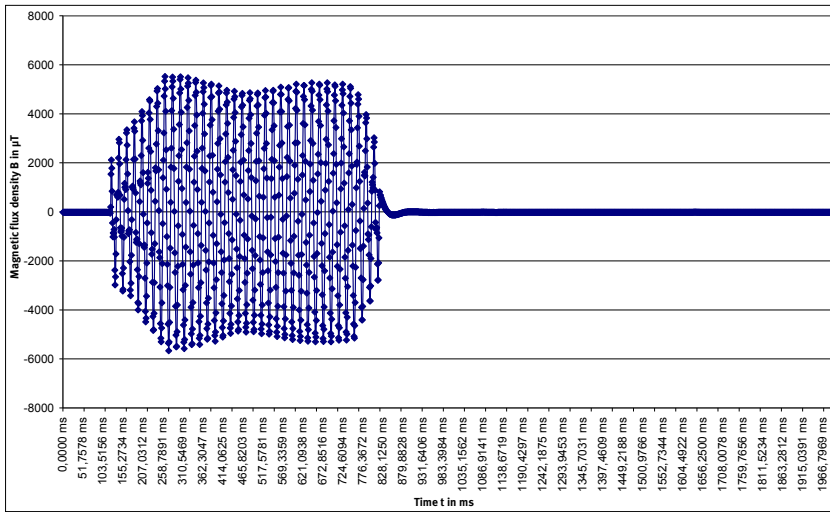
b)
Spot-welding gun No. 2 in the centre of the electrode, measured in sensor axis Y at a distance of 20 cm



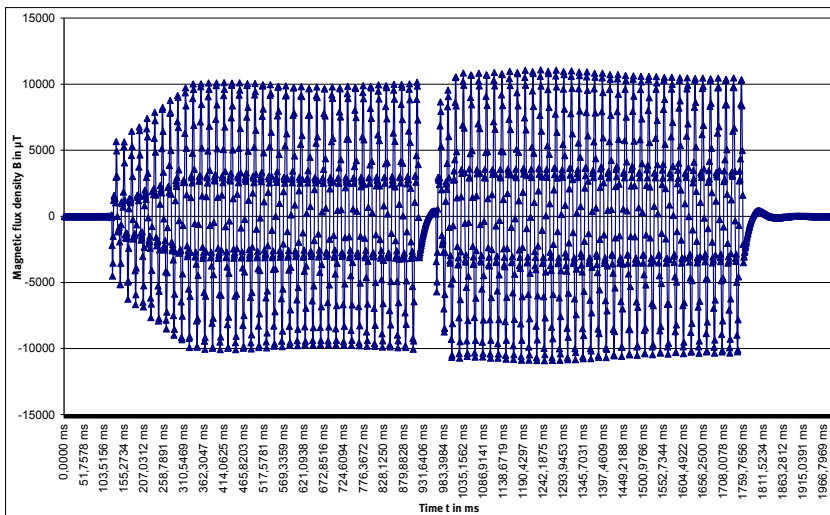
c)
Spot-welding gun No. 3 in the centre of the electrode, measured in sensor axis Y at a distance of 20 cm



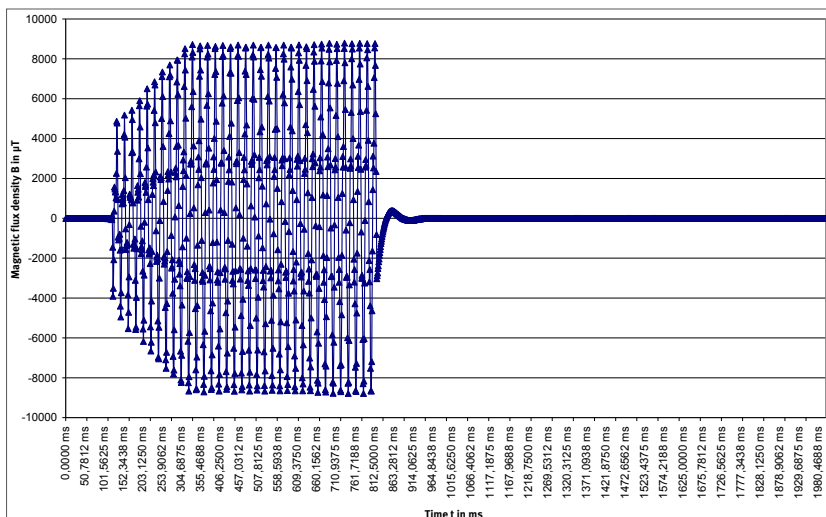
d) Spot-welding gun No. 4 in the centre of the electrode, measured in sensor axis Z at a distance of 20 cm



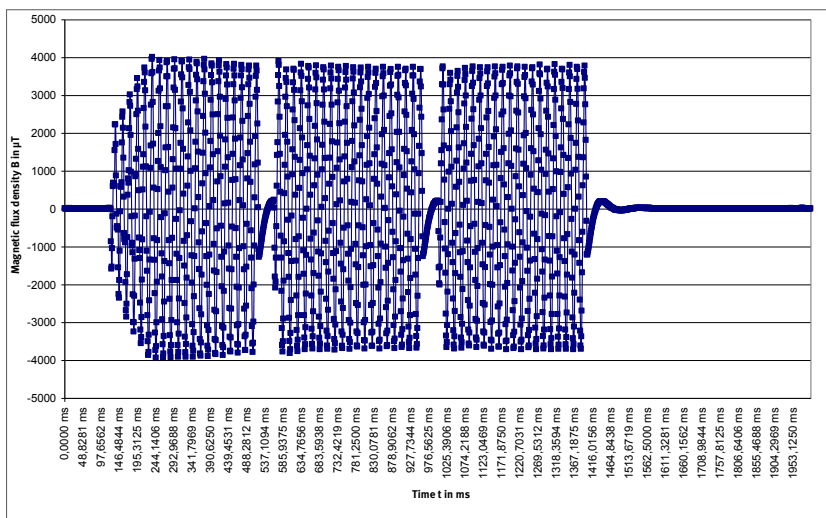
e) Spot-welding gun No. 5 in the centre of the gun window, measured in sensor axis X at a distance of 20 cm



f) Spot-welding gun No. 6 in the centre of the gun window, measured in sensor axis X at a distance of 20 cm



g) Spot-welding gun No. 7 in the centre of the gun window, measured in sensor axis Z at a distance of 20 cm



h) Spot-welding gun No. 8 in the centre of the gun window, measured in sensor axis Y at a distance of 20 cm

Table 1: Peak values of the magnetic flux density (B_{max}) determined on eight spot-welding guns as a function of the points of measurement

Point of measurement	B_{max} in mT for welding machine No.							
	1	2	3	4	5	6	7	8
Gun window, centre	21.0	5.1	5.5	7.9	6.0	11.7	10.0	5.5
Centre of the electrode at the front	7.8	2.8	2.9	2.65	1.8	2.4	3.15	1.75
Centre of the electrode to the side	19.0	3.7	3.5	3.3	1.95	4.5	4.2	3.3
Cable	53.0	34.0	37.5	20.5	43.0	32.5	28.0	32.6

5.5 Evaluation of the measurement results

For each spot-welding gun, the permissible values to BGV B11, Annex 1, Section 3 and BGI 5011 [2], Annex 1, Section 1.1 were calculated from the measured time behaviour of the welding current/magnetic flux density. The parameters used for calculation for the welding process concerned for each spot-welding gun studied and the permissible peak values of the magnetic flux density are shown in Table 2.

Comparison of the peak values for the magnetic flux density (Table 1) determined from the measured values with the

permissible values shown in Table 2 reveals that the latter are exceeded in various working positions on all spot-welding guns studied for the exposure area 1 and the increased exposure area (as defined in each case in BGV B11).

The highest exposure for the welders occurred in the vicinity of the welding cable and the centre of the gun window. The highest magnetic flux density was measured on spot-welding gun No. 1. Since the permissible „derived values“ to BGV B11 are exceeded, a check must be performed for observance of the basic values to BGV B11, Annex 1, Table 1.

Table 2:
Characteristic parameters and permissible values of eight spot-welding guns in use at the user's site

Parameters	Welding equipment at the user's site								
	No. 1	No. 2	No. 3	No. 4	No. 5	No. 6	No. 7	No. 8	
Number of periods of the welding current ($f = 50$ Hz)	2×40	30	35	35	35	2×40	35	3×20	
Duration of phase cut per half-wave, in ms	1.0	2.04	1.96	3.6	0.72	3.24	3.2	0.6	
Welding duration, in ms	1,40	477.6	563	434	649.6	1,082	476	1,128	
Weighting factor [V]	1	1.44	1.21	1.51	1.24	1	1.45	1	
Duration of field change τ_{pmin} , in ms	4.5	3.98	4.02	3.1	4.64	3.38	3.4	4.7	
Frequency of the field change f_p , in Hz	55	63	62	80	54	74	74	53	
Permissible peak value of the magnetic flux density, in mT	Ex 1 ¹⁾	1.74	2.21	1.8	1.8	2.2	1.29	1.84	1.81
	Incr-ex-a ²⁾	3.27	4.14	3.5	3.38	4.13	2.43	3.44	3.39

¹⁾ Exposure area 1; ²⁾ Increased exposure area

5.6 Analysis of the welders' working positions on the spot-welding guns studied at the user's site

5.6.1 Performance of the analysis

The behaviour of the welders was studied during production welding work at the user's production sites. For this purpose, the various working procedures were observed on all spot-welding machines and documented by means of videos and photographs. The data material was studied in consideration of the following aspects:

- How does the welder hold the spot-welding gun?
- How does the welder stand at the spot-welding gun?

- What are the distances between various parts of the welder's body, the spot-welding gun, and the welding cables?
- What parts of the welder's body make contact with the spot-welding gun?
- How are the welding cables guided past the welder's body?
- What differences exist between the holding of spot-welding guns with large vs. small gun windows?

Figures 3 to 10 show typical working positions on the spot-welding guns studied.

Figure 3:
Spot-welding gun No. 1 studied at the user's site



Figure 4:
Spot-welding gun No. 2 studied at the user's site



Figure 5:
Spot-welding gun No. 3 studied at the user's site



Figure 6:
Spot-welding gun No. 4 studied at the user's site

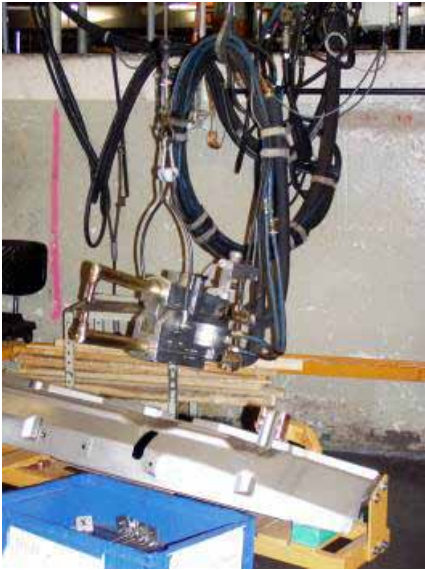


Figure 7:
Spot-welding gun No. 5 studied at the user's site



Figure 8:
Spot-welding gun No. 6 studied at the user's site



Figure 9:
Spot-welding gun No. 7 studied at the user's site



Figure 10:
Spot-welding gun No. 8 studied at the user's site



5.6.2 Results

Observations found that the welders using the welding equipment did not handle the spot-welding guns in a uniform way. This is due essentially to differences in the design of the welding equipment. The principal differences are between spot-welding guns that are held vertically (spot-welding guns Nos. 2, 3, 6, 7 and 8) and those held horizontally (spot-welding guns Nos. 4 and 5), and between large-format and small-format spot-welding guns.

On the spot-welding guns mainly held vertically, the welders generally stand with the upper body parallel to the gun window. On the spot-welding guns which the welders guide above the electrode arms with both hands (Nos. 2, 3 and 8), the distance between the upper body and the gun window is generally greater than 20 cm. The welding cables may however be placed past the welder's head and close to it in this case.

For positioning of spot-welding guns Nos. 6 and 7, a handle is fitted to one of the two electrode arms and another handle above the electrode arms. The welding cables are placed upwards. The possibility cannot be excluded in this case of the welder's upper body making contact with the electrode arms during welding work and the welding cables passing close to the head.

Spot-welding guns held mainly horizontally are held by the workers at around stomach height. The welders stand to the side of the gun window in this case, close to the welding cable terminals. During welding, the spot-welding gun is held by one handle and one electrode arm. The electrode arm is enclosed by the hand. The welding cables are placed to the side of the spot-welding gun away to the ceiling. The distance between the welder's upper body and the spot-welding gun is approximately 0 to 20 cm.

Large-format spot-welding guns (No. 1) are almost always guided parallel to the front of the body. The centre of the gun window is approximately at stomach level. During welding, the possibility

cannot be excluded of the welder making contact with the frame of the spot-welding gun.

5.7 Conclusions regarding the subsequent procedure

During evaluation of the exposure with reference to the basic values, a distinction must be drawn between:

- The design of the spot-welding gun (small and large gun window)
- The position of the spot-welding gun and of the gun window (horizontal, vertical)
- The welder's position at the spot-welding gun (to the side or centrally in relation to the gun window)
- The distance between the welder and the spot-welding gun
- The run of the welding cables

6 Project Step 2: studies in the laboratory

6.1 Objective of the studies performed in the laboratory

Studies were to be performed on two spot-welding guns with different gun windows, in order to determine the distribution of the magnetic flux density in the vicinity of the spot-welding guns as a function of the welding current, in several planes and at different distances from the spot-welding gun.

6.2 Studies in the laboratory

One spot-welding gun with small and one with large gun window were selected for the purpose of the study. These spot-welding guns and their dimensions are shown in Figures 11 and 12.

Figure 11:

Selected spot-welding guns with small (top) and large (bottom) gun window

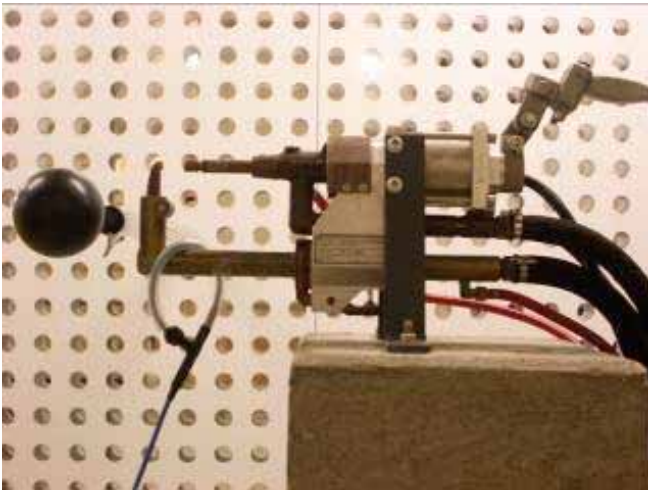
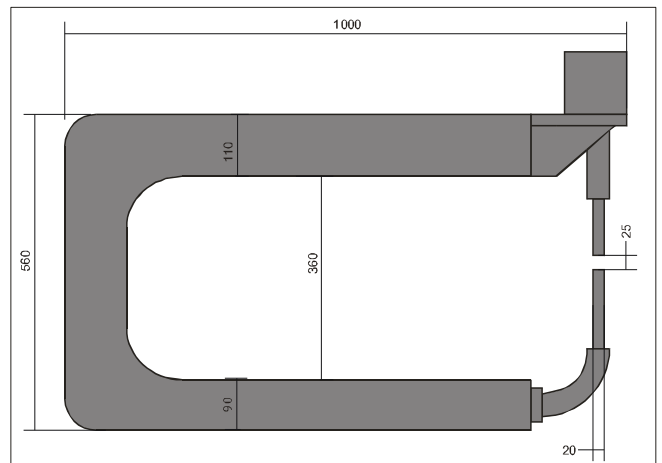
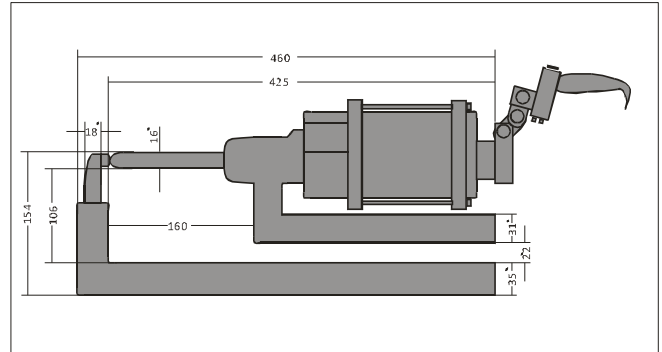


Figure 12:

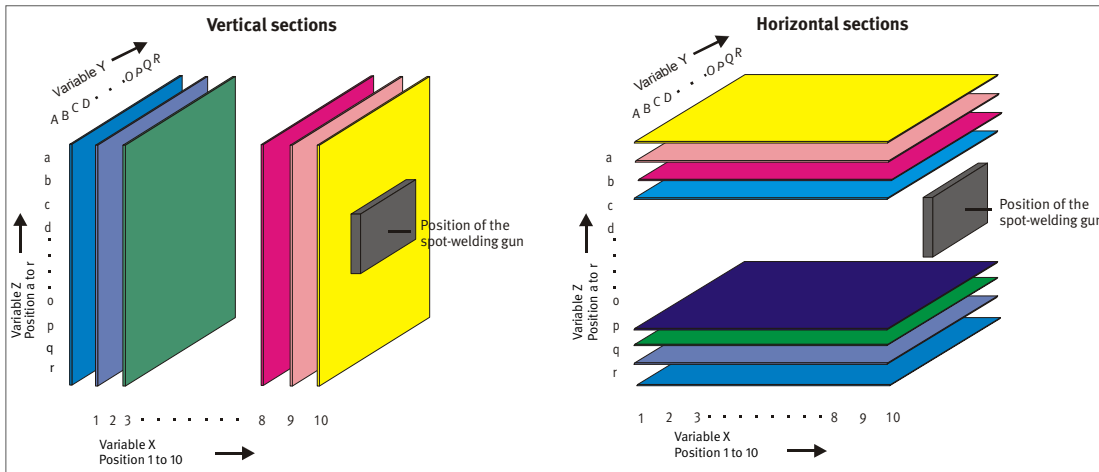
Schematic diagram of the selected spot-welding guns. Top: spot-welding gun with small gun window; bottom: spot-welding gun with large gun window; dimensions in mm



The variation of the magnetic flux density over time in front of the spot-welding gun during a welding process was measured and recorded on a 10 cm grid in a space with a height of 2 m, width of 2 m and depth of 1 m. The measurements were taken in the three mutually perpendicular axes and with identical welding parameters, such as welding current, duration of welding, frequency and phase control. To permit measurement of the maximum possible magnetic flux densities, the spot-welding guns were operated in short-circuit mode, i.e. without a workpiece.

The peak value of the magnetic flux density was determined for each measurement point from the recorded time behaviour in the magnetic flux density. The horizontal and vertical distributions of these peak values were then calculated in several sections (Figure 13). The sections were determined with reference to the measurement grid.

Figure 13:
Sections in which the magnetic flux density was measured



The Chauvin Arnoux CA 42 field measurement system and M 400 field measurement probe were used to measure the magnetic flux density. In addition, the time behaviour of the welding current was measured and recorded by means of a Rogowski coil and a digital memory oscilloscope.

The experimental setup used for this purpose is shown in Figures 14 to 16. Figure 14 shows the measurement and study arrangement for determining the distribution of the magnetic

flux density on the spot-welding guns with small and large gun window. The spot-welding gun with small gun window is mounted on four metal-free concrete blocks (Figure 14 a); the spot-welding gun with large gun window is mounted on a wooden strut (Figure 14 b). The wall with holes in a 10 cm grid and the field sensor with gauge rod can be seen on the left-hand side of the images. The measurement arrangement is shown schematically and the measurement points in side view and plan view in Figures 15 and 16.

Figure 14:
Measurement and study arrangement



a)
Spot-welding gun with small gun window



b)
Spot-welding gun with large gun window

Figure 15:
Side view of the measurement point (see also Figure 13, „horizontal plane“).
Top: spot-welding gun with small gun window; bottom: spot-welding gun with large gun window

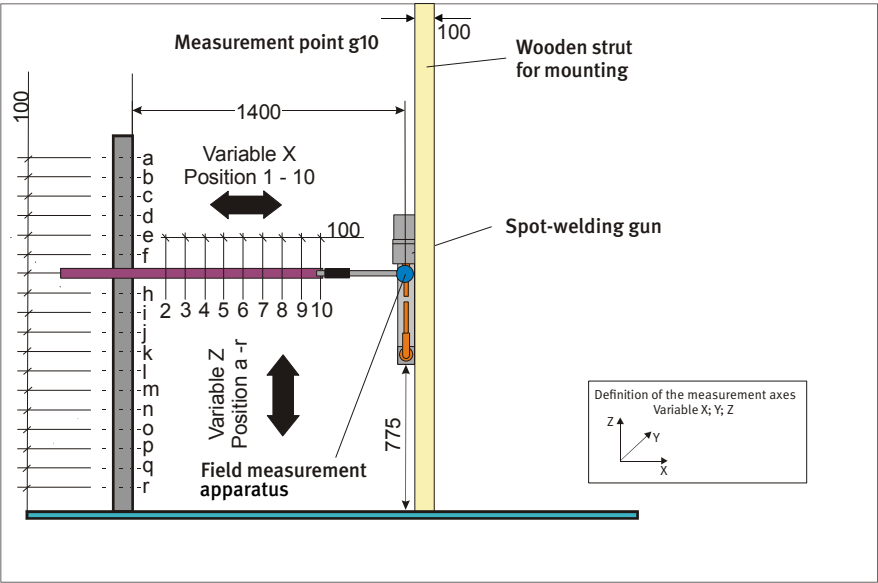
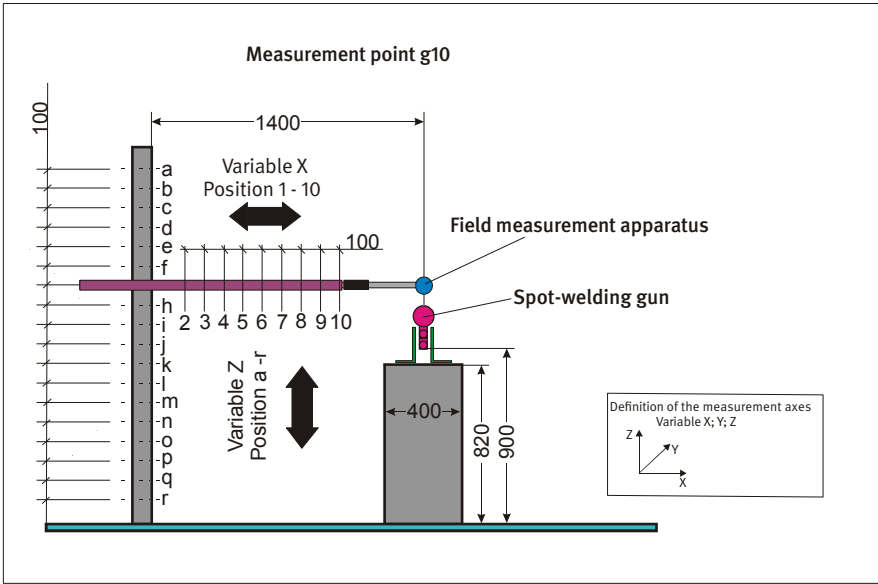
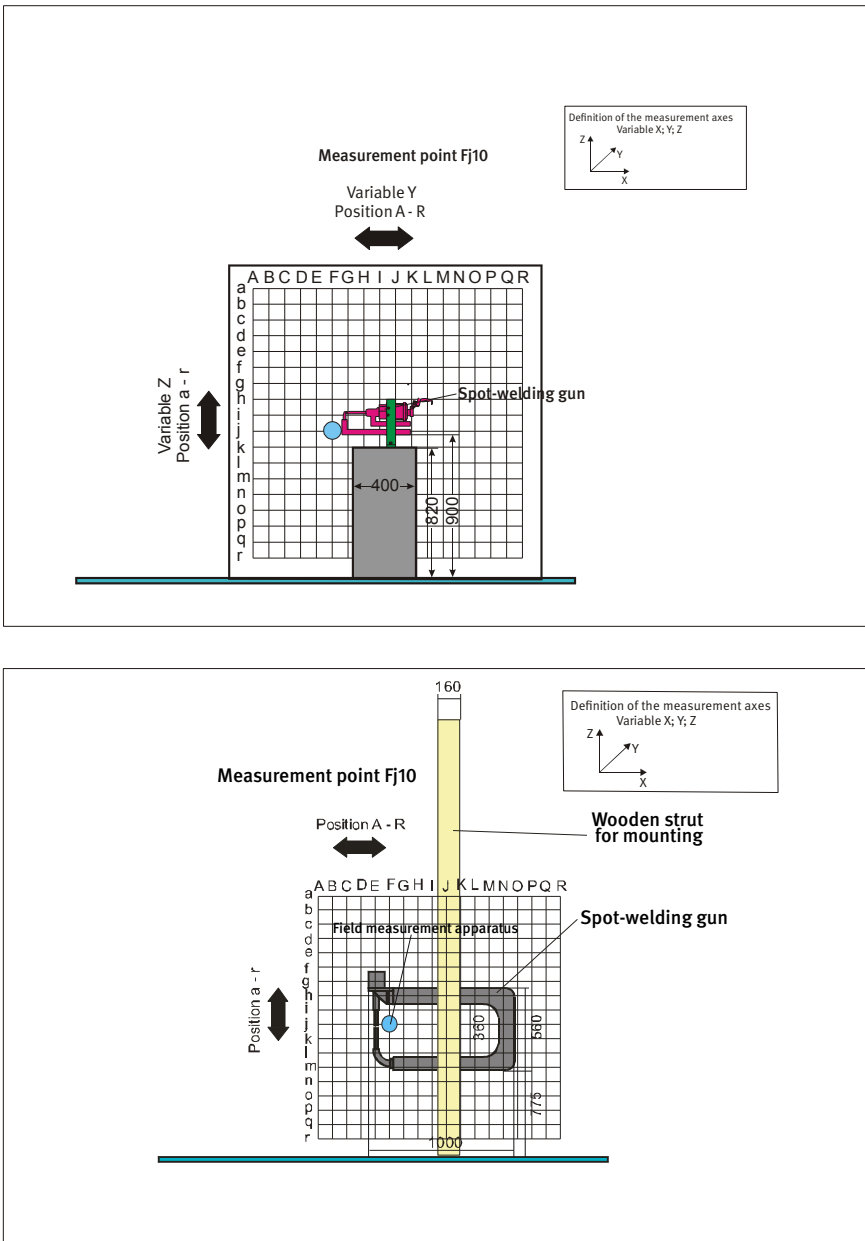


Figure 16:
Plan view of the measurement point (see also Figure 13, „vertical plane“).
Top: spot-welding gun with small gun window; bottom: spot-welding gun with large gun window



The distribution of the magnetic flux density was studied in the following steps:

1. Determining the spatial distribution and evaluation of the magnetic flux density on the spot-welding gun with small gun window
2. Measurement of the magnetic flux density on the spot-welding gun with large gun window at selected measurement points
3. Comparison of the measurement results with the results from Project Step 3

The climatic conditions prevailing during the studies were as follows:

- Temperature: 22.5 to 24.4 °C
- Relative humidity: 45.0 to 55.5%

The following instruments were used:

- **Electromagnetic field measurement system**

Manufacturer:	Chauvin Arnoux
Type:	CA 42
H-field probe	
Manufacturer:	Chauvin Arnoux
Type:	M 400
Bandwidth:	10 Hz to 400 kHz

Directional pattern: X, Y, Z
 Measurement range: 10 nT to 25 mT
 Uncertainty of measurement: $\pm 3\%$ of the display

- **Oscilloscope**

Manufacturer: Tektronix
 Type: TDS2012
 Serial No: C046119

- **Rogowski current wave transducer**

Manufacturer: Power Electronic Measurements Ltd.
 Type: IRF150 D12
 Serial No: 6394-1546
 Peak current rating: 30 kA/5 kHz

The duration of welding and the level of the welding current can be abstracted from the time behaviour of the welding current shown in Figure 17. The welding duration comprises 15 cycles each lasting 20 ms. The maximum welding current is 9.5 kA. The actual behaviour of the welding current can be seen in Figure 18. Owing to the phase control employed in the welding power supply, the welding current deviates from a purely sinusoidal form and is marked by interruptions. The duration of the interruption in the welding current is approximately 1 ms per half wave.

Figures 19 and 20 provide an overview of the distributions of the magnetic flux density on the spot-welding gun with small gun window in the horizontal and vertical sections. Figure 19 shows the horizontal distributions at a distance of 10 cm for distances of between 50 and 160 cm above the ground. For the positions 5 to 10 shown in Figure 15, the vertical distributions are shown in Figure 20 (see Page 36).

6.3 Results of the laboratory measurements

The time behaviour of the welding current upon which the measurements on the two spot-welding guns are based and a display detail from it are shown in Figures 17 and 18 respectively.

Figure 17:
 Welding current time behaviour during the laboratory measurement

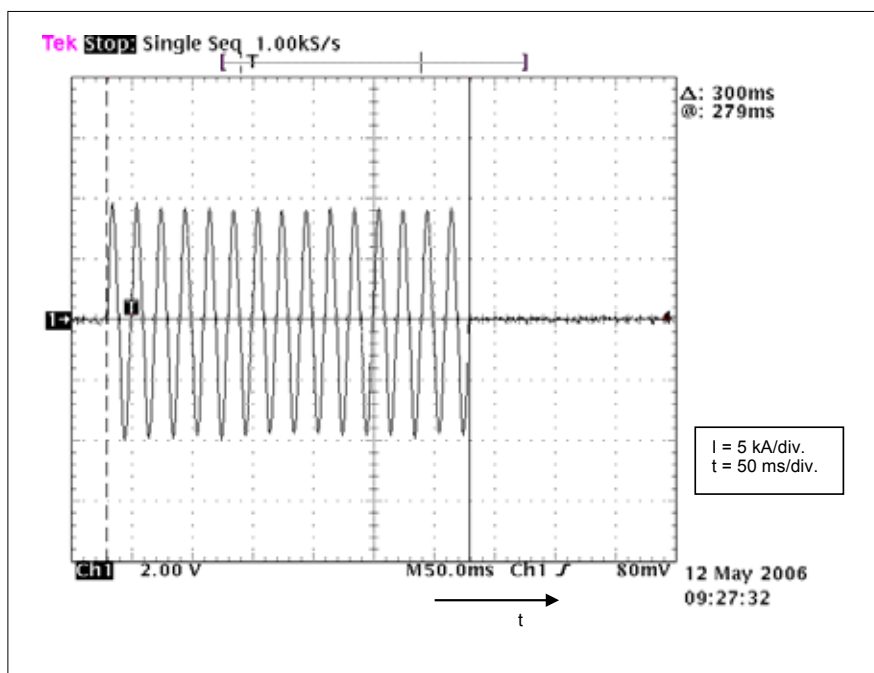


Figure 18:
Display detail from the welding current time behaviour during the laboratory measurement

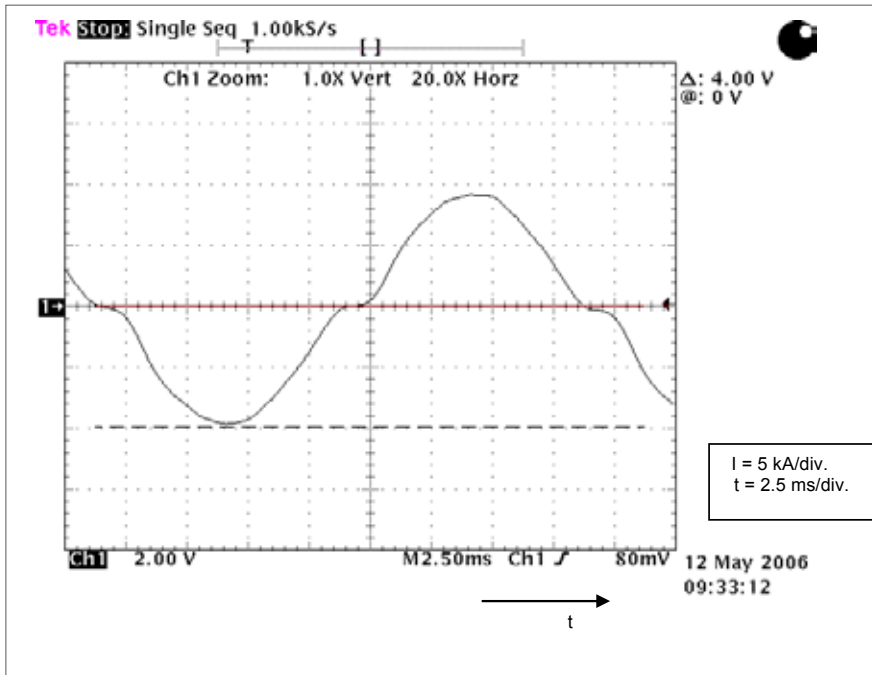
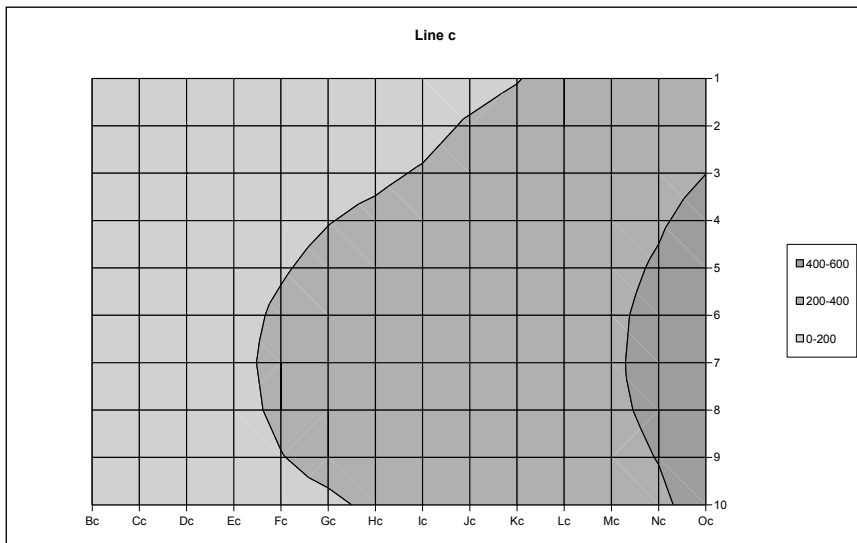
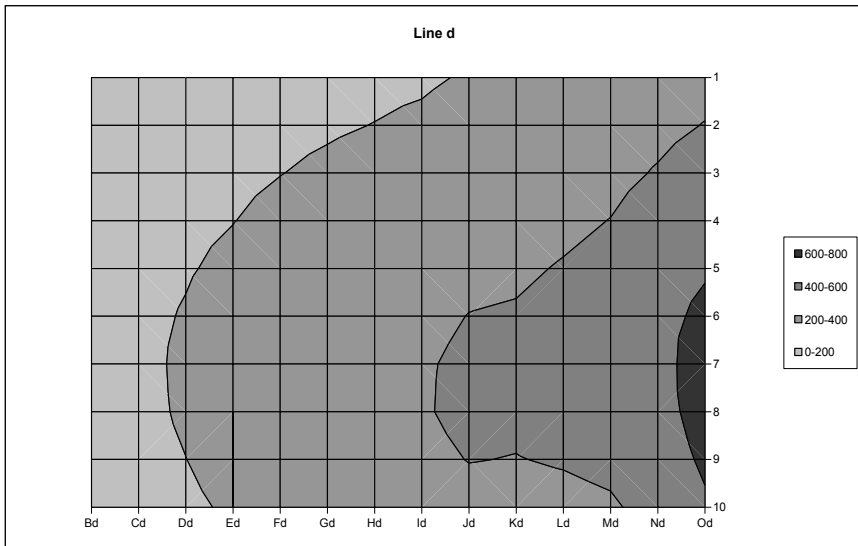


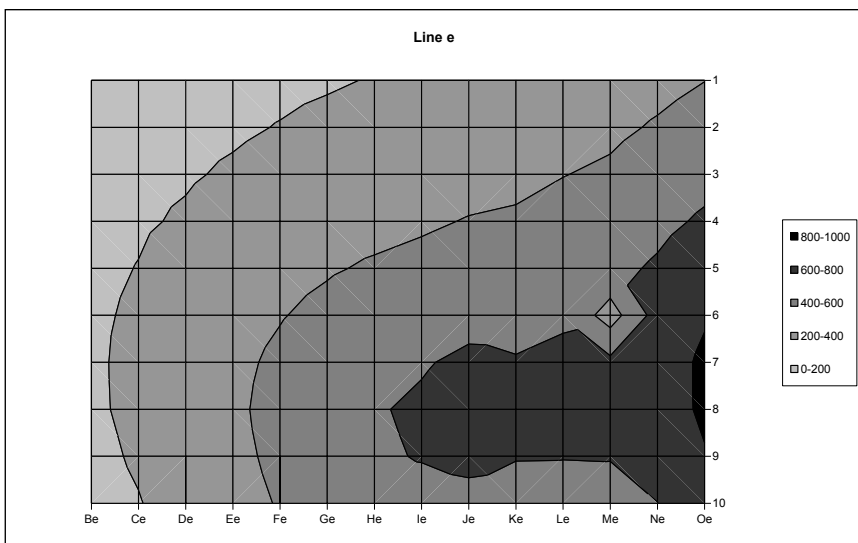
Figure 19:
Variation of the magnetic flux density at the spot-welding gun with small gun window in the horizontal plane as a function of the height h above the ground; values in the legends indicate the magnetic flux density in μT



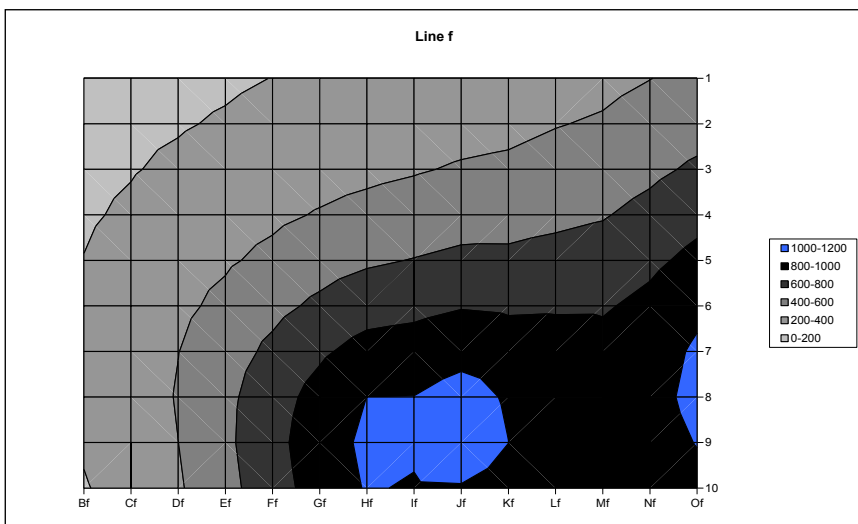
a) $h = 160 \text{ cm}$



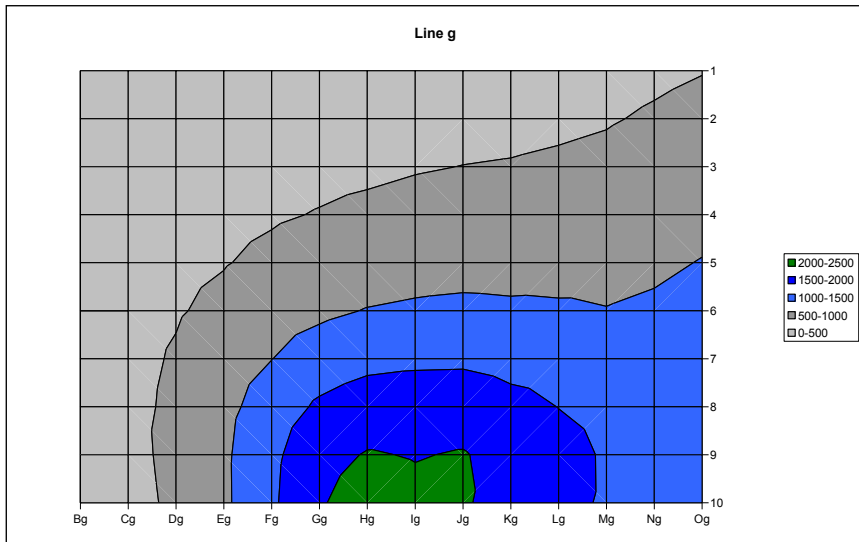
b) $h = 150$ cm



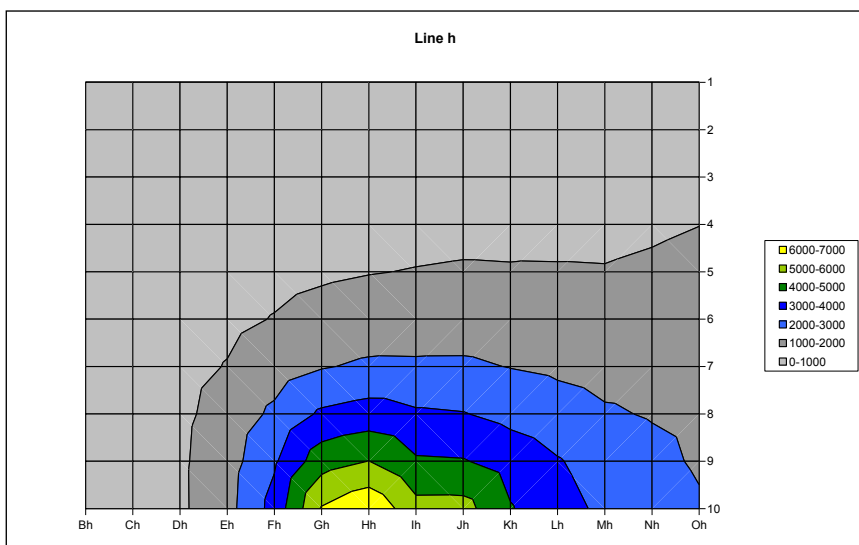
c) $h = 140$ cm



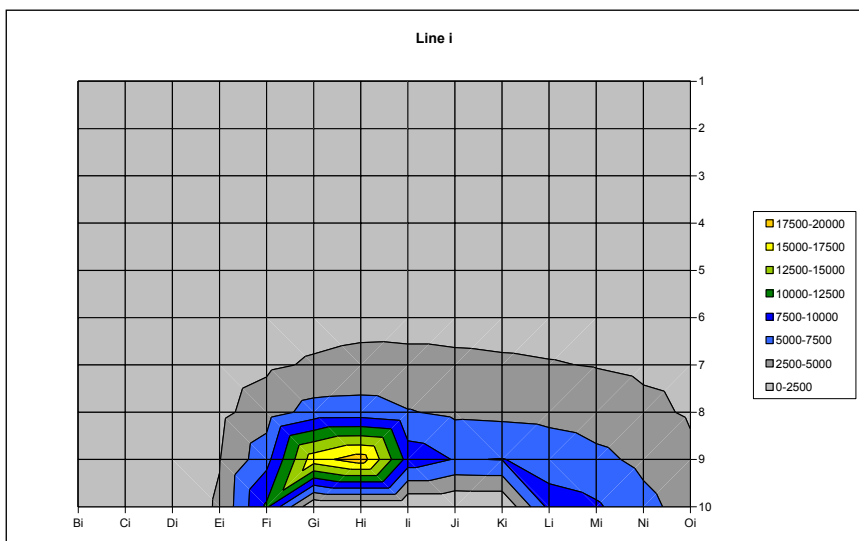
d) $h = 130$ cm



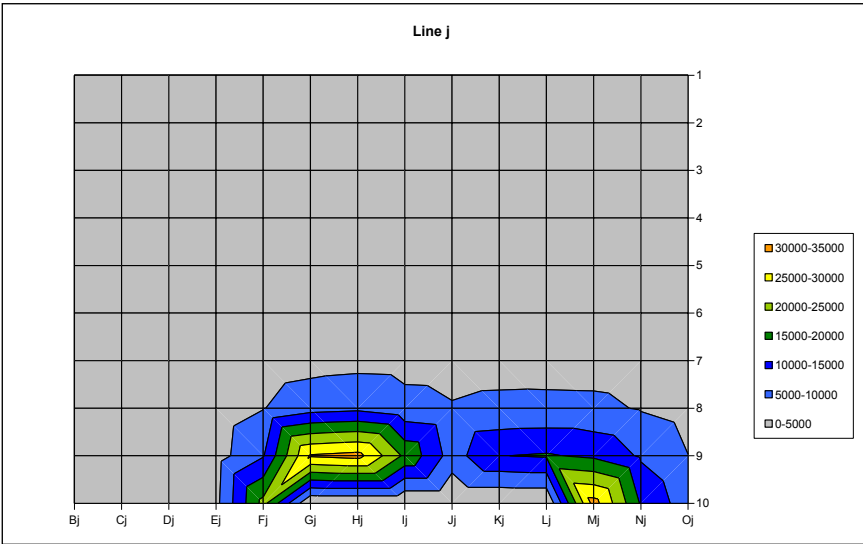
e) $h = 120$ cm



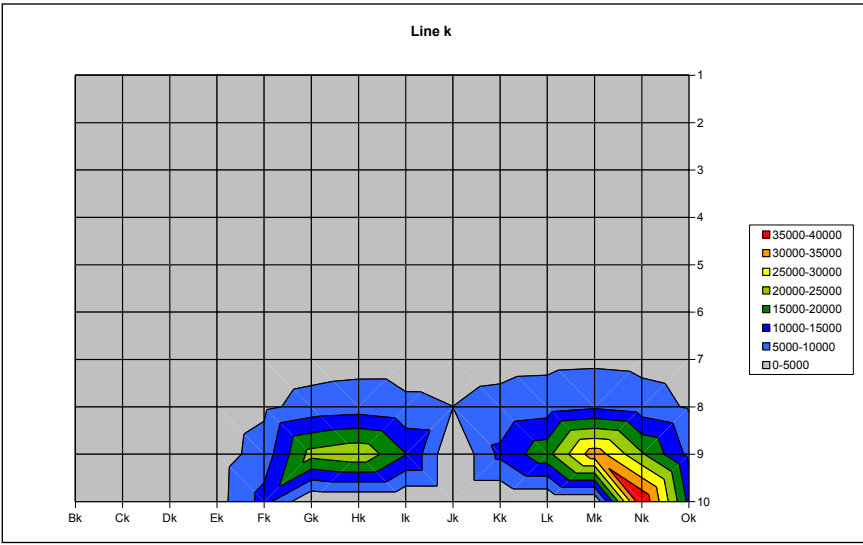
f) $h = 110$ cm



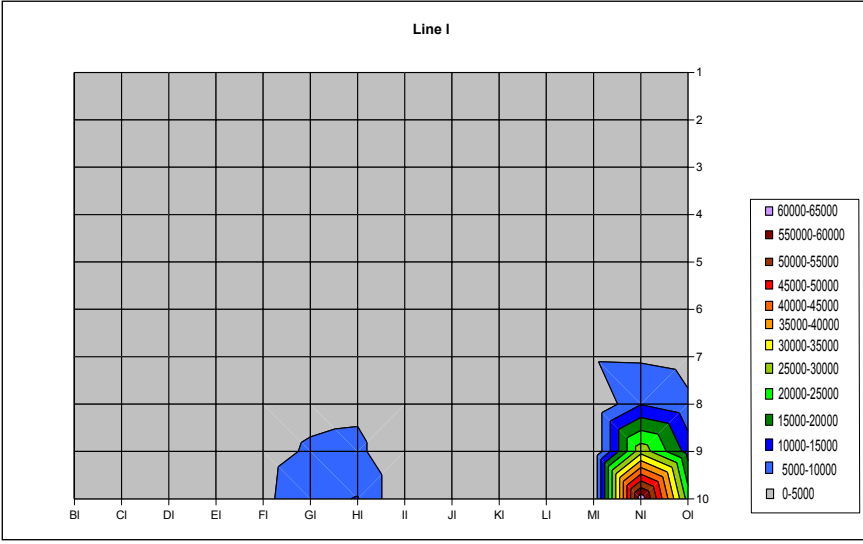
g) $h = 100$ cm



h) $h = 90$ cm

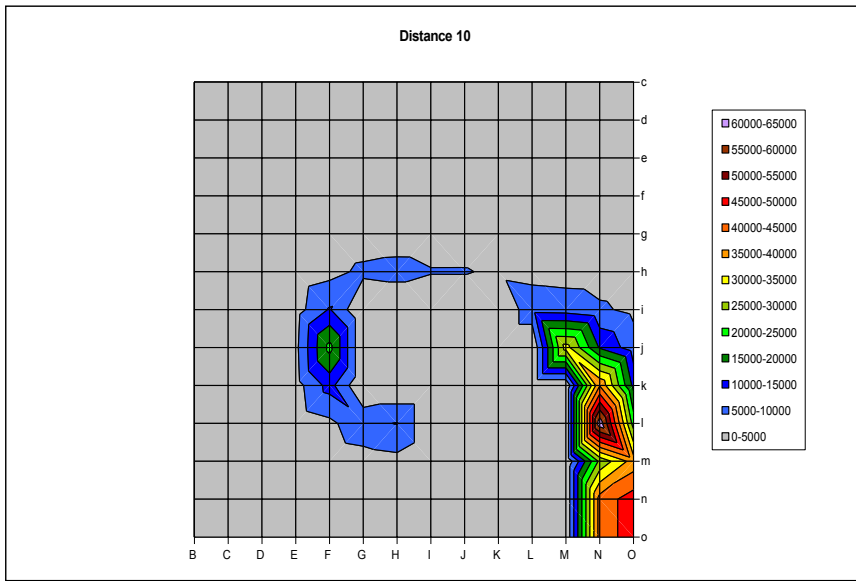


i) $h = 80$ cm

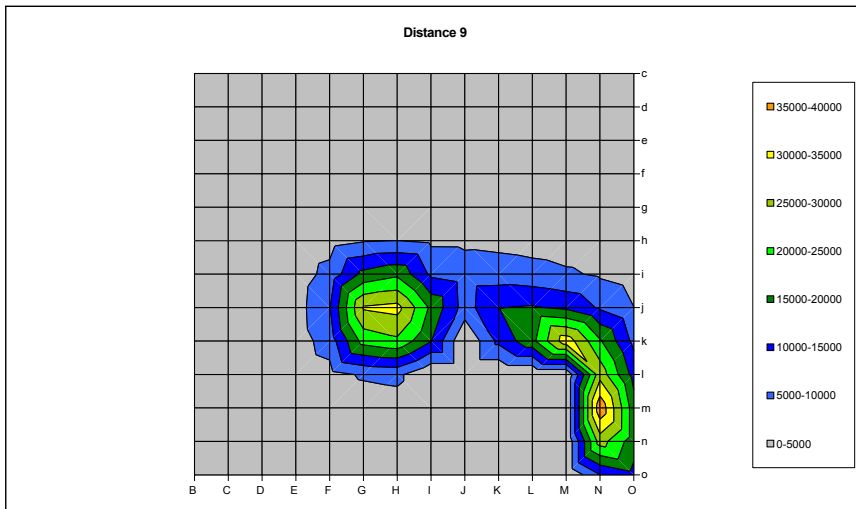


j) $h = 70$ cm

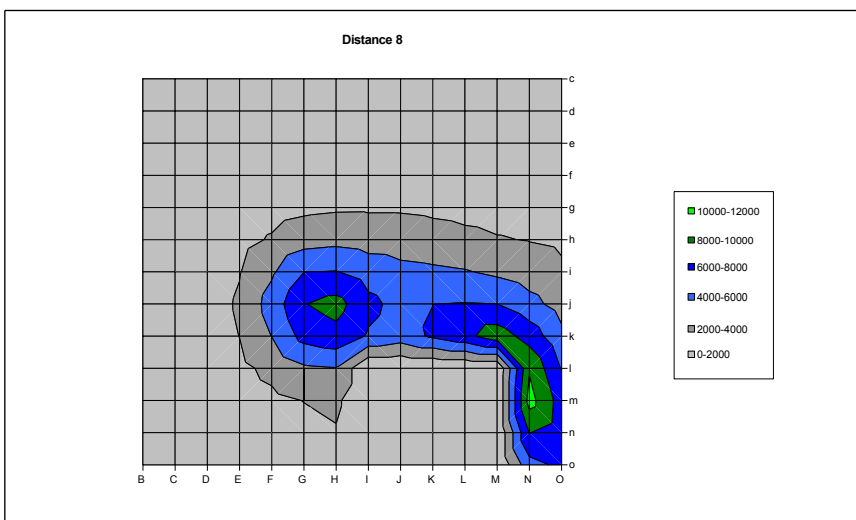
Figure 20:
Variation of the magnetic flux density at the spot-welding gun with small gun window in the vertical section as a function of the distanced from the spot-welding gun; values in the legends indicate the magnetic flux density in μT



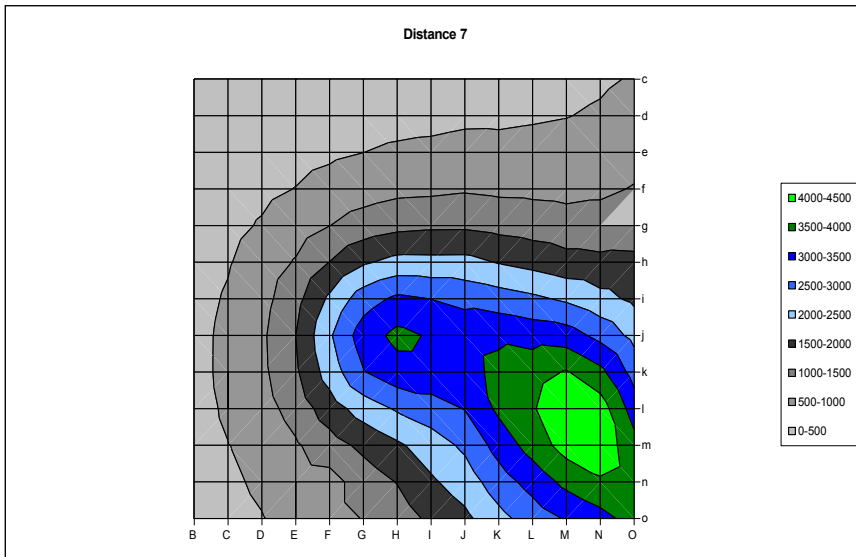
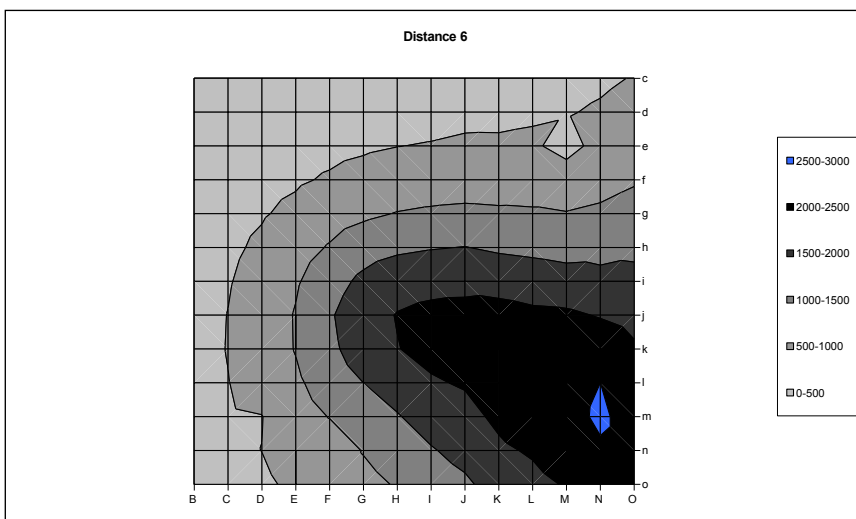
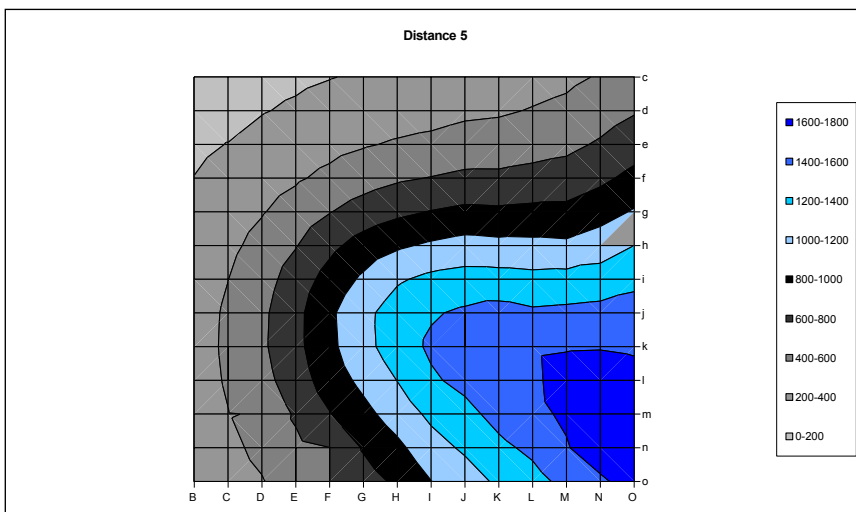
a) $d = 0$



b) $d = 10 \text{ cm}$



c) $d = 20 \text{ cm}$

d) $d = 30$ cme) $d = 40$ cmf) $d = 50$ cm

Magnetic flux densities were measured at selected measurement points in the measurement axes X, Y and Z on the spot-welding gun with large gun window. The following measurement points were selected for the measurement:

- X axis of measurement: Measurement point „1Jj“ to „10Jj“
- Y axis of measurement: Measurement point „8Aj“ to „8Qj“
- Z axis of measurement: Measurement point „8Jc“ to „8Jq“

The location of the measurement points on the spot-welding gun can be seen in Figures 15 b and 16 b. Figure 21 shows the measurement results in the three axes of measurement.

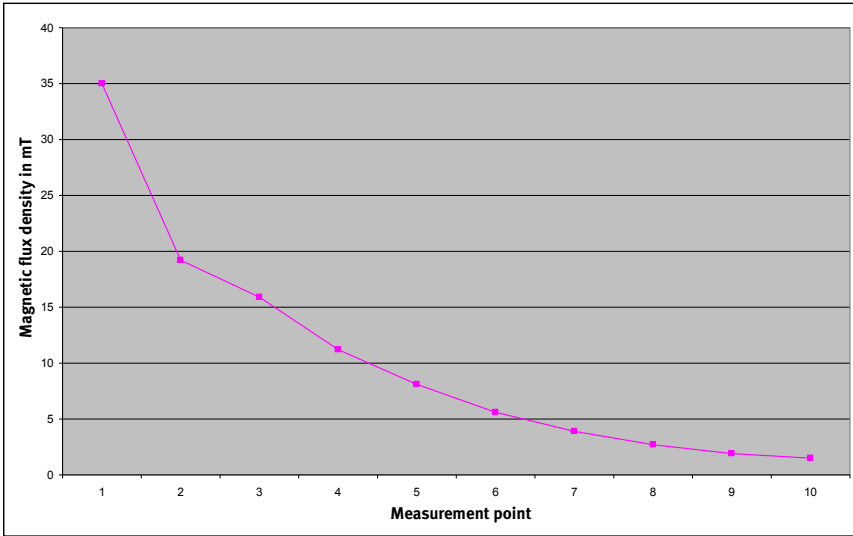
The highest value of the magnetic flux density, 63.5 mT, was measured on the welding cables at the measurement point Ni on the spot-welding gun with small gun window (see Figure 16, top).

Figures 22 and 23 (see Page 39) show the distributions of the magnetic flux density on the small welding gun for the planes with the highest flux density values. Figure 22 shows the field

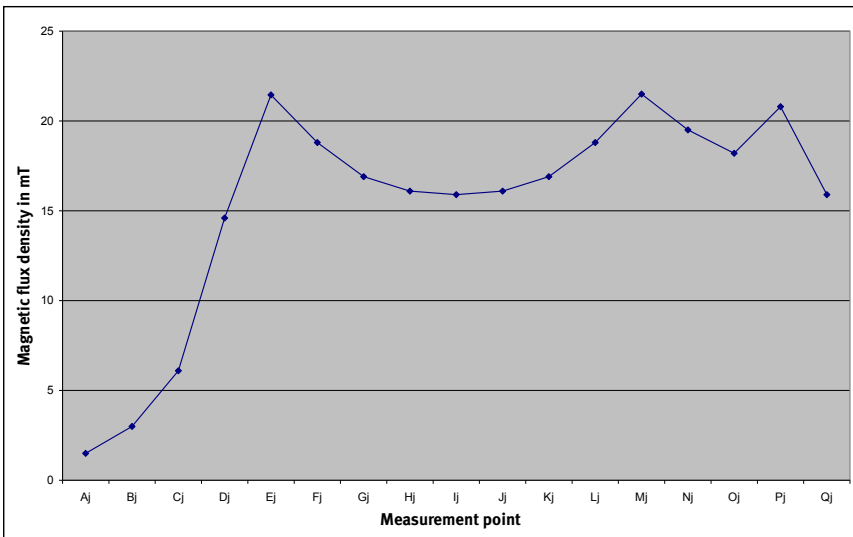
distribution in a vertical section at a distance of 10 cm from the welding electrode; Figure 23, that for the horizontal section (at a distance of 90 cm from the welding level). In both the vertical and horizontal sections, the highest values for the magnetic flux density, 30 to 35 mT, were measured on the welding electrodes and cables.

Both distributions show that high magnetic flux densities occur only in the immediate proximity of the spot-welding gun and cable. At a distance of 20 to 30 cm, the peak value of the magnetic flux density falls below 2 mT.

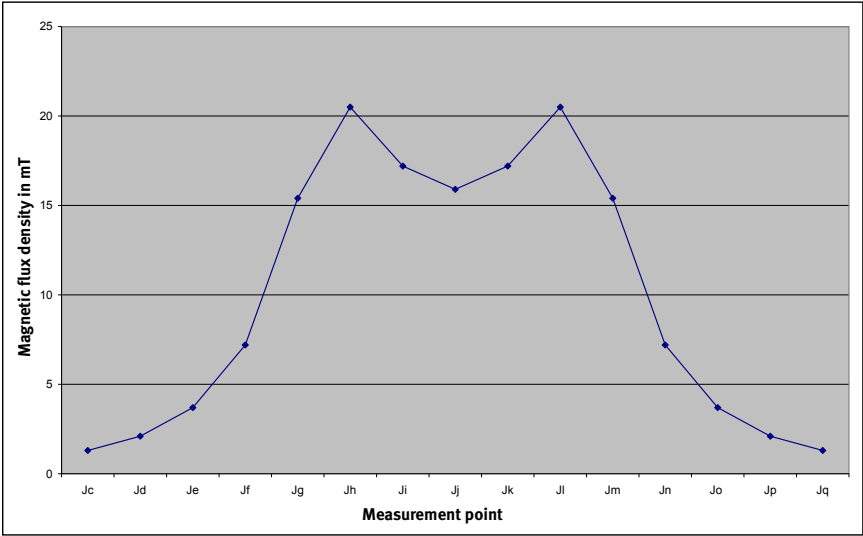
Figure 21: Magnetic flux densities measured on the spot-welding gun with large gun window



a) X axis of measurement: measurement points 1j to 10j, longitudinal direction



b) Y axis of measurement: measurement points 8Aj to 8Qj, horizontal direction



c) Z axis of measurement: measurement points 8Jc to 8Jo, vertical direction

Figure 22:
Example of a field distribution in the vertical section (distance d of 10 cm from the welding electrode), measured at the spot-welding gun with small gun window; the values in the legend indicate the magnetic flux density in μT

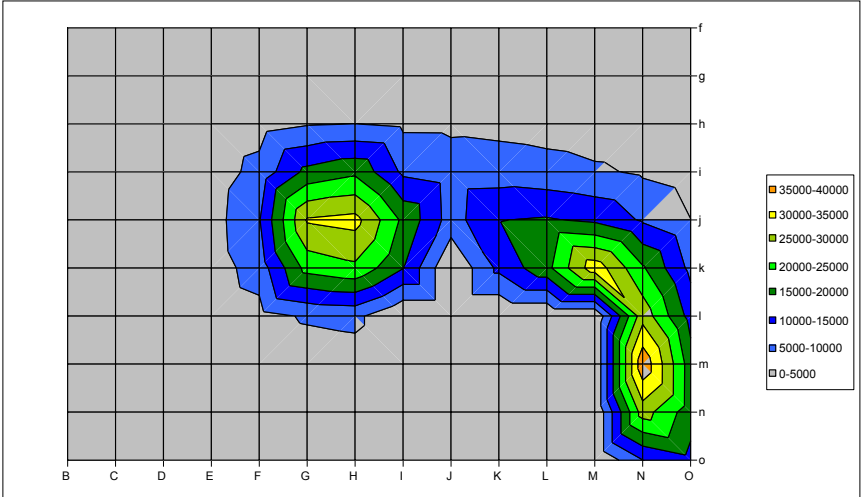
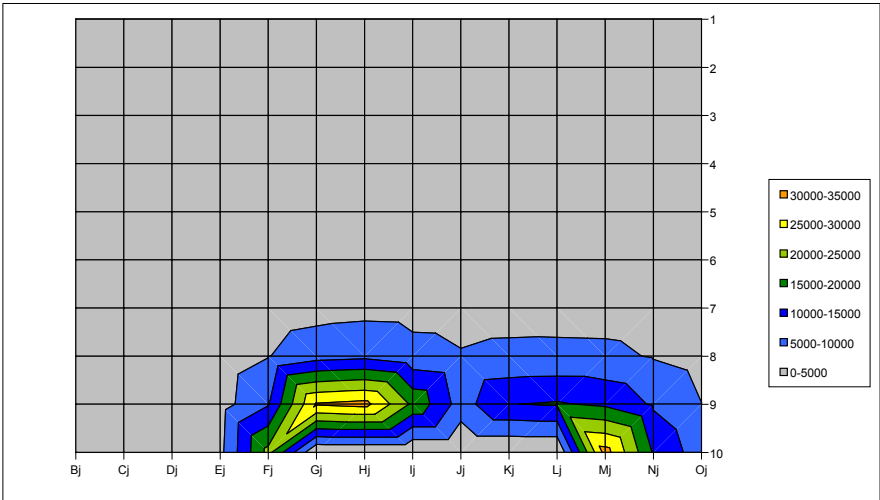


Figure 23:
Example of a field distribution in the horizontal section (distance h of 90 cm from the ground), measured at the spot-welding gun with small gun window; the values in the legend indicate the magnetic flux density in μT



6.4 Permissible values

The permissible peak value of the magnetic flux density is determined in accordance with BGV B11, Annex 1, Section 3, by the procedure to BGI 5011, Annex A 1.1. The parameters (Table 3) for calculation of the peak value are determined from the time behaviour of the welding current as shown in Figures 17 and 18. They apply for both spot-welding guns studied.

Table 3:
Parameters for determining the permissible values for the spot-welding guns used for the laboratory measurements

Parameter	Value
Number of welding cycles	15
Phase cut per half wave	1 ms
Duration of all field changes (current flow duration) τ_D	270 ms
Weighting factor [V]	1.92
Smallest value of the field-change duration τ_{pmin}	4.5 ms
Frequency of the field change f_p	55.5 Hz

Table 4 shows the permissible peak values for the magnetic flux densities derived in a number of areas of exposure in consideration of the maximum frequency of the field change ($f = 55.5$ Hz) and the weighting factor $V = 1.92$.

Table 4:
Permissible values for the magnetic flux density for the various areas of exposure

Area/part of the body	Permissible values Peak value of the magnetic flux density in mT
Area of exposure 1	3.28
Increased exposure area	6.22
Exposure of the extremities	8.2 ¹⁾ / 15.5 ²⁾
Hand/finger exposure	65.6 ¹⁾ / 124.4 ²⁾

¹⁾ Permissible peak value of the magnetic flux density for exposure of the extremities in exposure area 1

²⁾ Permissible peak value of the magnetic flux density for exposure of the extremities in the increased exposure area

6.5 Assessment and evaluation of the results

The results of measurement for the spot-welding guns with small and with large gun window reveal high magnetic flux densities in the proximity of the electrodes, electrode arms and welding cables (Figures 19 to 23). Either discrete or all permissible values shown in Table 4 are exceeded in this case, depending upon the distance and location of the exposure. In order for the permissible values for the increased exposure area to be observed, a minimum distance of approximately 30 cm must be observed from the various components of the spot-welding gun. The permissible values for the area of exposure 1 are however observed only upwards of a distance of approximately 40 cm. As explained in Section 5.2, the distance between the welder and the spot-welding gun is generally less than 20 cm. In the area occupied by the welder, the permissible values of BGV B11 are therefore almost always exceeded. Observance of the body current density values (basic values of BGV B11, Appendix 1, Table 1) must therefore be checked.

7 Project Step 3: field simulation

7.1 General

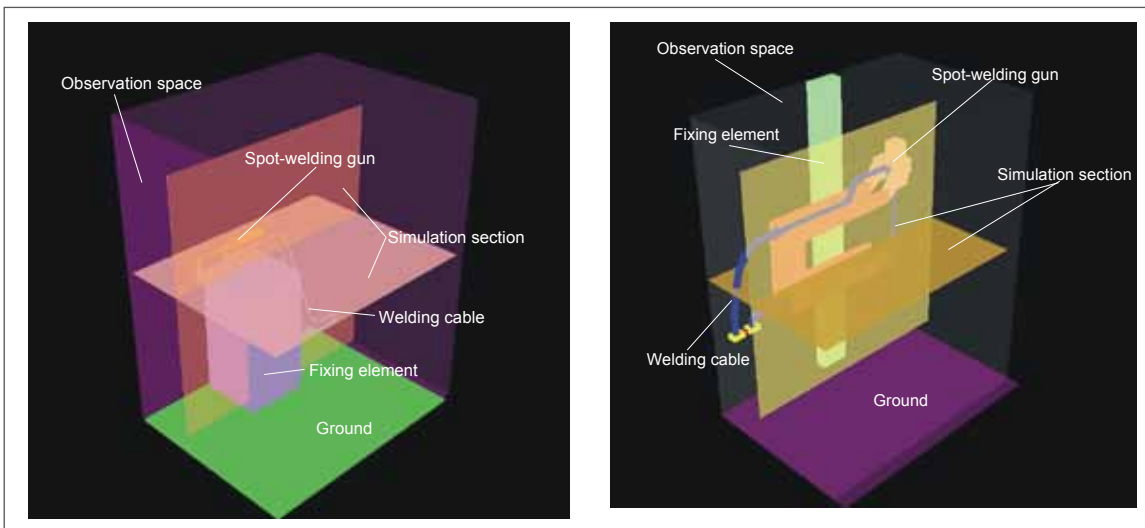
The magnetic fields at the spot-welding gun were calculated by means of the IMST EMPIRE™ field calculation program. This program enables the fields of specified structures to be simulated and visualized by analysis. It contains several modules the functionality of which is built upon a CAD program serving as a user interface. The geometrical structure, dimensions, material properties, architecture, location of the field source (spot-welding gun) and the space under consideration are programmed through this interface. The Finite Difference Time Domain (FDTD) method is employed for analysis of the magnetic fields.

7.2 Simulations

The analyses of the field distribution were based upon the simulations and arrangements for the spot-welding gun with small and large gun window shown in Figure 24.

The image corresponds to the measurement and study arrangement used in the laboratory during Step 2 of the project (refer to Figure 14). It shows the area of observation, two simulation sections (horizontal and vertical), the ground, and the location of the spot-welding guns and welding cables. In the simulations, the spot-welding guns were positioned above an electrically non-conductive floor, comparable to the ambient conditions in the laboratory arrangement.

Figure 24: Simulation of the measurement and study arrangement for analysis of the magnetic fields for spot-welding guns with small (left) and large (right) gun windows



7.3 Objective of the field simulation

The objective of the field simulation is to compare the measured and calculated field distributions in order to determine the suitability of the simulated measurement and study arrangement for use for calculation of the body current densities in a recognized body model. For this purpose, the calculated field distributions were compared with those measured in the laboratory. The purpose here was further to determine whether the two methods for determining the fields – based upon calculation and upon measurement – produce similar results, i.e. whether the distributions determined for the magnetic flux densities are identical or similar. For this purpose, the values for the magnetic flux density were determined from the horizontal and vertical field distributions for comparable locations, and compared.

7.4 Calculation of the field distribution

The distribution of the magnetic flux density was calculated for both simulations in a horizontal section approximately 1,000 mm above the ground, in a vertical section directly at the surface, and at a distance of 200 mm from the axis of symmetry of the spot-welding gun. As shown in Figures 15 and 16, this corresponds to the horizontal section (A-R)_i and the vertical sections (A-R)_(a-r) at points 8 and 10¹.

A welding current with a frequency of 50 Hz (without phase control) and a current of $I = 10$ kA served as the parameters for all field calculations.

¹ Measurement point position 10 = (position 10 according to figure 15 resp. 16) – (radius of the field probe and radius of the electrodes at the spot-welding gun)

7.5 Results of the field simulation

The results of the field calculations are shown in Figures 25 and 26. The diagrams show a three-dimensional plan view of the magnetic fields in the vicinity of the spot-welding gun in one horizontal and two vertical simulation sections.

Figure 25:
Results of the field calculation at the spot-welding gun with small gun window

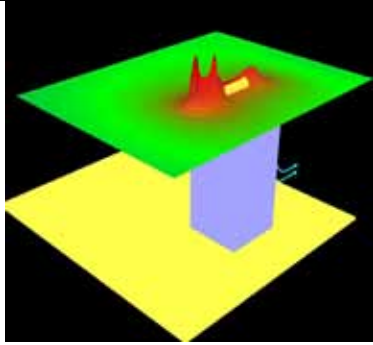
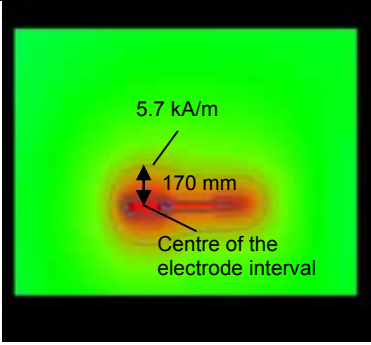
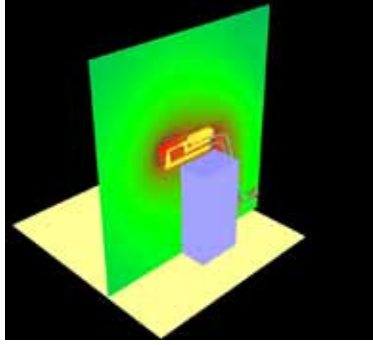
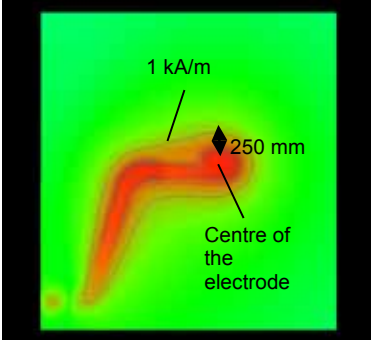
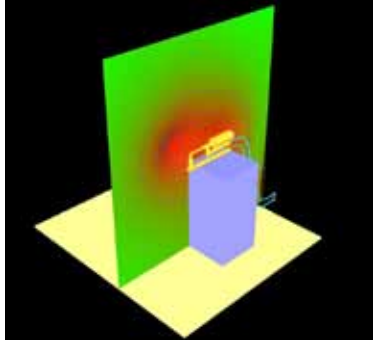
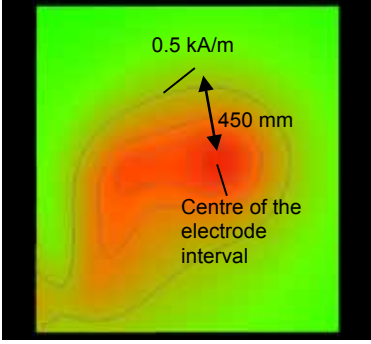
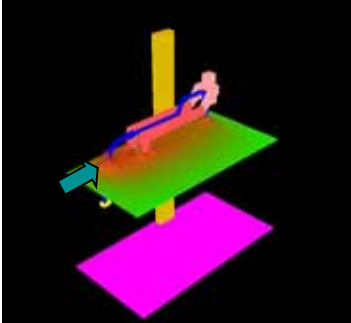
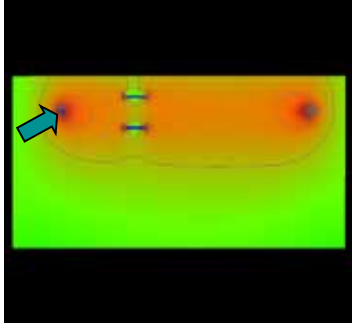
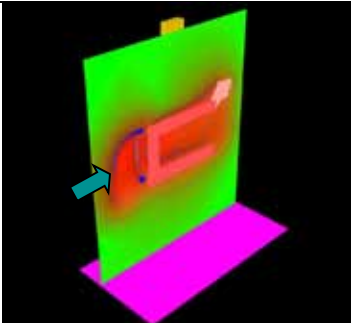
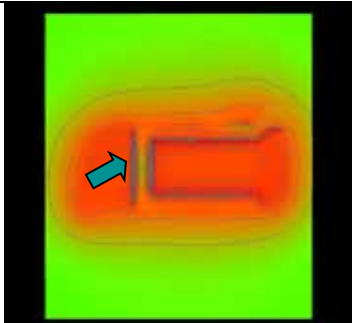
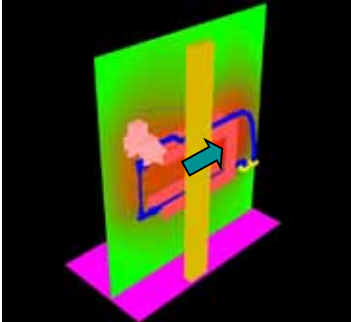
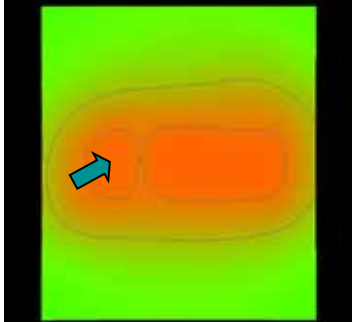
		Simulation and model	Field distribution Plan view	Legend/peak value $H_{max}^*)$
Simulation plane	Horizontal 1,000 mm above ground level			<ul style="list-style-type: none"> 120 000 kA/m 37 940 kA/m 12 000 kA/m 3 794 kA/m 1 200 000 A/m 379 400 A/m 100 000 A/m 37 940 A/m 12 000 A/m 3 794 A/m 1 200 A/m <p>$H_{max} = 127 \text{ kA/m}$</p>
	Vertically at the spot-welding gun			<ul style="list-style-type: none"> 50 000 kA/m 15 820 kA/m 5 000 kA/m 1 582 kA/m 500 000 A/m 158 200 A/m 50 000 A/m 15 820 A/m 5 000 A/m 1 582 A/m 500 000 mA/m <p>$H_{max} = 49 \text{ kA/m}$</p>
	Vertically 200 mm from the spot-welding gun			<ul style="list-style-type: none"> 10 000 kA/m 3 162 kA/m 1 000 kA/m 316 282 A/m 100 000 A/m 31 620 A/m 10 000 A/m 3 162 A/m 1 000 A/m 316 200 mA/m 100 000 mA/m <p>$H_{max} = 5.7 \text{ kA/m}$</p>

Figure 26: Results of the field calculation at the spot-welding gun with large gun window

		Simulation section and model	Field distribution Plan view	Legend/peak value H_{max} *)																																	
Simulation section	Horizontal 1,000 mm above the ground			 <table border="0"> <tr><td>50</td><td>000</td><td>kA/m</td></tr> <tr><td>15</td><td>820</td><td>kA/m</td></tr> <tr><td>5</td><td>000</td><td>kA/m</td></tr> <tr><td>1</td><td>582</td><td>kA/m</td></tr> <tr><td>500</td><td>000</td><td>A/m</td></tr> <tr><td>158</td><td>200</td><td>A/m</td></tr> <tr><td>50</td><td>000</td><td>A/m</td></tr> <tr><td>15</td><td>820</td><td>A/m</td></tr> <tr><td>5</td><td>000</td><td>A/m</td></tr> <tr><td>1</td><td>582</td><td>A/m</td></tr> <tr><td>500</td><td>000</td><td>mA/m</td></tr> </table> <p>$H_{max} = 48.92$ kA/m </p>	50	000	kA/m	15	820	kA/m	5	000	kA/m	1	582	kA/m	500	000	A/m	158	200	A/m	50	000	A/m	15	820	A/m	5	000	A/m	1	582	A/m	500	000	mA/m
	50	000	kA/m																																		
	15	820	kA/m																																		
5	000	kA/m																																			
1	582	kA/m																																			
500	000	A/m																																			
158	200	A/m																																			
50	000	A/m																																			
15	820	A/m																																			
5	000	A/m																																			
1	582	A/m																																			
500	000	mA/m																																			
	Vertically at the spot-welding gun			 <table border="0"> <tr><td>50</td><td>000</td><td>kA/m</td></tr> <tr><td>15</td><td>820</td><td>kA/m</td></tr> <tr><td>5</td><td>000</td><td>kA/m</td></tr> <tr><td>1</td><td>582</td><td>kA/m</td></tr> <tr><td>500</td><td>000</td><td>A/m</td></tr> <tr><td>158</td><td>200</td><td>A/m</td></tr> <tr><td>50</td><td>000</td><td>A/m</td></tr> <tr><td>15</td><td>820</td><td>A/m</td></tr> <tr><td>5</td><td>000</td><td>A/m</td></tr> <tr><td>1</td><td>582</td><td>A/m</td></tr> <tr><td>500</td><td>000</td><td>mA/m</td></tr> </table> <p>$H_{max} = 50.04$ kA/m </p>	50	000	kA/m	15	820	kA/m	5	000	kA/m	1	582	kA/m	500	000	A/m	158	200	A/m	50	000	A/m	15	820	A/m	5	000	A/m	1	582	A/m	500	000	mA/m
50	000	kA/m																																			
15	820	kA/m																																			
5	000	kA/m																																			
1	582	kA/m																																			
500	000	A/m																																			
158	200	A/m																																			
50	000	A/m																																			
15	820	A/m																																			
5	000	A/m																																			
1	582	A/m																																			
500	000	mA/m																																			
	Vertically 200 mm from the spot-welding gun			 <table border="0"> <tr><td>50</td><td>000</td><td>kA/m</td></tr> <tr><td>15</td><td>820</td><td>kA/m</td></tr> <tr><td>5</td><td>000</td><td>kA/m</td></tr> <tr><td>1</td><td>582</td><td>kA/m</td></tr> <tr><td>500</td><td>000</td><td>A/m</td></tr> <tr><td>158</td><td>200</td><td>A/m</td></tr> <tr><td>50</td><td>000</td><td>A/m</td></tr> <tr><td>15</td><td>820</td><td>A/m</td></tr> <tr><td>5</td><td>000</td><td>A/m</td></tr> <tr><td>1</td><td>582</td><td>A/m</td></tr> <tr><td>500</td><td>000</td><td>mA/m</td></tr> </table> <p>$H_{max} = 10.64$ kA/m </p>	50	000	kA/m	15	820	kA/m	5	000	kA/m	1	582	kA/m	500	000	A/m	158	200	A/m	50	000	A/m	15	820	A/m	5	000	A/m	1	582	A/m	500	000	mA/m
50	000	kA/m																																			
15	820	kA/m																																			
5	000	kA/m																																			
1	582	kA/m																																			
500	000	A/m																																			
158	200	A/m																																			
50	000	A/m																																			
15	820	A/m																																			
5	000	A/m																																			
1	582	A/m																																			
500	000	mA/m																																			

*) Field strengths of each colour graduation; H_{max} = calculated peak value of the magnetic field strength

The variation in the magnetic field strength is graded by colour in the individual images. The graduation runs from red through yellow and green to blue. Red in this context stands for high, blue for low magnetic field strength. For calculation of the magnetic flux density (B), all field strength values must be multiplied by the magnetic field constant $\mu_0 = 1.256 \times 10^{-6}$ Vs/Am.

As in the laboratory measurements, high local magnetic field strengths occur only in the proximity of the current-carrying cables (welding cables) and on the electrode arms/welding electrodes of the spot-welding gun. On the spot-welding gun with small gun window, a maximum value of 127 kA/m (Figure 25) was obtained in the calculations for the magnetic field strength in the horizontal simulation section; this corresponds to a

magnetic flux density of approximately 160 mT. The field distribution shows that this value occurs at the welding electrodes in the proximity of the welding point. Owing to the dimensions of the welding electrode, the electrode diameter and therefore the effective length of the magnetic field lines are at their lowest here, with the result that the magnetic field strength H assumes its highest value:

$$H = \frac{I}{\ell}$$

where:

H	magnetic field strength
I	current in the electrodes
ℓ	length of the field lines at the welding electrode

The variation of the field exhibits strong changes in the immediate vicinity of the spot-welding gun. In the proximity of the welding electrodes, electrode arms and welding cables in particular, the distance between field line pairs is very small. Above a distance of 200 mm from the axis of symmetry of the spot-welding gun (centre of the model), the rate of field reduction flattens out.

Figure 25 shows the variations of the magnetic field in the proximity of the spot-welding gun and the welding cables for the "at the spot-welding gun" and "200 mm from the spot-welding gun" vertical simulation sections. In these sections too, the magnetic field is seen to be localized. On the "vertically at the spot-welding gun" simulation section – the actual distance from the centre of the gun window is 45 mm – the variation of the magnetic field shows that the highest value of the magnetic field strength lies at the centre of the spot-welding gun and between the welding cables. The highest value of the field strength in the centre of the gun window is 49 kA/m (61 mT). It is thus lower by a factor of 2.5 than at the electrodes of the spot-welding gun. From the highest value, the magnetic field strength decreases in all directions with increasing distance; the exception is the field strength variation between the welding cables.

In Figure 25, the field variations in the vertical "200 mm from the spot-welding gun" simulation section show the calculated magnetic field strength for a vertical section 200 mm from the axis of symmetry of the spot-welding gun. The maximum magnetic field strength of 5.7 kA/m is once again to be found in the centre of the gun window. The magnetic field strength has decreased more than 20 times as much as the maximum value at the electrodes (127 kA/m).

Table 5:

Calculated and measured magnetic flux densities at the spot-welding gun with small gun window for the point „Hj“

Position in the laboratory measurements	Distance from the axis of symmetry of the spot-welding gun, in mm	Magnetic flux density, in mT Determined by:	
		Field simulation	Measurement
10	0	61.5	-
9	100	27.3	31.6
8	200	7.2	8.7
7	300	1.9	3.6
6	400	1.1	2.0
5	500	0.6	2.4
4	600	0.6	1.0

The field distributions in Figure 25 also show that with increasing distance, the field strength drops very quickly from its maximum value. To illustrate this relationship, the field strength and the maximum distance in millimetres measured from the centre of the gun window are stated for the field line at the transition from yellow to green in the field distributions shown in Figure 25.

Table 5 compares the magnetic flux densities measured at positions 4 to 10 at the measurement point „Hj“ (Figure 16, top) with the values calculated in the field simulation.

Figure 26 shows the field distributions for the spot-welding gun with large gun window. They reveal high magnetic field strengths on the electrodes, electrode arms and spot-welding gun chassis. The highest magnetic field strength is observed on the welding cables (see Figure 26, „horizontal 1000 mm above the ground“ simulation section). The highest value is around 50 kA/m (approx. 63 mT). In the region of the gun window, the field strengths are substantially lower, with values of between 5 and 15 kA/m.

The influence of the aluminium frame upon the field variation can also be seen. High field changes occur here at the edges which distort the field variation at the spot-welding gun. The field strengths are approximately as high as those on the welding cable and on the welding electrodes.

Table 6 compares the magnetic flux densities measured at measurement point „lj“ (Figure 16, bottom) at positions 4 to 10 (measurement column) and the corresponding values from the field simulation.

Table 6:
Calculated and measured magnetic flux densities at the spot-welding gun with large gun window for the point „Jj“

Position in the laboratory measurements	Distance from the axis of symmetry of the spot-welding gun, in mm	Magnetic flux density, in mT Determined by:	
		Field simulation	Measurement
10	0	36	35
9	100	22.7	19.2
8	200	13.4	15.9
7	300	8.3	11.2
6	400	5.1	8.1
5	500	3.6	5.6
4	600	3.0	3.9

7.6 Conclusions

The comparison of the magnetic flux densities shown in Tables 5 and 6 and the comparison of the field distributions calculated from the measurements and from the field simulations (Figures 22 and 23, 25 and 26) show a high degree of correlation between the field variations and the magnetic flux densities.

The simulations and arrangements for the spot-welding gun are suitable for the exposure calculations. The EMPIRE program can be used to calculate the welder's actual exposure to a high degree of precision. The calculations of the body current densities can therefore be based upon real field conditions.

8 Project Step 4: calculation of the body-current densities

8.1 General

For calculation of the body-current densities in human tissue, a three-dimensional anatomical model of the human body was integrated into a field simulation model. The model developed in the Visible Human project of the Air Force Research Laboratory was used as the body model. This model contains more than 40 different tissue types, structured from anatomical perspectives, such as muscles, lung, brain, skin, bone, fat, eyes and blood, with a resolution per voxel of $[3 \times 3 \times 3] \text{ mm}^3$. The voxel size of the model is $x = 196$, $y = 114$ and $z = 626$ voxels. This corresponds to the following body model dimensions: shoulder width = 588 mm, body width = 342 mm, body height = 1,878 mm.

In order for typical work positions of a welder to be simulated, the working position of a welder was adopted for the body model in the simulations of the laboratory arrangement (Figure 24). Since this depends upon the welder's location, position of the welding equipment/gun window, dimensions of the welding equipment and the place of the welding cables, the influence of these variables was taken into account in the exposure models.

A distinction was therefore drawn in the exposure models between:

- The form taken by the spot-welding gun (small and large gun window)

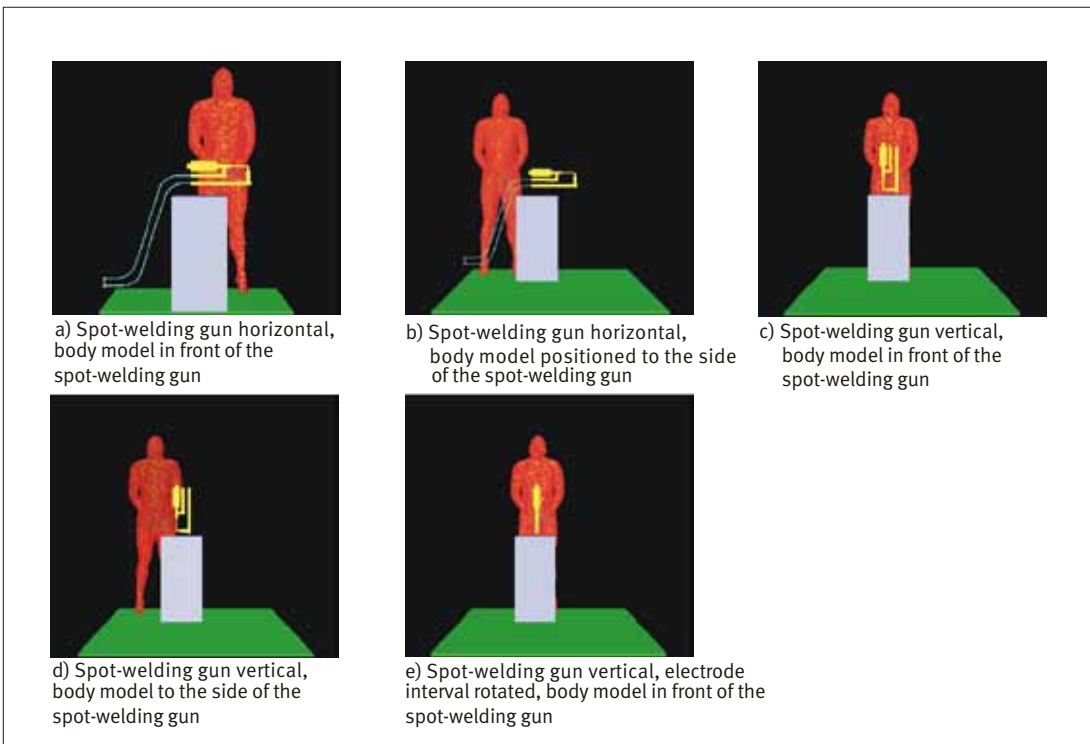
- The position of the spot-welding gun and of the gun window (horizontal, vertical)
- The position of a welder at the spot-welding gun (body model to the side or central with respect to the gun window)
- The distance between the body model and the spot-welding gun
- The place of the welding cables

The parameters determined in practice were used for all calculations of body current densities. The calculations were based upon a 50 Hz AC current without phase cut and with a peak value of $I = 10 \text{ kA}$. These values correspond to those from the field measurements in Project Step 2.

8.2 Exposure simulation

Figures 27 and 28 show the exposure simulations for different work scenarios on the spot-welding guns with small and large gun window. They simulate various work scenarios on the spot-welding gun. The body current densities were determined for five different working positions of a welder on the spot-welding gun with small gun window (see Figure 27).

Figure 27: Exposure simulations for work scenarios on the spot-welding gun with small gun window



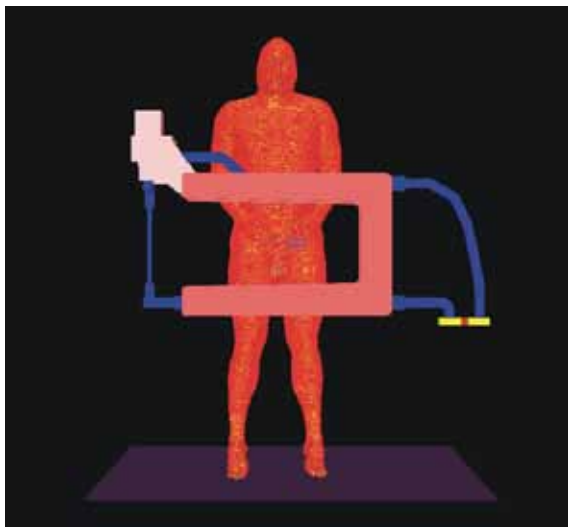
As can be seen in Figure 27 a) to d), the gun window of the spot-welding gun is positioned in front of the body model such that the main orientation of the magnetic flux impacts upon the front of the body model. In the simulation model shown in Figure 27 e), the gun window is rotated through 90°; the main orientation of the magnetic flux therefore runs parallel to the front of the body model. The influence of the welding cables upon the exposure was considered only in the exposure simulations with the spot-welding gun in the horizontal arrangement: see Figure 27 a) and 27 b). Both are simulations of the laboratory arrangement used in the studies conducted in Project Step 2.

On the spot-welding gun with large gun window, the exposure was calculated only for one working position in the centre of the

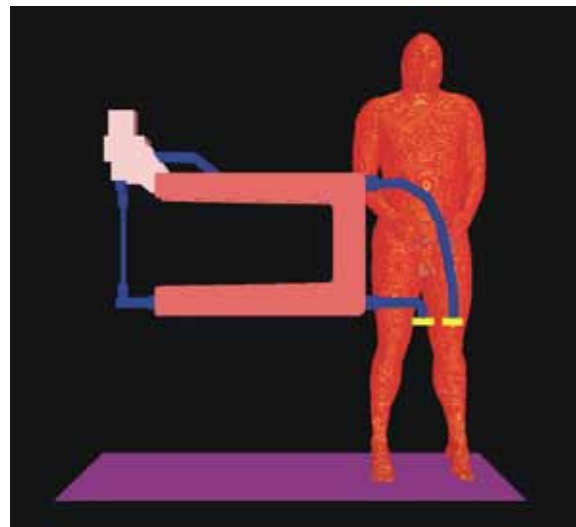
gun window and one position close to the forward conductor of the welding cable (Figure 28).

For the work scenarios in Figures 27 and 28, the body-current densities in the body model were calculated for different distances between the body model and the gun window: for the exposure model with the spot-welding gun with small gun window, at 0, 200 and 400 mm; for the spot-welding gun with large gun window, at 0, 200, 400 and 600 mm. Figures 29 and 30 show, for each simulated work scenario, a plan view of the exposure simulations for which body current densities were calculated. The images show the simulation space, the simulated instrumentation and study arrangement, the spot-welding gun, the place of the welding cable, and the various locations of the body model.

Figure 28:
Exposure simulations for two typical work scenarios on the spot-welding gun with large gun window



a) Spot-welding gun horizontal, body model central in front of the spot-welding gun



b) Spot-welding gun horizontal, body model to the side of the spot-welding gun

Figure 29:
Schematic diagram of the five different work scenarios for the spot-welding gun with small gun window

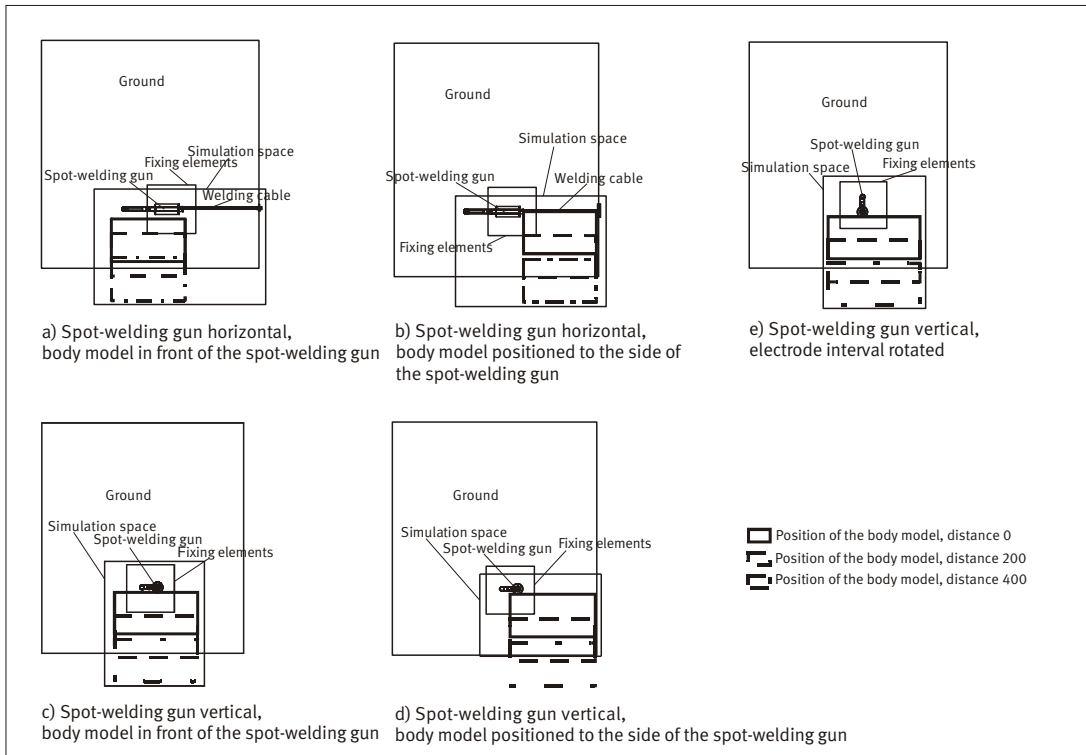
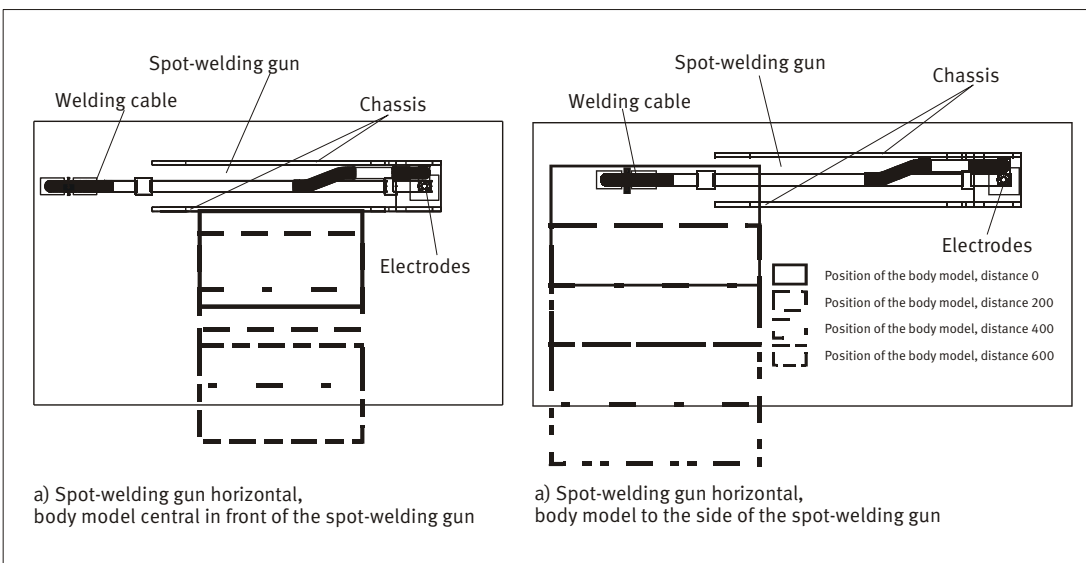


Figure 30:
Schematic diagram showing two typical work scenarios on the spot-welding gun with large gun window

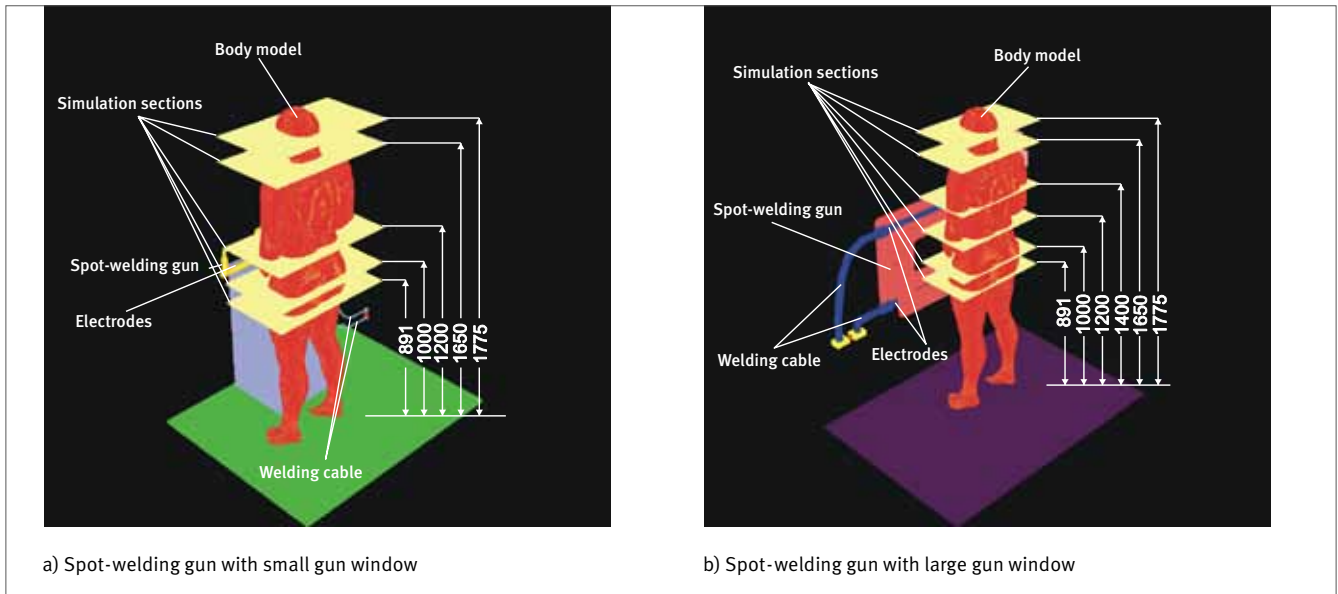


8.3 Simulation sections

Owing to the high computing overhead, the distribution of the body current densities over the body height was not calculated with the same resolution in all cases. Calculations with high resolution, corresponding to the voxel size of the body model, were performed as shown in Figure 31 in five/six simulation sections. Measured from ground level, these sections were at

heights of 891, 1,000, 1,200, 1,400, 1,650 and 1,775 mm. The heights of these sections were selected such that the distributions of the body current densities could be determined in the genital area (891 mm), the trunk (1,000, 1,200 and 1,400 mm), the neck (1,650 mm) and the head/brain (1,775 mm). Figure 31 shows the relationships and locations of these sections in the body model.

Figure 31: Simulation sections in the body model for determining the body current density



8.4 Cable influences

The influence exerted by the welding cables was studied with reference to several simple exposure simulations (Figure 32, Page 62). A double cable with forward and return line with a diameter of 10 cm and a distance of 10 mm between the cables was arranged for this purpose in the longitudinal axis of the body model in front of the chest and on the back directly over the spinal canal at a distance of 10 mm from the surface of the body model. Figure 32 shows the arrangement of the body model and the two conductors, and the simulation sections.

In addition, the exposure caused by welding cables was determined in a body model for two particular cable routings (Figure 33).

Figure 33 shows, on the left, the simulation with cable routing to prEN 50444; on the right, with cable routing to Figure 22 of BGI 5011. For all cable routings in Figures 32 and 33, the body current densities in the body model were determined in two simulation sections, namely those at 1,200 and 1,775 mm.

Figure 32: Exposure simulation for study of the exposure caused by welding cables. Left: welding cable with forward and return line in front of the chest of the body model; right: welding cable with forward and return line on the back of the model

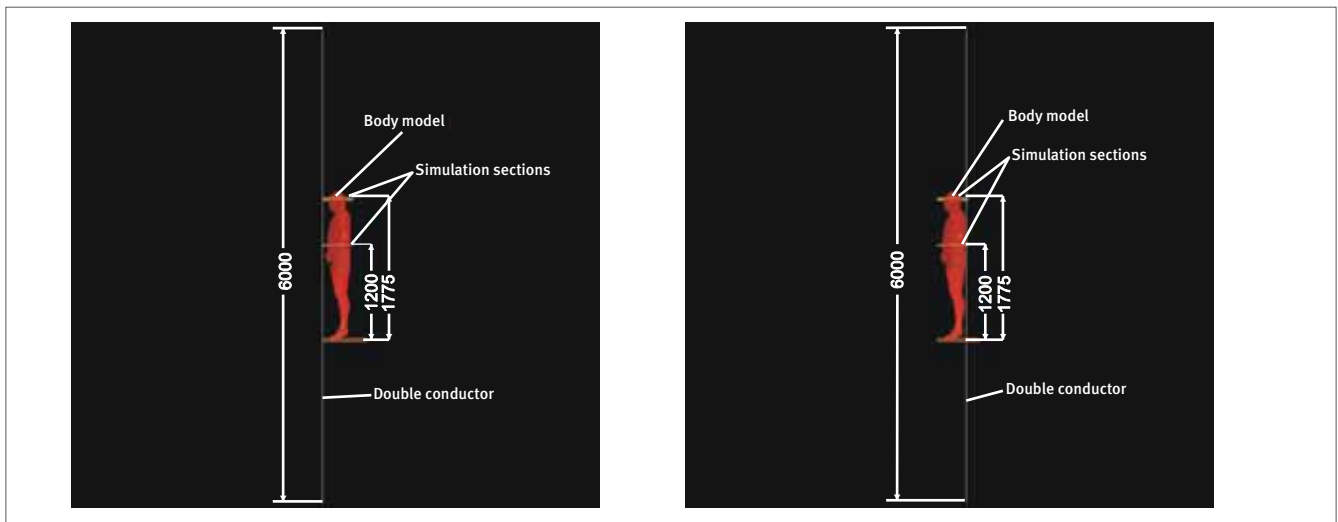
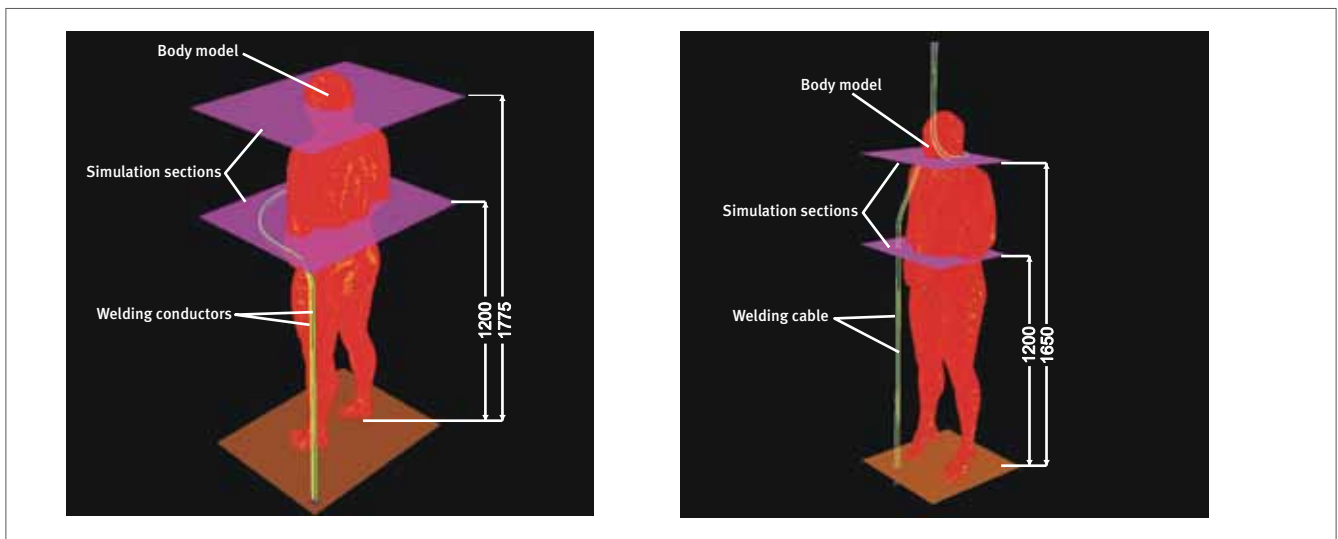


Figure 33:
Exposure simulation for study of the exposure caused by welding cables with particular cable routing.
Left: welding cable to prEN 50444; right: welding cable to BGI 5011, Figure 22



8.5 Results

The calculated body current densities are shown in Figures 34 and 43 (see Page 65 ff.) for the various exposure simulations of the two spot-welding guns and cable routings. The figures contain series of images with sectional views. Each sectional view refers to a distance and a simulation section corresponding to the location of the body model. Each image shows the distributions of the body current densities in a body model on a transverse section for a particular section height which corresponds to the distance between the simulation section and the ground (see Figures 31 to 33).

The variations of the body current densities in the sectional views are graduated in colour from red, through green, to blue. Red and blue stand in this case for high and low body current densities respectively (refer also to the legend for Figures 34 to 43). The calculated peak value of the body current density is also shown on the right of each sectional view.

8.5.1 Spot-welding gun with small gun window

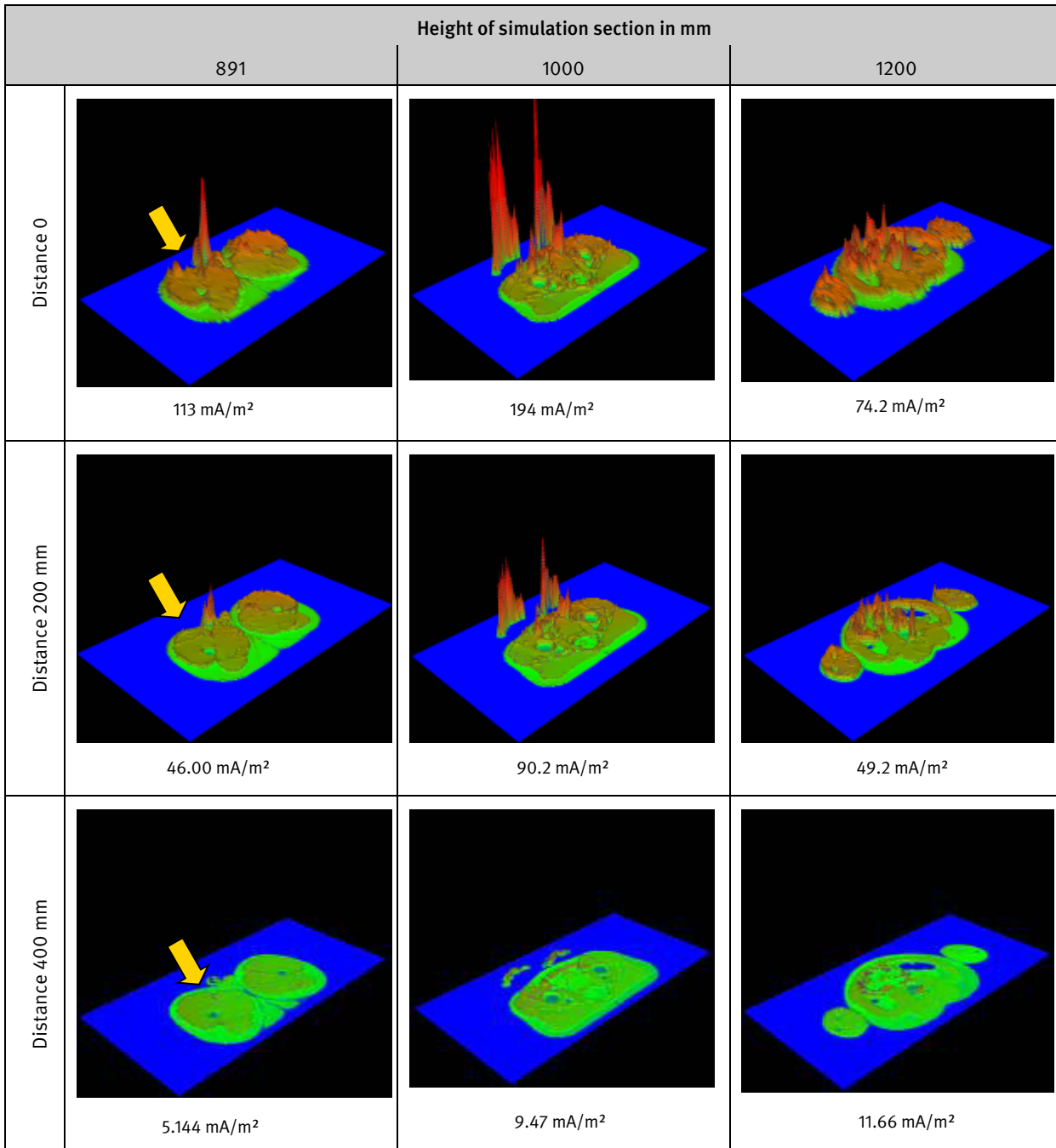
All sectional views in Figures 34 to 38 exhibit an inhomogeneous variation of the tissue current density, with peaks and troughs. Different variations and values of the current density occur in

each exposure model studied and in each simulation section, even within the body model (genital region, trunk, neck and head/brain). For example, high current densities in the 1,000 mm simulation section do not result in the same in the adjacent simulation section, for example that at 1,200 mm. This can be seen for example from Figures 34 and 35.

It can also be seen that the highest current densities in the body model do not generally occur in the tissue layers opposite the spot-welding gun. Depending upon the distance from the body model, the current densities in the neck and head may be higher than those in the trunk area, which is located in front of the welding equipment. Differences in the variation and level of the tissue current density also depend upon the size and position of the spot-welding gun and upon the position of the body model.

The exposure models studied are similar only in terms of the variation of the current density values as a function of the distance of the body model from the spot-welding gun: the sectional views of the different simulation sections show that the current densities (including the peak values) decrease with increasing distance. For the distance of 400 mm, Figures 34 to 38 show almost identical current density variations and, with the exception of Figure 35, identical current density values.

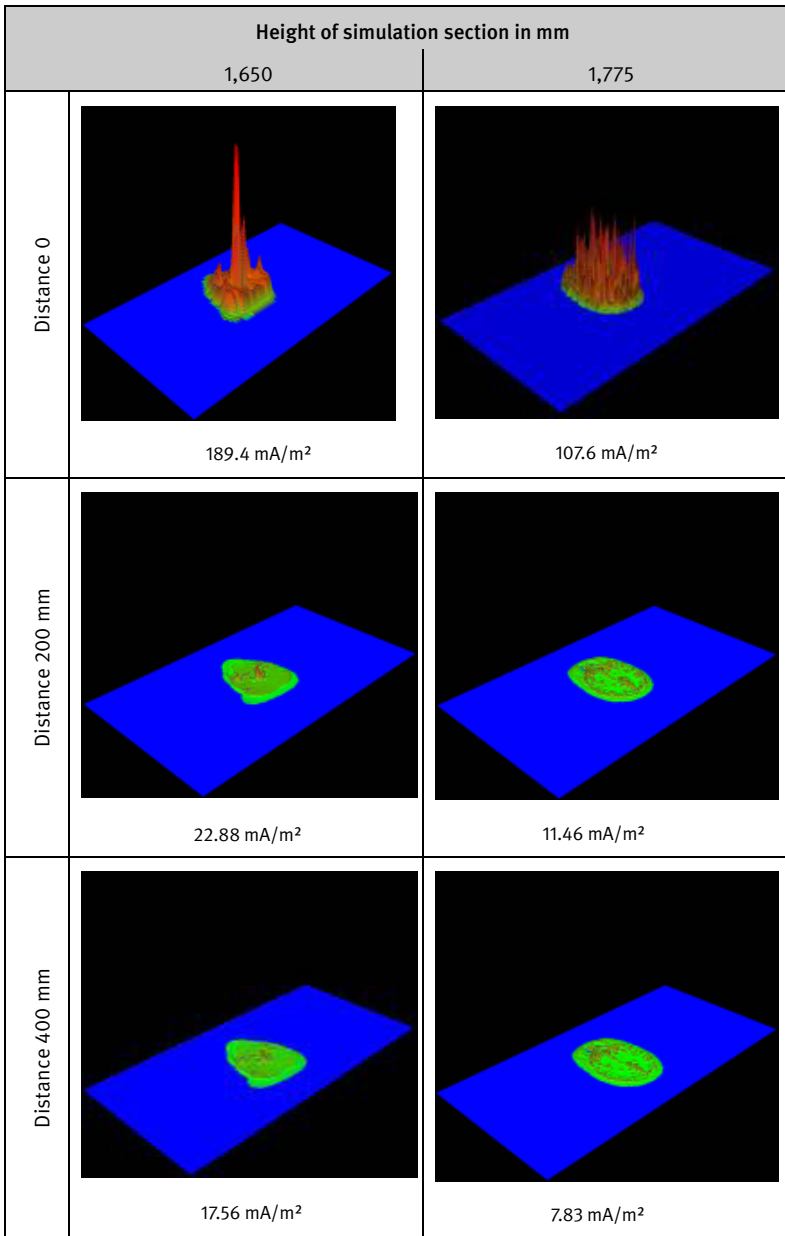
Figure 34:
Body current densities calculated for the spot-welding gun with small gun window,
spot-welding gun horizontal, body model in front of the spot-welding gun



Legend:

	100.000 mA/m ²		3.162 mA/m ²		100.000 μA/m ²		3.162 μA/m ²
	36.620 mA/m ²		1.000 mA/m ²		31.620 μA/m ²		1.000 μA/m ²
	10.000 mA/m ²		316.200 μA/m ²		10.000 μA/m ²		

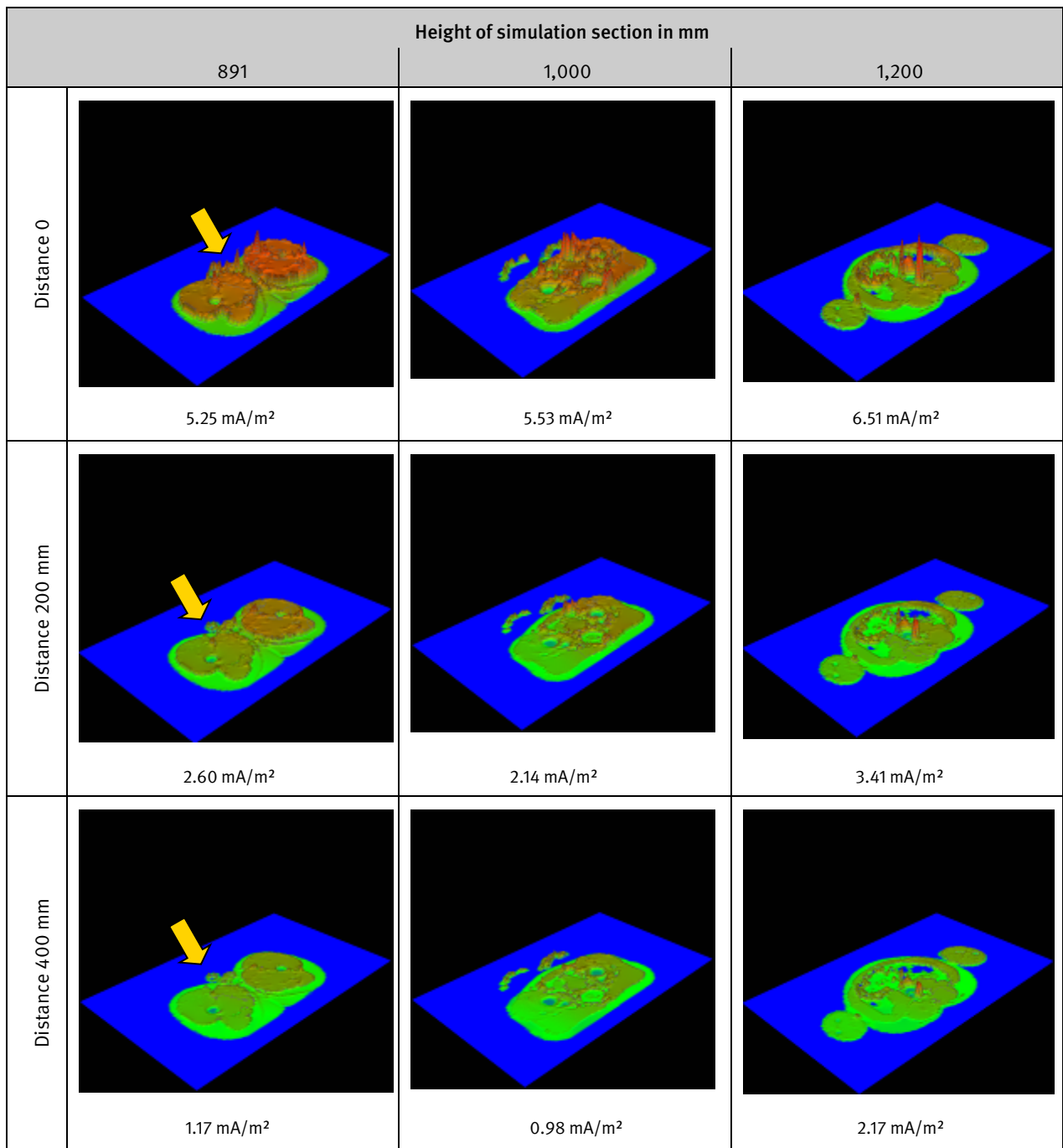
Figure 34: continued



Legend:

	100.000 mA/m ²		3.162 mA/m ²		100.000 μA/m ²		3.162 μA/m ²
	36.620 mA/m ²		1.000 mA/m ²		31.620 μA/m ²		1.000 μA/m ²
	10.000 mA/m ²		316.200 μA/m ²		10.000 μA/m ²		

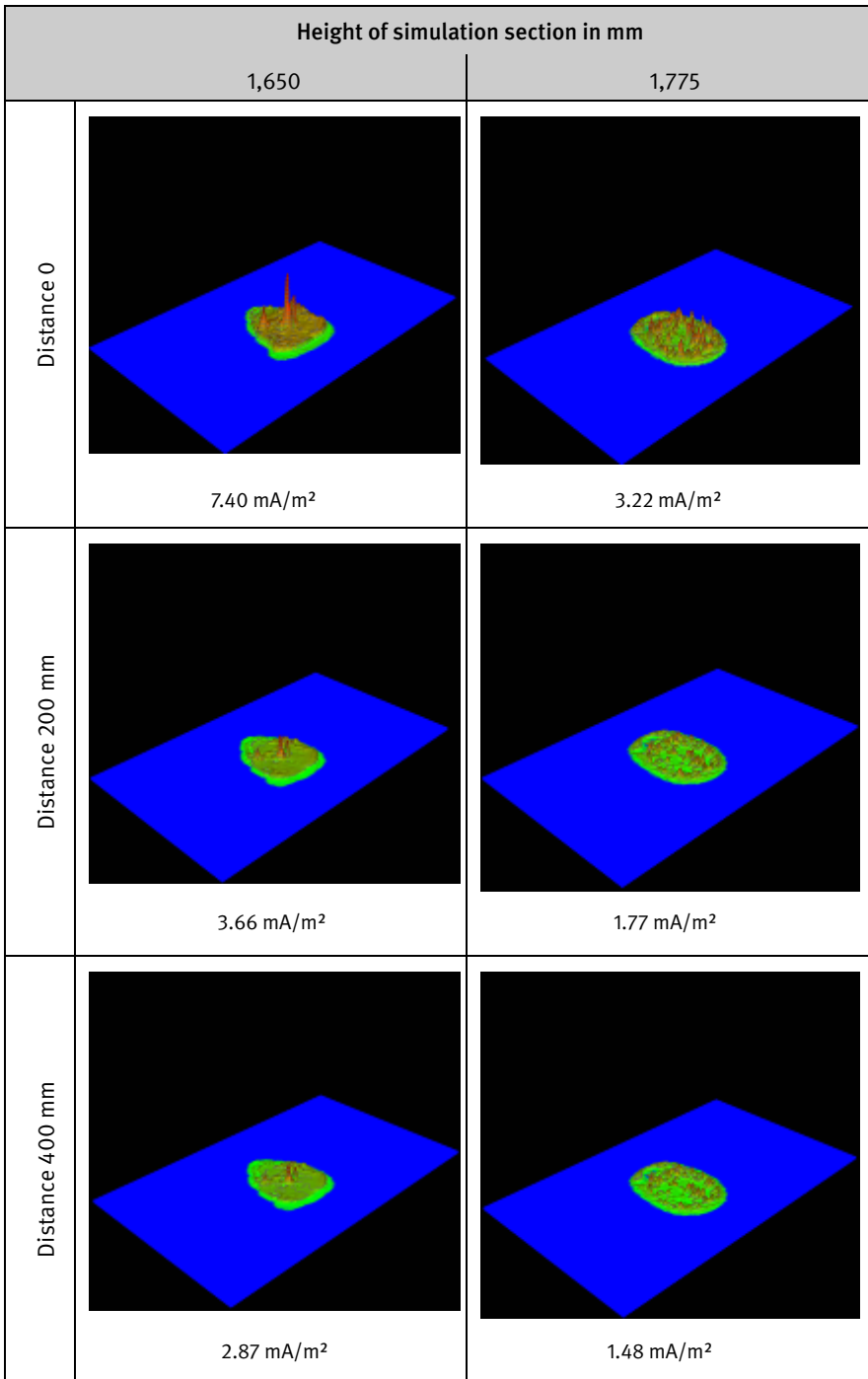
Figure 35:
Body current densities calculated for the spot-welding gun with small gun window,
spot-welding gun horizontal, body model to the side of the spot-welding gun



Legend:

	10.000 mA/m ²		316.200 μA/m ²		10.000 μA/m ²		316.200 nA/m ²
	3.162 mA/m ²		100.000 μA/m ²		3.162 μA/m ²		100.000 nA/m ²
	1.000 mA/m ²		31.620 μA/m ²		1.000 μA/m ²		

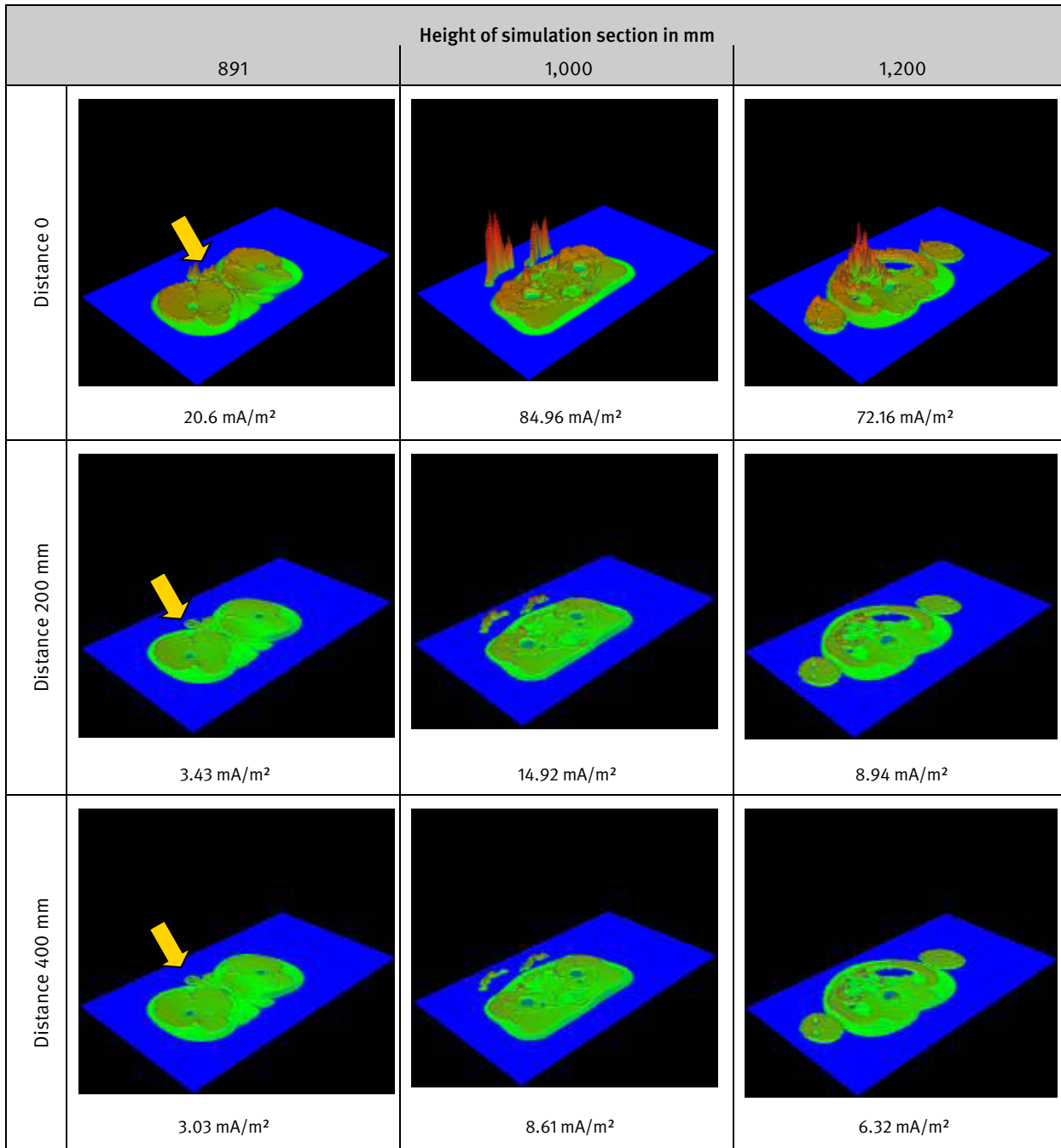
Figure 35: continued



Legend:

	10.000 mA/m ²		316.200 μA/m ²		10.000 μA/m ²		316.200 nA/m ²
	3.162 mA/m ²		100.000 μA/m ²		3.162 μA/m ²		100.000 μA/m ²
	1.000 mA/m ²		31.620 μA/m ²		1.000 μA/m ²		

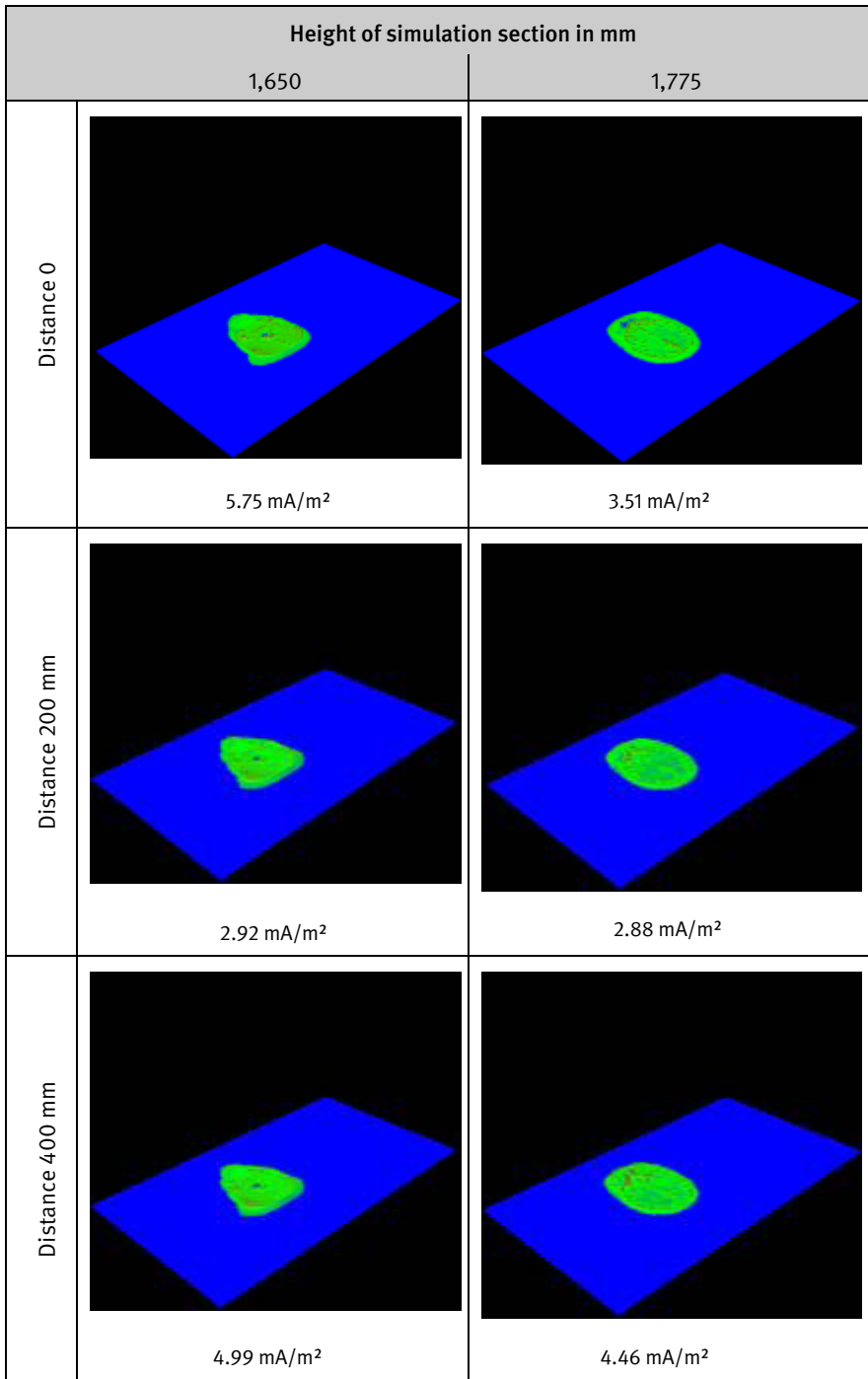
Figure 36:
Body current densities calculated for the spot-welding gun with small gun window,
spot-welding gun vertical, body model in front of the spot-welding gun



Legend:

	100.000 mA/m ²		3.162 mA/m ²		100.000 μA/m ²		3.162 μA/m ²
	36.620 mA/m ²		1.000 mA/m ²		31.620 μA/m ²		1.000 μA/m ²
	10.000 mA/m ²		316.200 μA/m ²		10.000 μA/m ²		

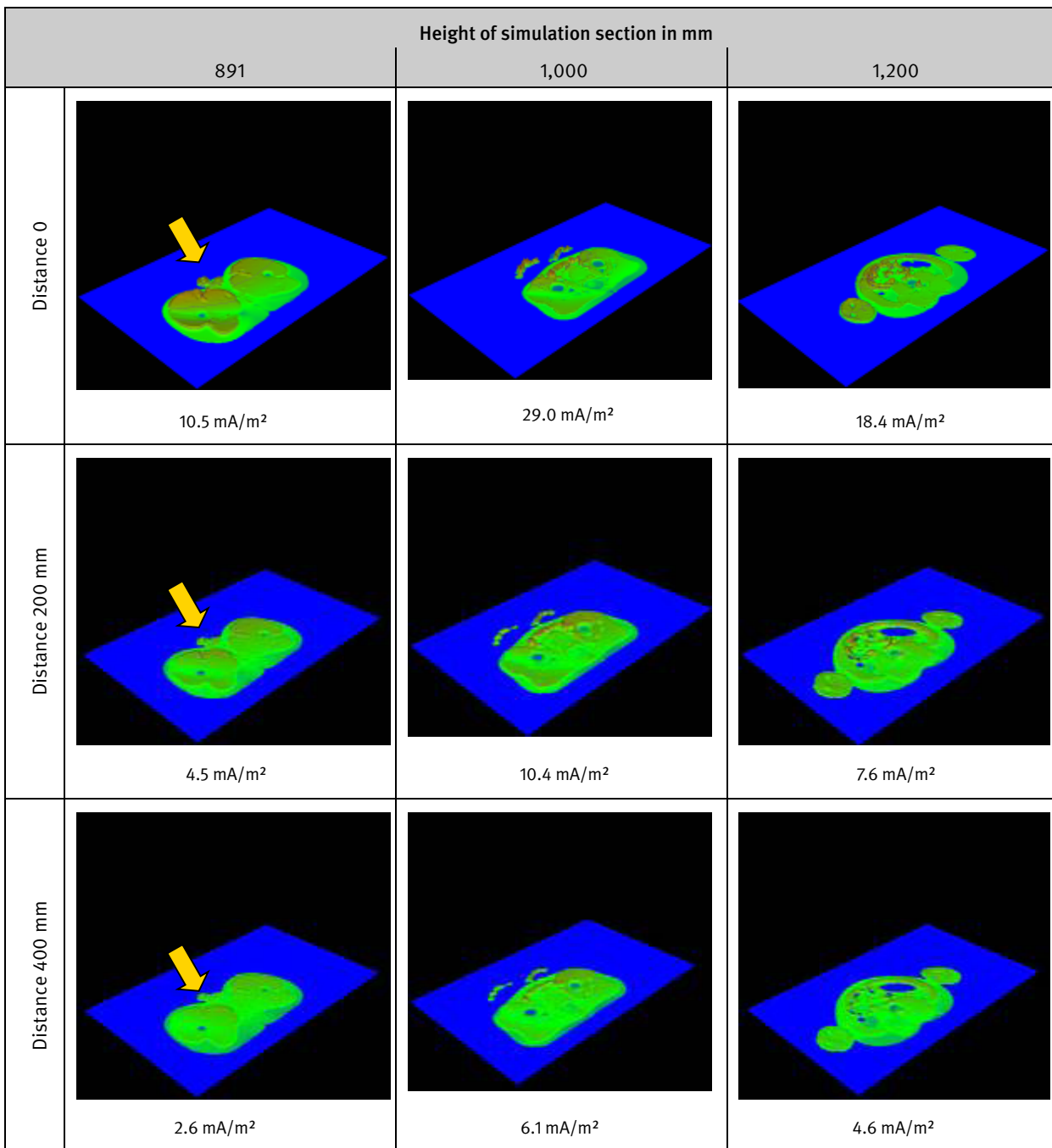
Figure 36: continued



Legend:

	100.000 mA/m ²		3.162 mA/m ²		100.000 μA/m ²		3.162 μA/m ²
	36.620 mA/m ²		1.000 mA/m ²		31.620 μA/m ²		1.000 μA/m ²
	10.000 mA/m ²		316.200 μA/m ²		10.000 μA/m ²		

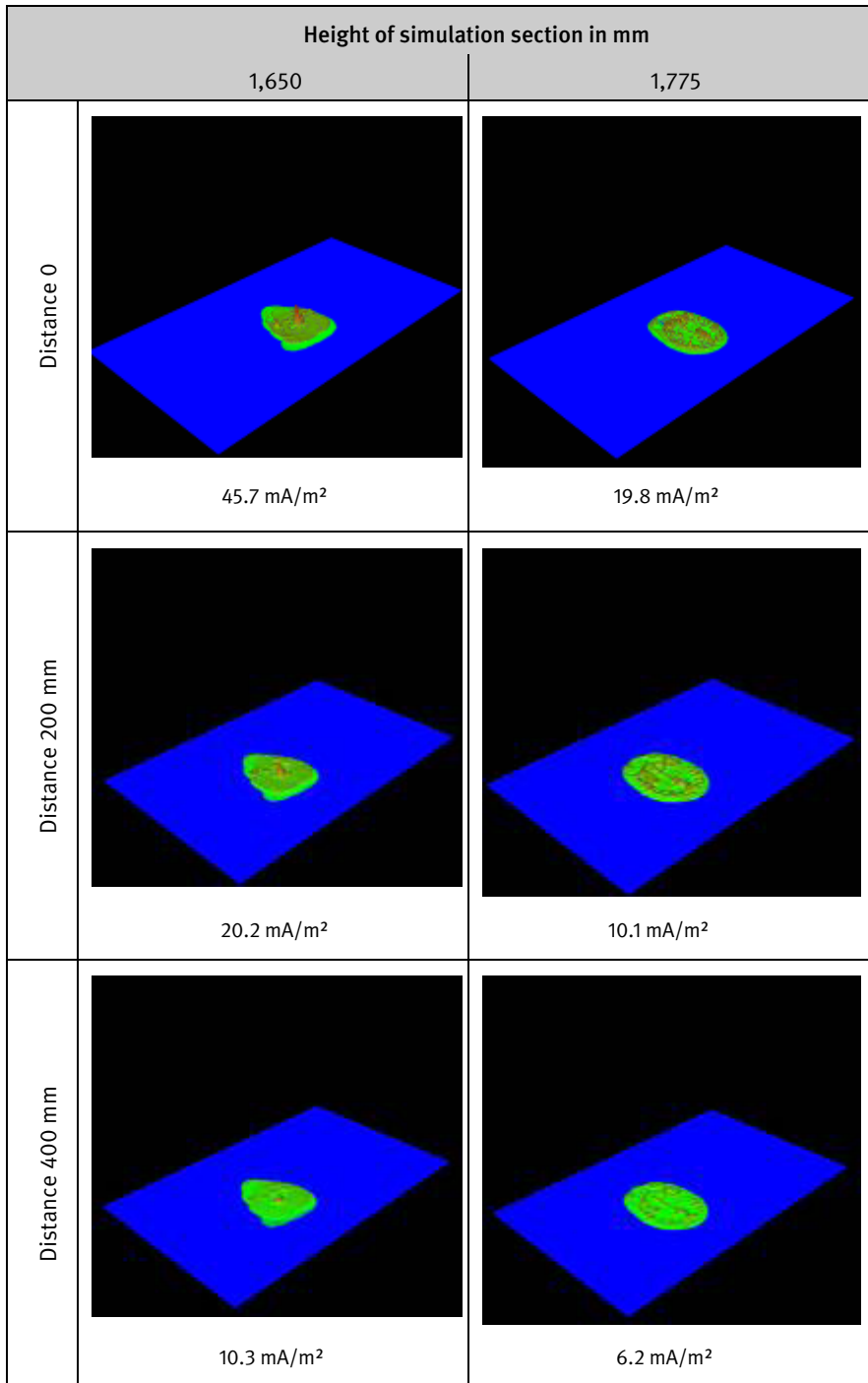
Figure 37:
Body current densities calculated for the spot-welding gun with small gun window,
spot-welding gun vertical, body model to the side of the spot-welding gun



Legend:

	100.000 mA/m ²		3.162 mA/m ²		100.000 μA/m ²		3.162 μA/m ²
	36.620 mA/m ²		1.000 mA/m ²		31.620 μA/m ²		1.000 μA/m ²
	10.000 mA/m ²		316.200 μA/m ²		10.000 μA/m ²		

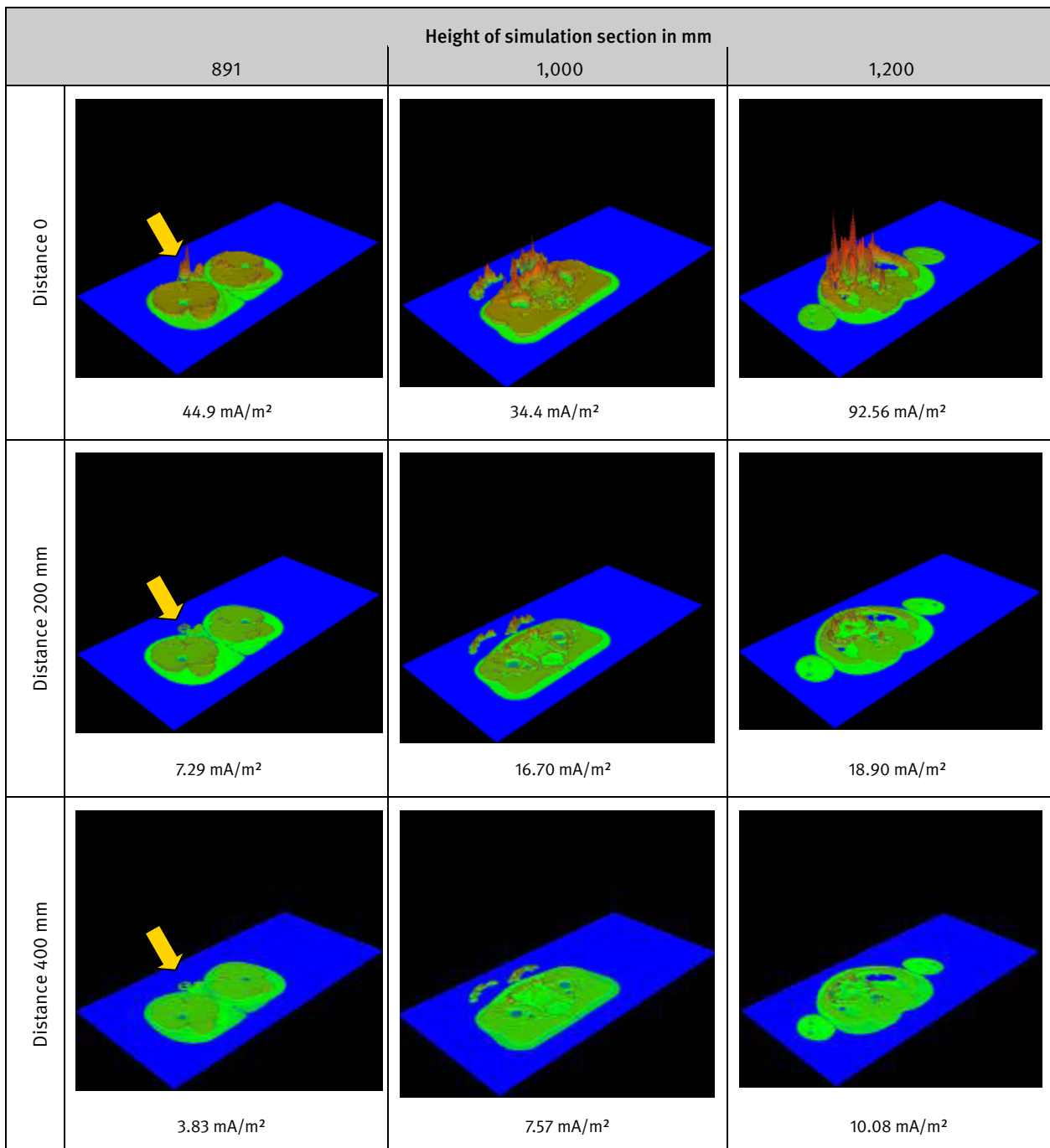
Figure 37: continued



Legend:

	100.000 mA/m ²		3.162 mA/m ²		100.000 μA/m ²		3.162 μA/m ²
	36.620 mA/m ²		1.000 mA/m ²		31.620 μA/m ²		1.000 μA/m ²
	10.000 mA/m ²		316.200 μA/m ²		10.000 μA/m ²		

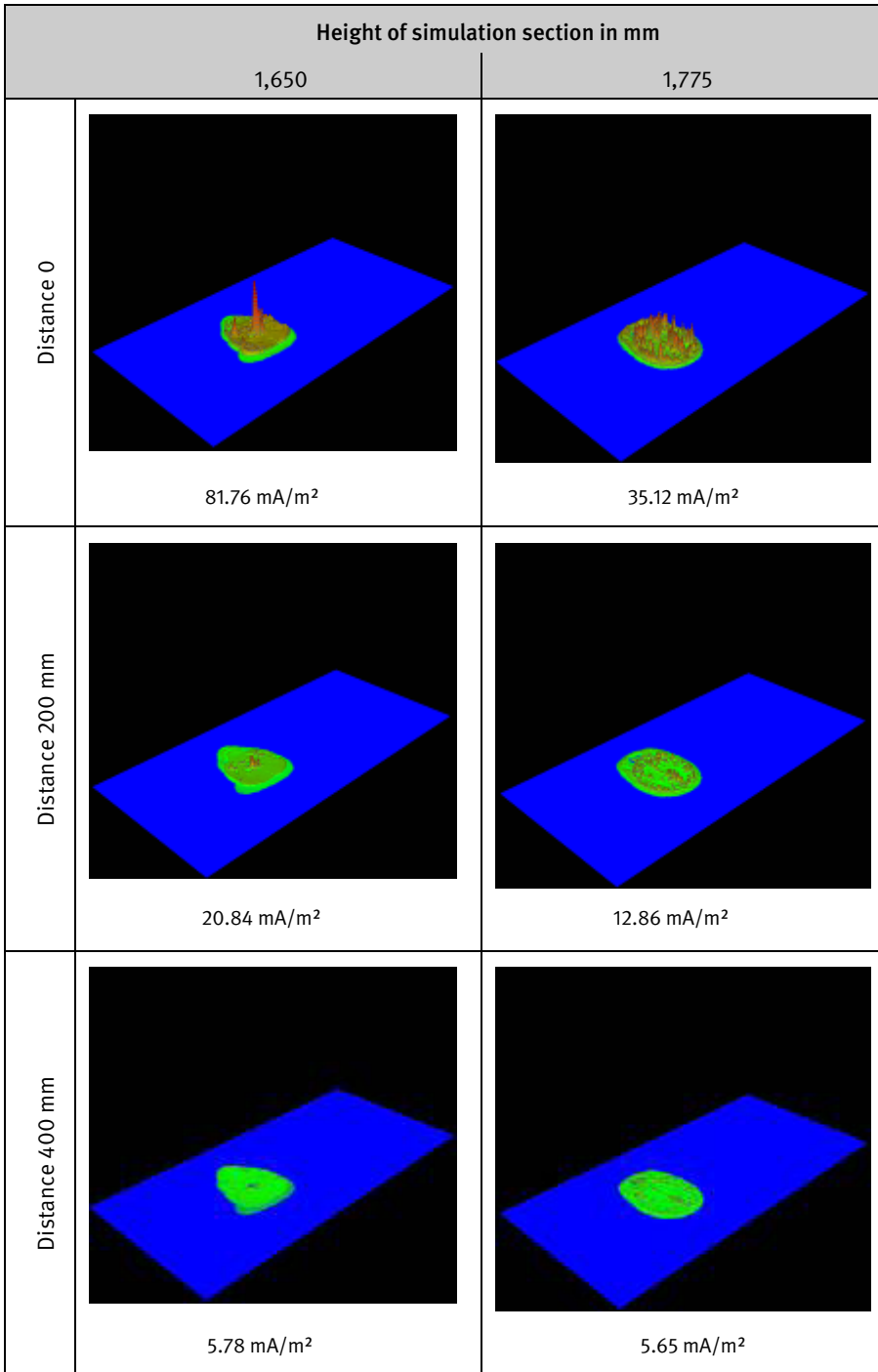
Figure 38:
Body current densities calculated for the spot-welding gun with small gun window,
spot-welding gun vertical, gun window rotated, body model in front of the spot-welding gun



Legend:

	100.000 mA/m ²		3.162 mA/m ²		100.000 μA/m ²		3.162 μA/m ²
	36.620 mA/m ²		1.000 mA/m ²		31.620 μA/m ²		1.000 μA/m ²
	10.000 mA/m ²		316.200 μA/m ²		10.000 μA/m ²		

Figure 38: continued



Legend:

	100.000 mA/m ²		3.162 mA/m ²		100.000 μA/m ²		3.162 μA/m ²
	36.620 mA/m ²		1.000 mA/m ²		31.620 μA/m ²		1.000 μA/m ²
	10.000 mA/m ²		316.200 μA/m ²		10.000 μA/m ²		

8.5.2 Spot-welding gun with small gun window, positioned horizontally

In this exposure model, the tissue current densities in the body models positioned to one side and centrally in front of the spot-welding gun differ fundamentally from each other (Figures 34 and 35). In the body model positioned to the side of the gun window (Figure 35), the current density can be seen to be distributed almost homogeneously, with low values and a pronounced peak value in the spinal region. In the body model positioned to the front (Figure 34), considerably higher current densities occur than in the body model positioned to the side. The distribution of the current density changes as a function of the distance between the body model and the gun window. At small distances from the gun window (0 and 200 mm), high current density peaks arise in the body model on the side facing the gun window up to the middle of the model. Only at greater distances between the body model and the gun window (approx. 400 mm) is the current density distribution comparable to that in the body model positioned to the side. The maximum tissue current densities in the body models positioned to the front and side are 194 mA/m^2 and 7.40 mA/m^2 respectively.

8.5.3 Spot-welding gun with small gun window, positioned vertically

In this exposure model too, the body current densities in the body models positioned to the side and front (Figures 36 and 37) differ fundamentally from each other. As with the spot-welding gun positioned horizontally, the body current densities in the body model positioned to the front are higher in the simulation sections facing the spot-welding gun than in the model positioned to the side. In the simulation sections for the neck and the head however, precisely the reverse is the case: high current densities occur in these parts of the body only in the body model positioned to the side. At a distance of 400 mm, the current density variations in the tissue of the body model positioned to the side and the front are once again almost identical. The calculated maximum value of the body current density is 84.96 mA/m^2 in the body model positioned to the front and 45.7 mA/m^2 in that positioned to the side.

8.5.4 Spot-welding gun with small gun window, positioned vertically rotated through 90°

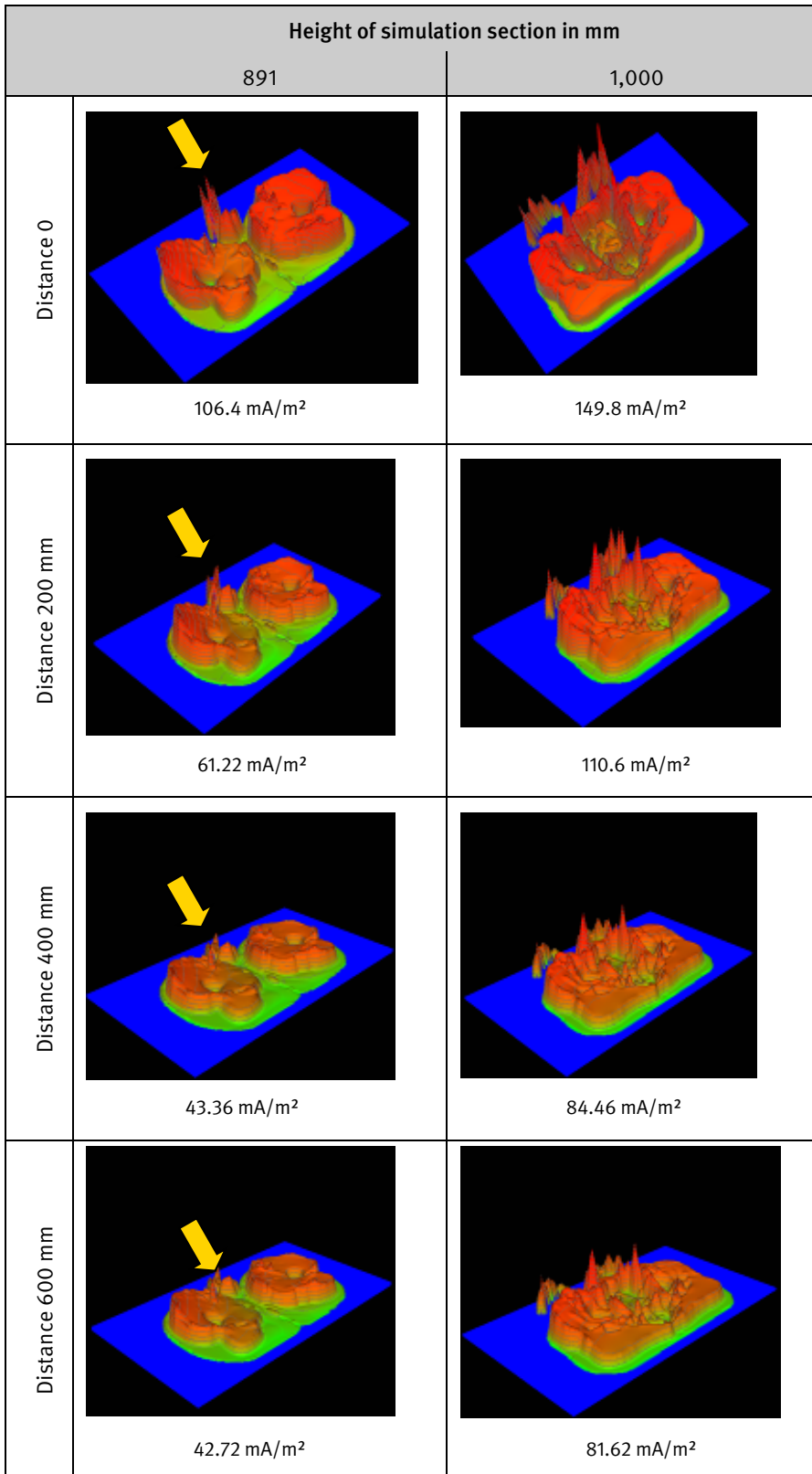
In the exposure model with a spot-welding gun positioned vertically and rotated through 90° (Figure 38), the current density variations in the sectional views are very similar to those shown in Figure 34. The values of the current density are however substantially lower. This does not apply to the current densities of the 1,200 mm simulation section calculated for a distance of 0 mm; the maximum value of the current density calculated for this exposure model is 92.56 mA/m^2 .

8.5.5 Spot-welding gun with large gun window

The variations of the tissue current density for the exposure models with the spot-welding gun with large gun window are shown in Figures 39 and 40.

The virtually identical colouring of the tissue structure on all sectional views is an indication of high current density values. Above the 1000 mm simulation section, pronounced current density peaks are observed in the centre of the body cross-section. In the 891, 1,000 and 1,200 mm simulation sections at a distance of 0, the current density values on the side of the body model facing the spot-welding gun are higher than on the side facing away from it. These current density peaks decrease more rapidly with increasing distance from the spot-welding gun than the current density values in other tissue areas. Upwards of a distance of approximately 400 mm, this behaviour can no longer be observed in the current density variation. The diagrams also show that the body current densities of the body model positioned in the centre of the gun window (Figure 40) exhibit higher values in the simulation sections below 1,400 mm than those in the body model positioned to the side (Figure 39): in the latter arrangement, the peak values of the body current density in the two simulation sections for the neck and the head are higher than those in the body model positioned in the centre of the gun window. The influence of the spot-welding gun chassis is evident from the variation of the body current densities in the sectional views of the other simulation sections. The current densities are higher than on the left-hand side of the image, irrespective of the distance. The maximum value of the calculated body current density is 222 mA/m^2 for both body model positions.

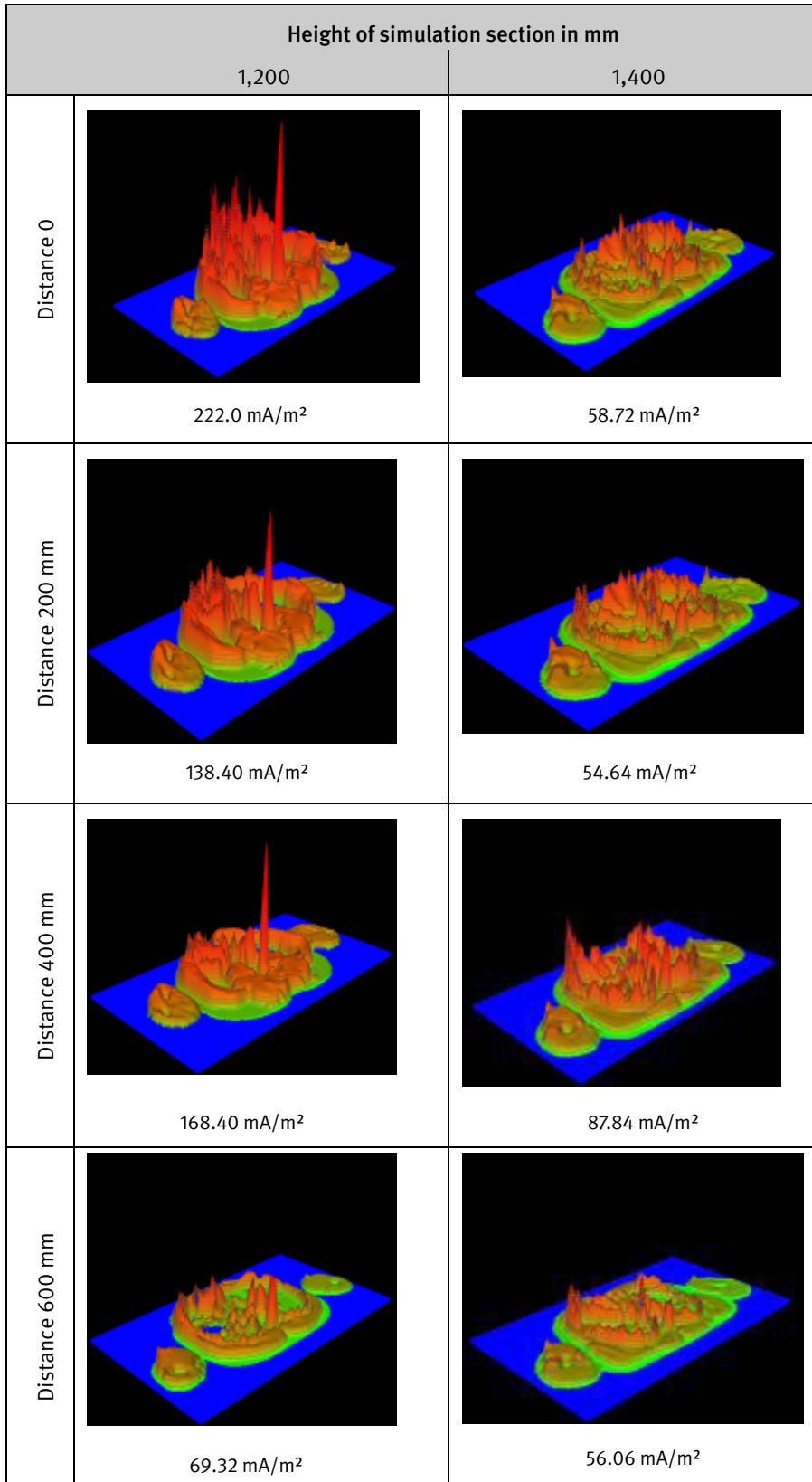
Figure 39:
Body current densities calculated for the spot-welding gun with large gun window,
spot-welding gun positioned horizontally, body model in the centre of the spot-welding gun



Legend:

	100.000 mA/m ²		3.162 mA/m ²		100.000 μA/m ²		3.162 μA/m ²
	36.620 mA/m ²		1.000 mA/m ²		31.620 μA/m ²		1.000 μA/m ²
	10.000 mA/m ²		316.200 μA/m ²		10.000 μA/m ²		

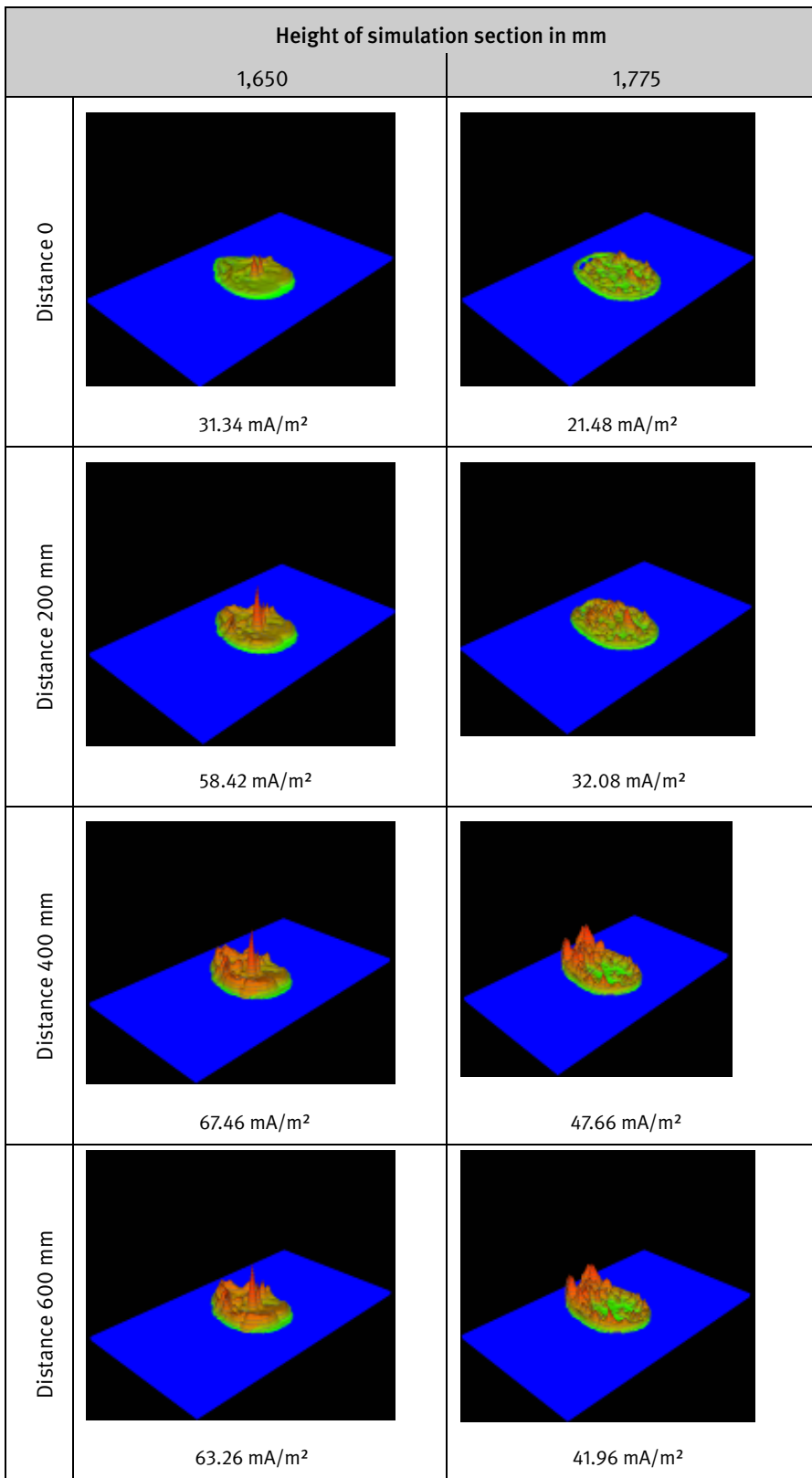
Figure 39: continued



Legend:

	100.000 mA/m ²		3.162 mA/m ²		100.000 μA/m ²		3.162 μA/m ²
	36.620 mA/m ²		1.000 mA/m ²		31.620 μA/m ²		1.000 μA/m ²
	10.000 mA/m ²		316.200 μA/m ²		10.000 μA/m ²		

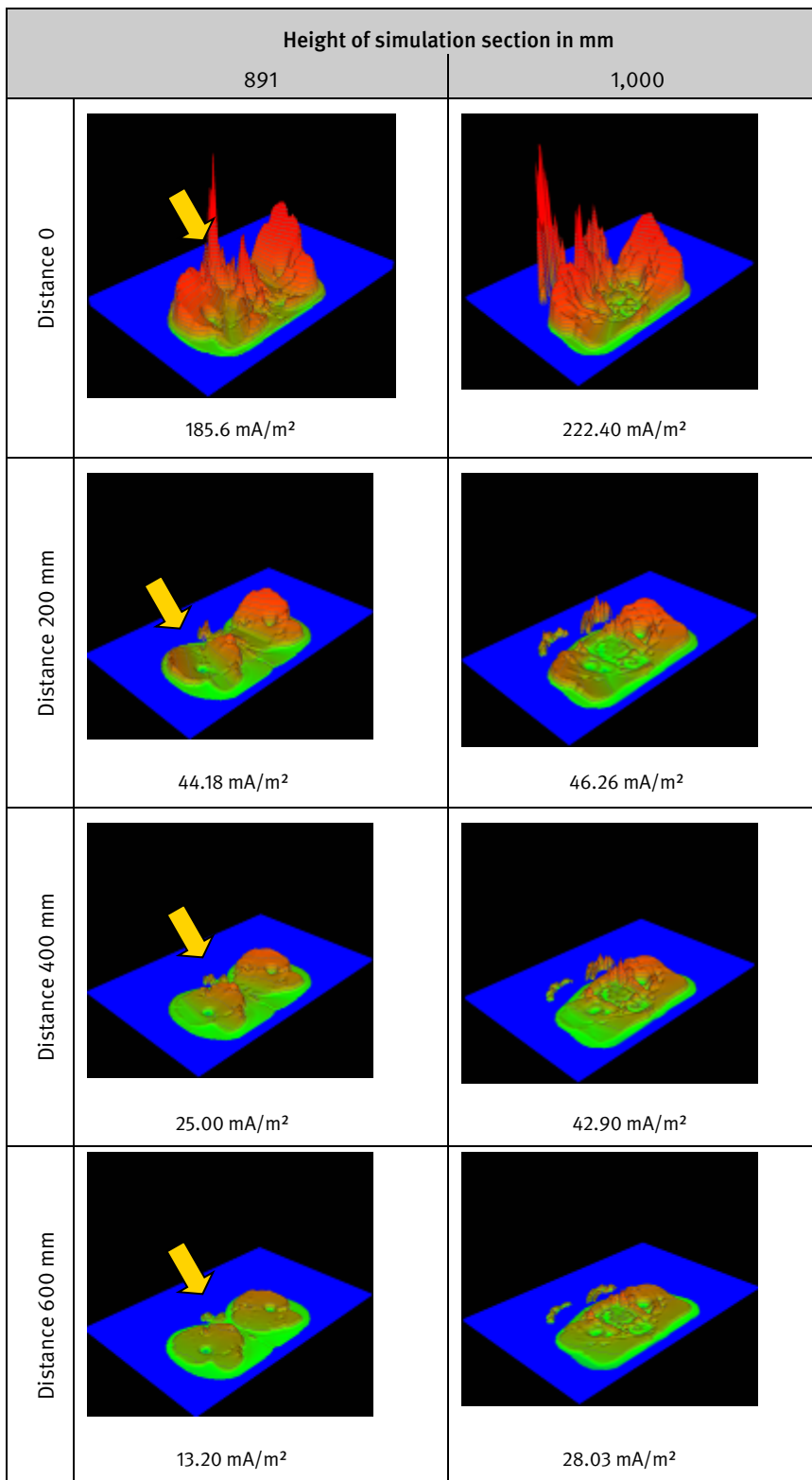
Figure 39: continued



Legend:

	100.000 mA/m ²		3.162 mA/m ²		100.000 μA/m ²		3.162 μA/m ²
	36.620 mA/m ²		1.000 mA/m ²		31.620 μA/m ²		1.000 μA/m ²
	10.000 mA/m ²		316.200 μA/m ²		10.000 μA/m ²		

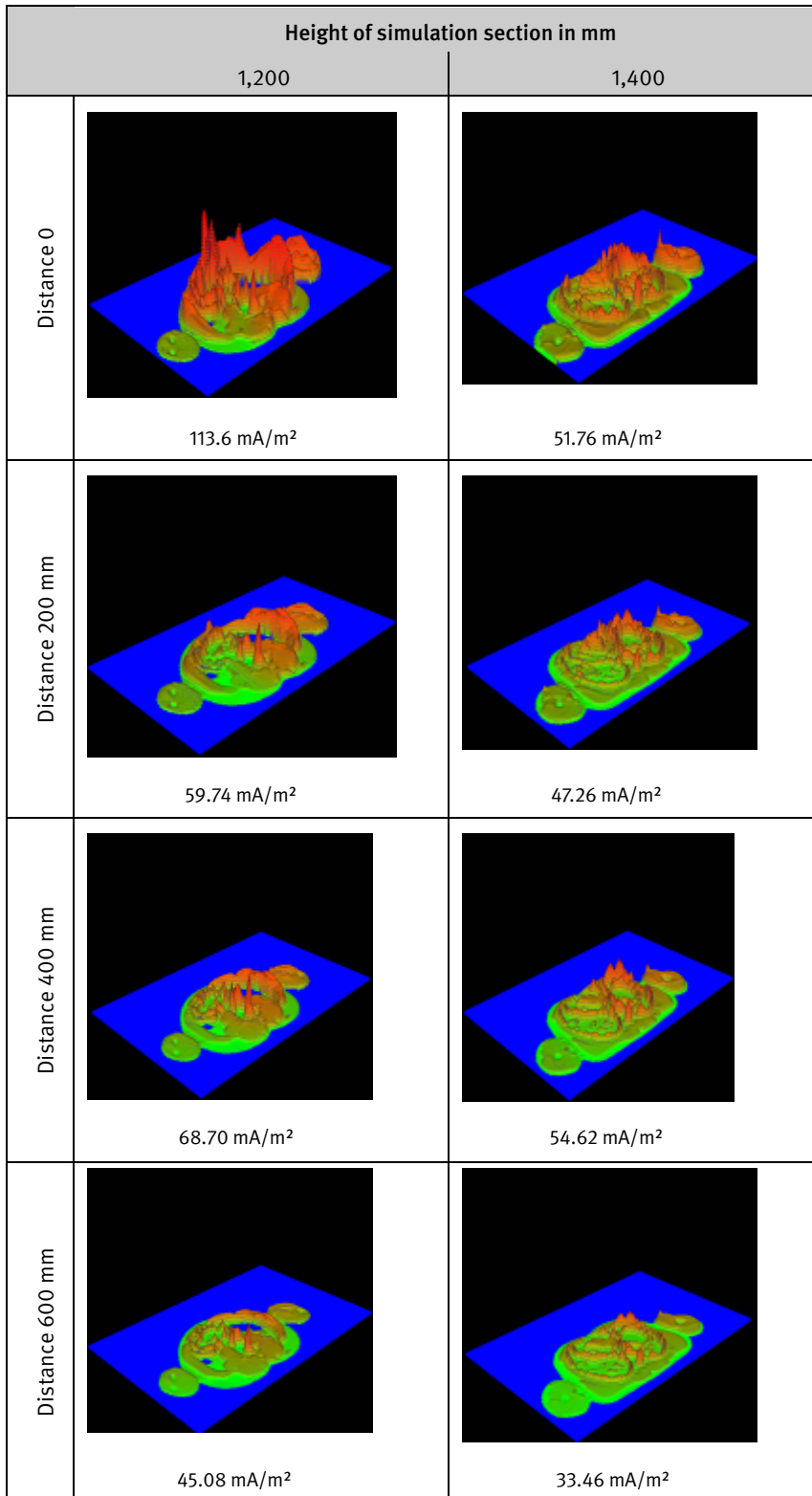
Figure 40:
Body current densities calculated for the spot-welding gun with large gun window,
spot-welding gun positioned horizontally, body model to the side of the spot-welding gun



Legend:

	100.000 mA/m ²		3.162 mA/m ²		100.000 μA/m ²		3.162 μA/m ²
	36.620 mA/m ²		1.000 mA/m ²		31.620 μA/m ²		1.000 μA/m ²
	10.000 mA/m ²		316.200 μA/m ²		10.000 μA/m ²		

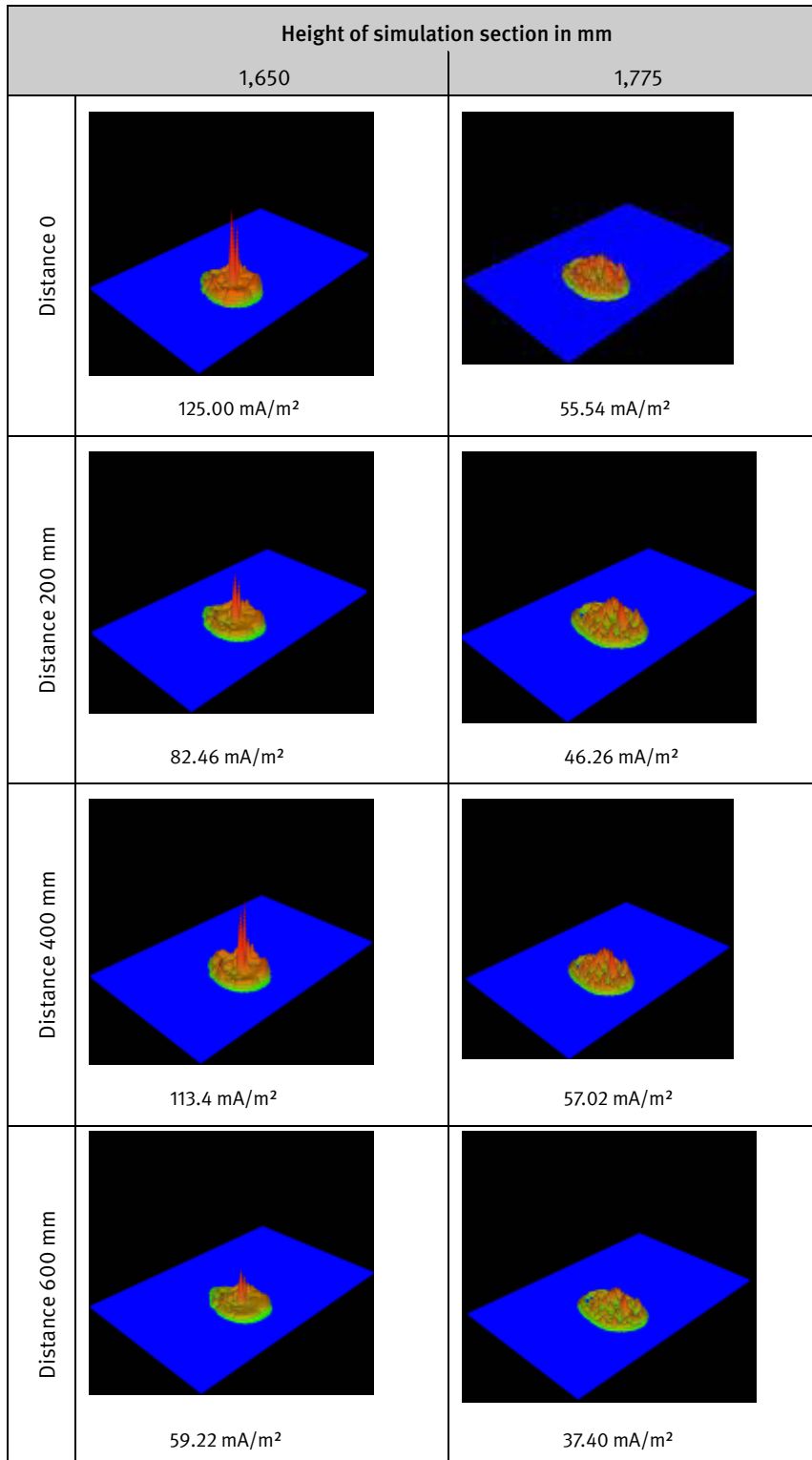
Figure 40: continued



Legend:

	100.000 mA/m ²		3.162 mA/m ²		100.000 μA/m ²		3.162 μA/m ²
	36.620 mA/m ²		1.000 mA/m ²		31.620 μA/m ²		1.000 μA/m ²
	10.000 mA/m ²		316.200 μA/m ²		10.000 μA/m ²		

Figure 40: continued



Legend:

	100.000 mA/m ²		3.162 mA/m ²		100.000 μA/m ²		3.162 μA/m ²
	36.620 mA/m ²		1.000 mA/m ²		31.620 μA/m ²		1.000 μA/m ²
	10.000 mA/m ²		316.200 μA/m ²		10.000 μA/m ²		

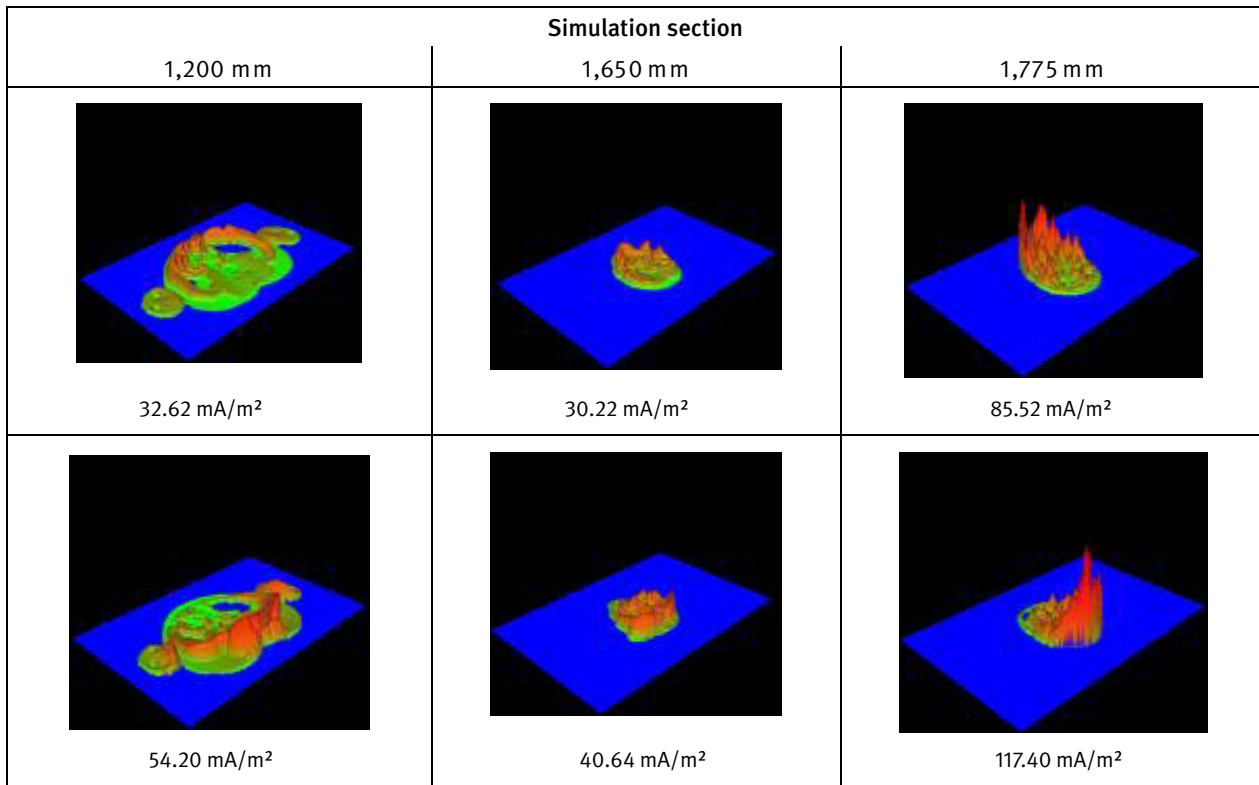
8.5.6 Results concerning cable routing

8.5.6.1 Double conductor

The calculated variations in body current density for the exposure simulations with the double conductor in front of the chest and in front of the back are shown in Figure 41. The sectional

views of the three simulation sections show high corresponding body current densities only on the tissue side located closest to the cable, i.e. either on the back or on the chest side. The peak value of the current densities is in the 1,775 mm section, i.e. in the head. The calculated maximum value is 117 mA/m². On the two other simulation sections, the peak value of the current density lies between 30 and 54 mA/m².

Figure 41
Calculated body current densities with routing of a double conductor close to the body.
Top: double conductor in front of the chest (distance: 10 mm); bottom: double conductor in front of the back (distance: 10 mm)



Legend:

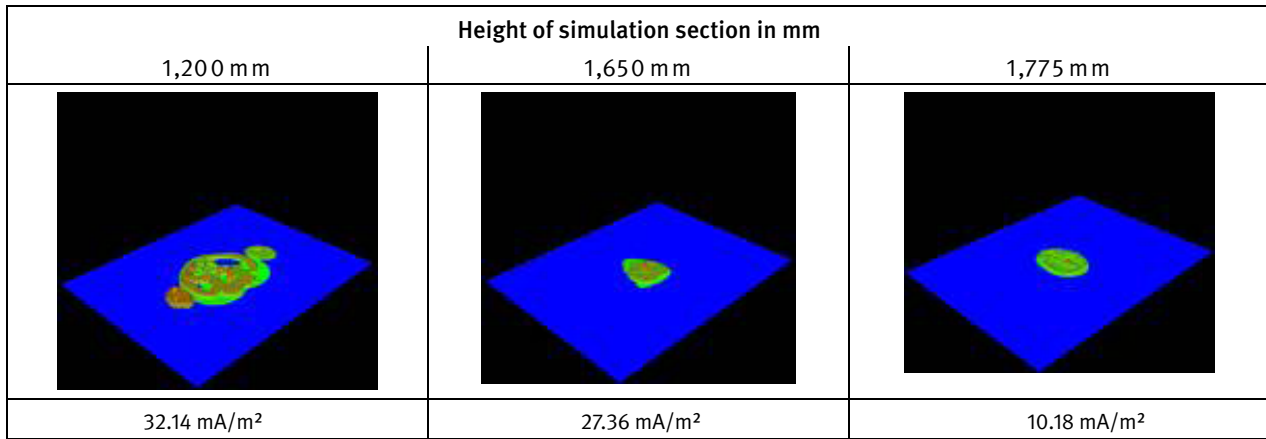
	100.000 mA/m ²		3.162 mA/m ²		100.000 μA/m ²		3.162 μA/m ²
	36.620 mA/m ²		1.000 mA/m ²		31.620 μA/m ²		1.000 μA/m ²
	10.000 mA/m ²		316.200 μA/m ²		10.000 μA/m ²		

8.5.6.2 Cable routing to prEN 50444

Figure 42 shows the calculated body current densities with cable routing to prEN 50444. Owing to the cable routing, the current densities in the 1,200 mm simulation section are somewhat higher on the left-hand side (in the direction of view of the body model) than on the right-hand side. The peak value is located approximately in the middle of this section, with a value of approximately 32 mA/m². In the two other simulation sections,

the influence of the cable routing is no longer evident. A current density peak is observed in the middle of the tissue structure in the 1,650 mm simulation section, on the neck. At approximately 27 mA/m², its value is in the same order of magnitude as in the trunk. The 1,775 mm simulation section exhibits no prominent current density peaks; the current densities in this section are substantially lower than those in the two other simulation sections.

Figure 42:
Calculated body current densities with cable routing to prEN 50444



Legend:

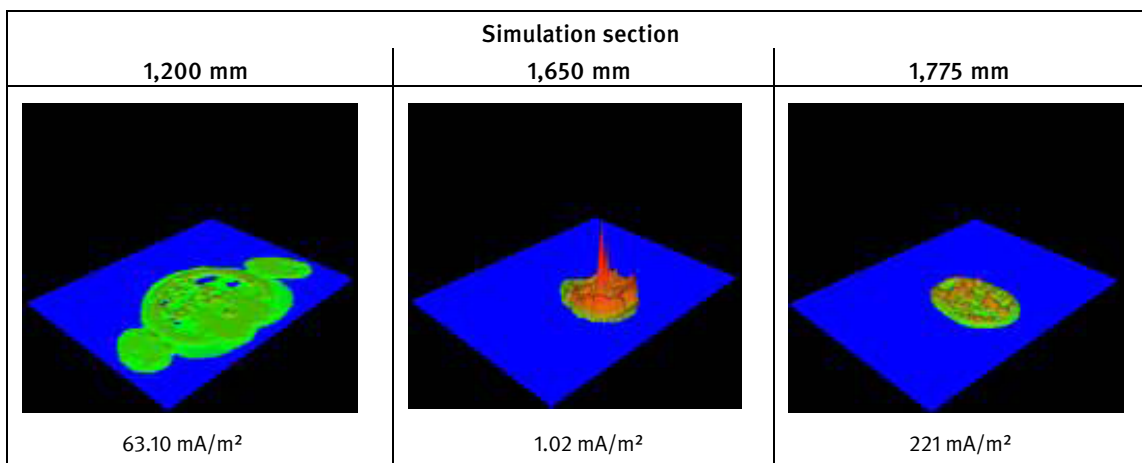
	100.000 mA/m ²		3.162 mA/m ²		100.000 μA/m ²		3.162 μA/m ²
	36.620 mA/m ²		1.000 mA/m ²		31.620 μA/m ²		1.000 μA/m ²
	10.000 mA/m ²		316.200 μA/m ²		10.000 μA/m ²		

8.5.6.3 Cable routing to BGI 5011 Figure 22

Figure 43 shows the body current densities calculated for the cable routing shown in Figure 22 of BGI 5011. The current density in the neck exhibits the highest value with this cable routing (half a conductor loop around the neck), with a peak value of approximately 1 A/m² in the centre of the tissue structure. The current density variations in the two other simulation sections

exhibit substantially lower current densities. A current density peak is evident in the centre of the tissue structure in the 1,200 mm simulation section (trunk). The current density in this case is approximately 63 mA/m². The current densities in the surrounding tissue are substantially lower: as shown by the graduation, they are between 1 and 30 mA/m². The current densities in the head are substantially higher, with a peak value of approximately 220 mA/m².

Figure 43:
Calculated body current densities with cable routing based upon BGI 5011, Figure 22



Legend:

	100.000 mA/m ²		3.162 mA/m ²		100.000 μA/m ²		3.162 μA/m ²
	36.620 mA/m ²		1.000 mA/m ²		31.620 μA/m ²		1.000 μA/m ²
	10.000 mA/m ²		316.200 μA/m ²		10.000 μA/m ²		

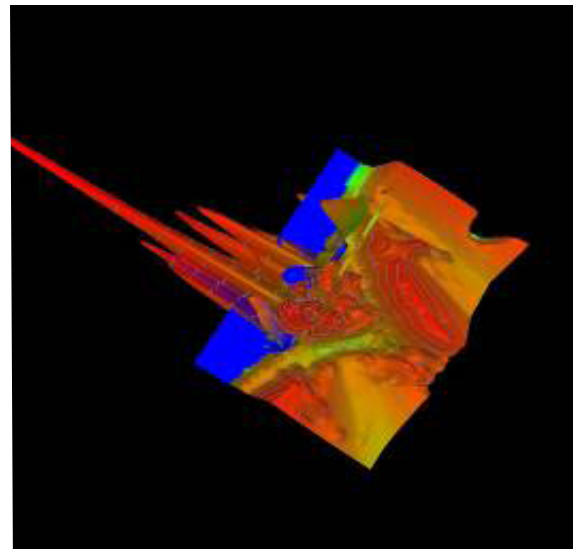
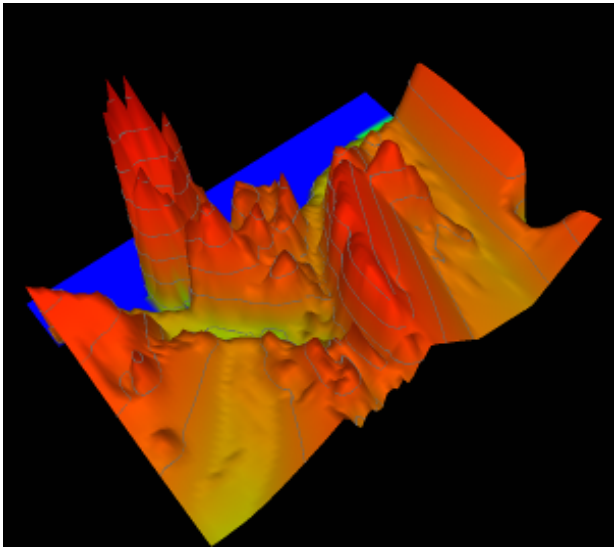
8.5.7 Results for the genital region

The body current densities in the genital region (testicles and penis) are shown in Figures 34 to 40 in the sectional views of the 891 mm sectional section: approximately in the middle of the image, in the middle of the upper outer tissue structure. An arrow indicates this region. The highest current densities occur in this region at a distance of 0 mm to the gun window, i.e. the gun window is in contact with the body model; the peak value of the tissue current density is approximately 185 mA/m². This

value was calculated for the body model positioned to the side of the spot-welding gun with large gun window (see Figure 40). Figure 44 shows two excerpts from the current density variations in the genital region of Figure 40: on the left, the plan view of the current densities in the genital region in the horizontal direction; on the right, the current densities in the testicles in the vertical direction. These images exhibit approximately identical current densities. Table 6 provides an overview of the calculated peak values of the current density in the genital region, as a function of the work scenario studied.

Figure 44

Distribution of the current density in the genital region at the spot-welding gun with large gun window, with the body model positioned to the side. Left: plan view of the variation of the tissue current density in the horizontal direction; right: plan view of the variation of the tissue current density in the horizontal and vertical direction



Legend:

	100.000 mA/m ²		3.162 mA/m ²		100.000 μA/m ²		3.162 μA/m ²
	36.620 mA/m ²		1.000 mA/m ²		31.620 μA/m ²		1.000 μA/m ²
	10.000 mA/m ²		316.200 μA/m ²		10.000 μA/m ²		

Table 6:

Peak values of the current density J in the genital region as a function of the work scenario and the distance between the gun window (ZF) and the body model (KM)

Work scenario		Current density in the genital region, in mA/m ²	
Spot-welding gun	Body model	Distance 0 mm	Distance 200 mm
with small gun window positioned horizontally	in front of the spot-welding gun	113.00	46.88
	positioned to the side of the spot-welding gun	5.25	2.60
with small gun window positioned vertically, gun window parallel to the body model	in front of the spot-welding gun	20.60	3.43
	positioned to the side of the spot-welding gun	10.50	4.50
with small gun window positioned vertically, gun window rotated through 90° to the body model	in front of the spot-welding gun	44.90	7.29
with large gun window, positioned horizontally	in front of the spot-welding gun	106.40	61.22
	positioned to the side of the spot-welding gun	185.60	44.18

9 Project Step 5: Assessment and evaluation of the results

9.1 Limit values

The effects of an external low-frequency magnetic field in the human body are described with reference to the induced body currents. Owing to the body's electrically inhomogeneous tissue structure, the current densities occurring in the tissue differ and fluctuate over time. In tissue capable of electrical excitation, these current densities may cause stimulation of the nerves. In order to prevent such stimulation, the International Commission on Non-Ionizing Radiation Protection (ICNIRP), in conjunction with the World Health Organization (WHO), has set out exposure limit values in the ICNIRP Guidelines [3]. These values also form the basis for the exposure limit values set out in EU Directive 2004/40/EC [4] and the basic values formulated in the BGV B11 accident prevention regulation [1]. The basic values found in Annex 1, Table 1 of BGV B11 form the basis below for the body current densities calculated for evaluation of the various work scenarios described. BGV B11 sets out current densities, as a function of the frequency, for the head and trunk for low-frequency external electric and magnetic fields.

The frequencies of the magnetic fields studied on the two spot-welding guns are used to determine the permissible body current densities. Since the frequencies are derived from the welding currents and the frequency of the welding current is $f = 50$ Hz on both spot-welding guns, this is the frequency which must be used for determining the limit values. In accordance with BGV B11, the permissible body current density for the frequency $f = 50$ Hz is 10 mA/m^2 .

The limit values are intended solely to protect against acute exposure of the tissue of the central nervous system in the head and trunk, i.e. they provide protection against harmful exposure of the central nervous system. In body tissue other than the central nervous system, higher current densities are permitted under the same exposure conditions. Refer in this context to the ICNIRP Response to questions and comments on the guidelines for limiting exposure to time-varying electric, magnetic, and electromagnetic fields (up to 300 GHz) [3].

„Question:

Is the basic restriction of 10 mA/m^2 based only on the threshold for acute effects in the central nervous system, or does it apply to other tissues in the trunk or body?

Answer:

The basic restriction of 10 mA/m^2 is intended to protect against acute exposure effects on central nervous system tissues in the head and trunk of the body with a safety factor of 10. ICNIRP recognizes that this basic restriction may permit higher current densities in body tissues other than the central nervous system under the same exposure conditions.“

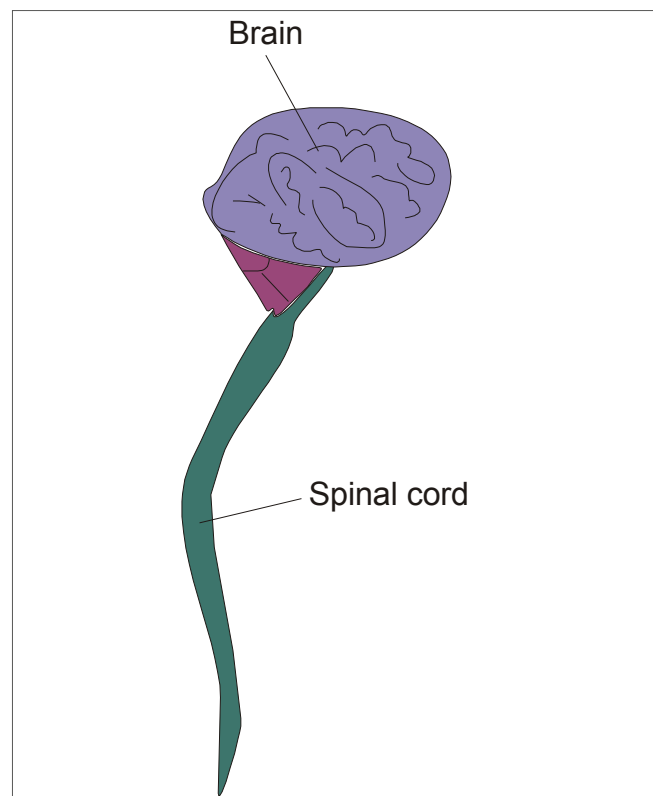
9.2 The central nervous system

9.2.1 Structure

The human central nervous system (CNS) comprises the spinal cord and the brain. This encompasses all areas within the body that are enveloped by the meninges (Figure 45).

The tissue of the CNS is divided into grey matter (*substantia grisea*) and white matter (*substantia alba*). Grey matter is located in the outer part of the brain and in the inner part of the spinal cord. The two forms can be distinguished in a tissue section by the naked eye according to the colour after which they are named. Grey matter consists primarily of nerve cell bodies, white matter of their nerve fibres (axons), the conduction paths.

Figure 45:
Schematic diagram of the human central nervous system



9.2.2 The brain

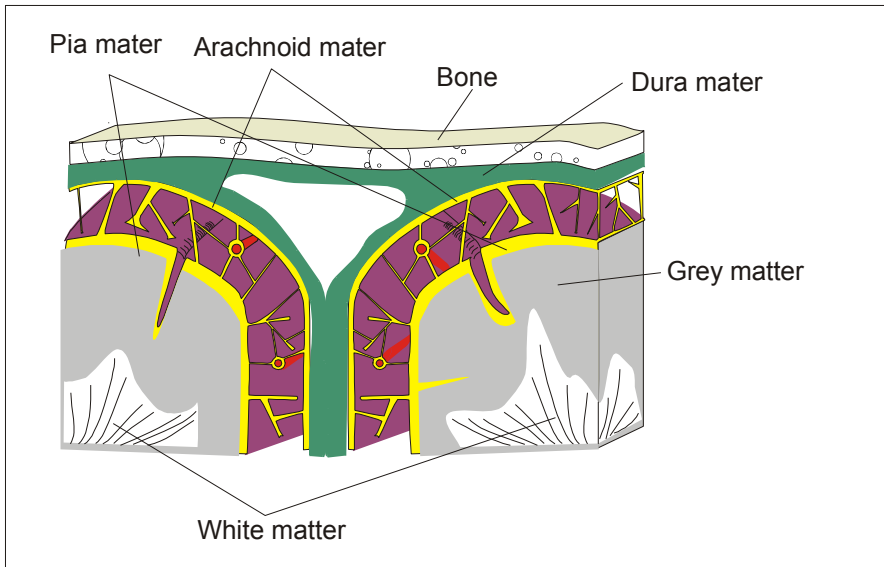
The brain is the part of the central nervous system located in the head. It is situated in the cranial cavity, where it is protected, and is surrounded by three meninges (Figure 46):

- The *dura mater*
- The *arachnoid mater*
- The *pia mater*

The arachnoid mater contains the blood vessels. The space between the arachnoid mater and the pia mater is filled with

cerebrospinal fluid. The brain is therefore housed within a liquid cushion.

Figure 46:
Schematic cross-section of the tissue in the brain



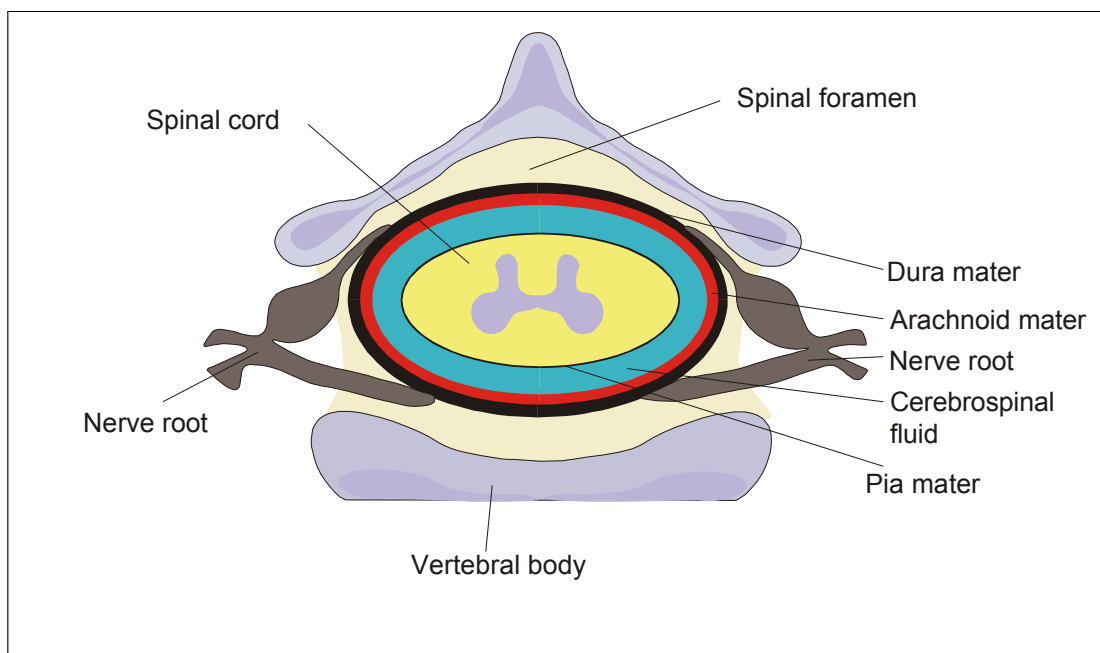
9.2.3 The spinal cord

The spinal cord is the central bundle of nerves along which information is transported between the brain and the body. The spinal cord of an adult human of average height is approximately 45 cm in length and runs in the spinal canal, i.e. through the spinal foramens of the individual vertebral bodies. Nerve fibres emerge from the spinal cord and combine to form spinal nerves. There are 31 pairs of spinal nerves in total. The spinal nerves

emerge from the spinal cord through intervertebral foramens, and disperse into the peripheral regions of the body.

Like the brain, the spinal cord is also protected by bone, the cerebrospinal fluid, and three meninges. Here too, the cerebrospinal fluid fills the space between the arachnoid mater and the pia mater, and dampens movements, impacts and shocks (see Figure 47).

Figure 47:
Schematic cross-sectional diagram of the spinal cord



9.2.4 The CNS in the body model

The course of the CNS in the body model and in the individual simulation sections is shown by the tissue sectional views in Figures 48 and 49. Figure 48 shows a longitudinal section through the centre of the body model, showing the various different types of tissue. The nervous tissue in the back is located close to the spine (blue colouring). The grey matter (nerve cell bodies) in the brain is shown in pink. The cerebrospinal fluid is shown in both areas in yellow.

Figure 48:
Course of the CNS in the body model

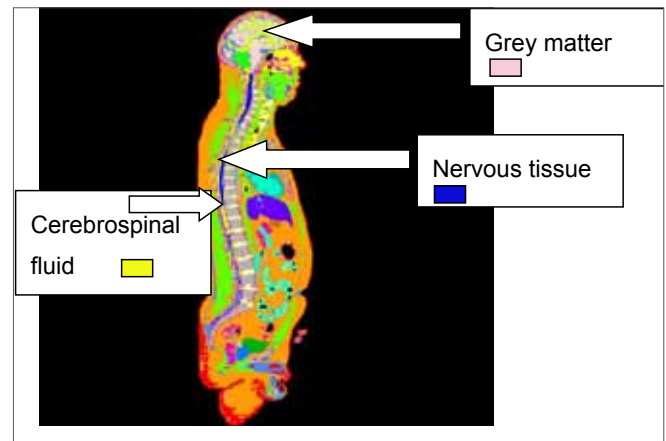
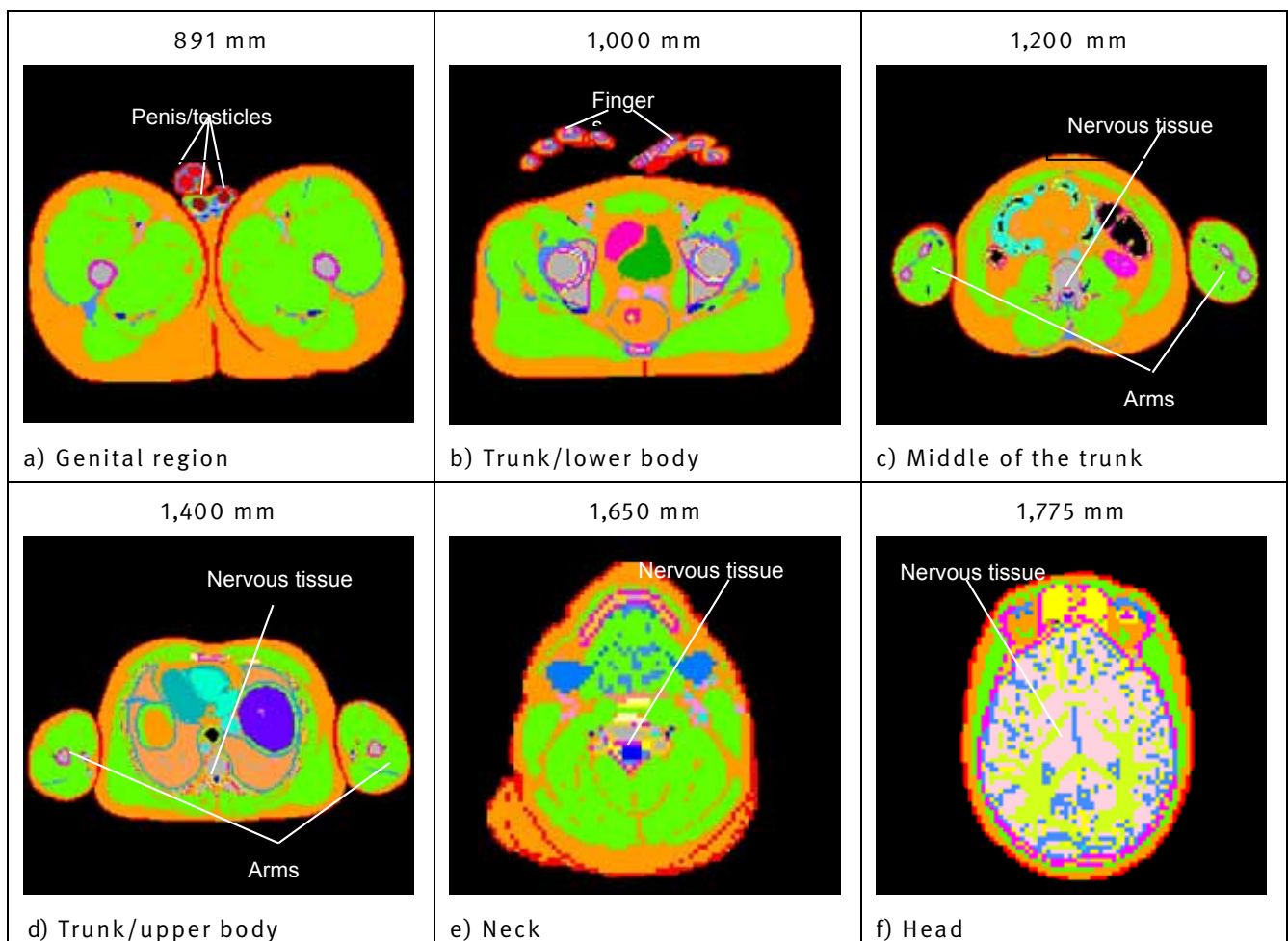


Figure 49:
Tissue sectional views of a transversal horizontal section through the body model in the 891, 1,000, 1,200, 1,400, 1,650 and 1,775 mm simulation sections; nervous tissue = blue; cerebrospinal fluid = yellow; a) and b): without nervous tissue



The sectional views in Figure 49 show the tissue structure of the body model in the simulation sections studied. The locations of the nervous tissue and the cerebrospinal fluid are marked. The tissue consists for the greater part of muscle (green) and fat (orange). For evaluation of the current density with the exception of the head, the maximum value of the current density is to be

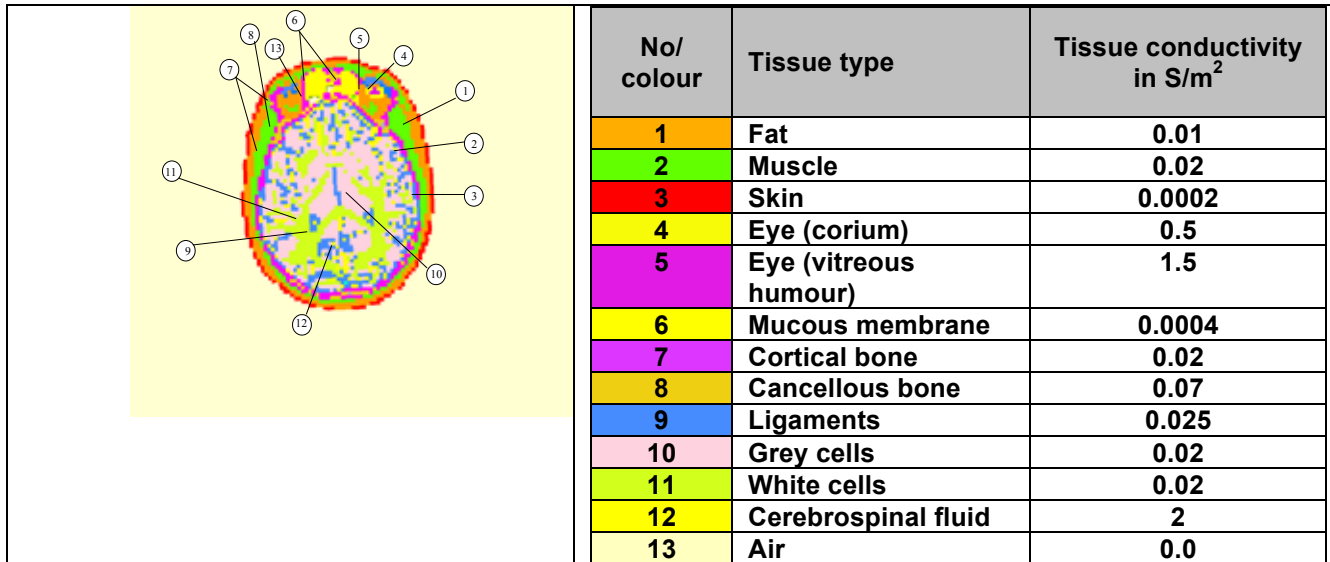
determined from the variations in the body current density (see Figures 34 to 43).

9.3 Electrical tissue properties

The electrical properties of human tissue, i.e. its electrical conductivity, permittivity and permeability, vary according to the frequency and the type of tissue. In other words, the human body is a highly inhomogeneous electrical conductor. The distribution of induced currents within this conductor thus varies strongly

according to the conductivity of the exposed tissue. Owing to the associated low electrical resistance, substantially higher currents flow in regions with high conductivity than in those with low conductivity. At a given tissue cross-section, the electric current density in tissue with high conductivity is also higher. The values of the electrical conductivity for the different tissue types in the head of the body model used are shown in Figure 50.

Figure 50:
Electrical conductivity of the different tissue types in the head of the body model



The forms of tissue of the CNS are characterized by the values of the electrical conductivity for the grey matter and the cerebrospinal fluid. The cerebrospinal fluid has the higher conductivity of the two, by a factor of 100 (2 S/m² vs. 0.02 S/m²). Owing to this property and to the low cross-section, it can be assumed that when an external magnetic field is present, the electric current density is higher in the cerebrospinal fluid than in the nervous tissue of the spinal cord and the brain.

- The nervous tissue and its position were determined in the tissue sectional views.
- The sectional views were placed over the current density variations of the individual simulation sections.
- The current density in the nervous tissue was determined from the current density variations.

9.4 Assessment

The results are assessed by comparison of the calculated body current densities with the permissible values. For this purpose, the current densities for the CNS are determined from the individual current density distributions in the various simulation sections, and compared with the permissible body current density values to BGV B11 [1].

The following steps were performed for determination of the body current density in the CNS:

- Tissue sectional views were produced by transverse sections through the body model corresponding to the simulation section

The highest values of the body current densities were then determined in the various simulation sections. The results are shown in Table 7 (Page 94).

Since the body current density is the product of the electrical conductivity and the electric field strength, the results already available for the variation of the body current density and knowledge of the tissue conductivity are not sufficient on their own to permit conclusions regarding the current density in the spinal cord. Calculations of the body current density with substantially higher resolutions and/or knowledge of the distribution of the electric field in the tissue are required for this purpose. These were performed during evaluation of the results – by way of example – for the body model positioned at a distance of 0 mm in front of the spot-welding gun with small gun window. The distribution of the electric field was calculated in the 1,200, 1,650 and 1,775 mm simulation sections (Figure 51).

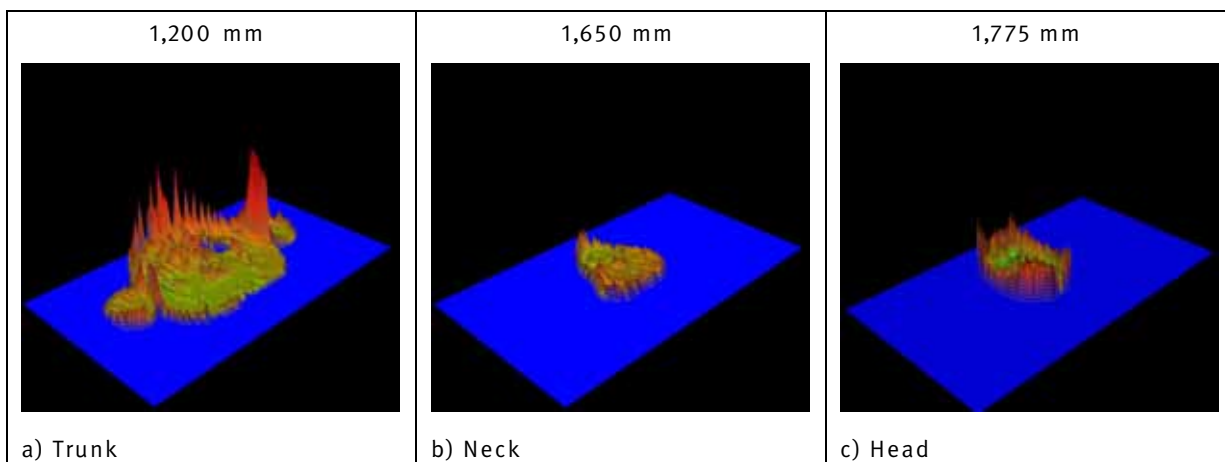
Table 7:

Maximum values of the body current density in the cerebrospinal fluid in the respective simulation sections

Height of simulation section in mm	Body current density, in mA/m ²		
	Spot-welding gun with small gun window	Spot-welding gun with large gun window	Cable routing
891	-	-	-
1,000	-	-	-
1,200	74.2	222.0	63.1
1,400	-	87.8	-
1,650	189.4	113.3	1,020
1,775	74.2	57.0	221

Figure 51:

Distribution of the electric field strength in several different simulation sections for a body model positioned at a distance of 0 mm from the front of the spot-welding gun with small gun window



Legend:

1.000 V/m	31.620 mV/m	1.000 mV/m	31.620 μ V/m
316.200 mV/m	10.000 mV/m	316.200 μ V/m	10.000 μ V/m
100.000 mV/m	3.162 mV/m	100.000 μ V/m	

High electric field strengths occur only on the surface of the body. Within the body, the changes in field strength are relatively minor. In the spinal cord region, they are in the order of 100 to 300 mV/m. On a logarithmic scale of the electric field, this change equates to around 10 dB. Compared to the ratio of the tissue conductivity of the cerebrospinal fluid to that of the grey matter (a factor of 100 or 40 dB), the change in the field strength in this region of the tissue has only a minor influence upon the current density in the nervous tissue. The electric current density in the nervous tissue of the CNS is therefore assumed to be lower than that in the cerebrospinal fluid by the factor K, which is calculated from the ratio of the tissue conductivity of the cerebrospinal fluid to the tissue conductivity of the grey matter. This assumption is confirmed by the results of model calculations of the body current density in a body model with a resolution of 1 mm \times 1 mm \times 1 mm in the CNS region in the back for the 1,200 mm simulation section (Figure 52, Page 74).

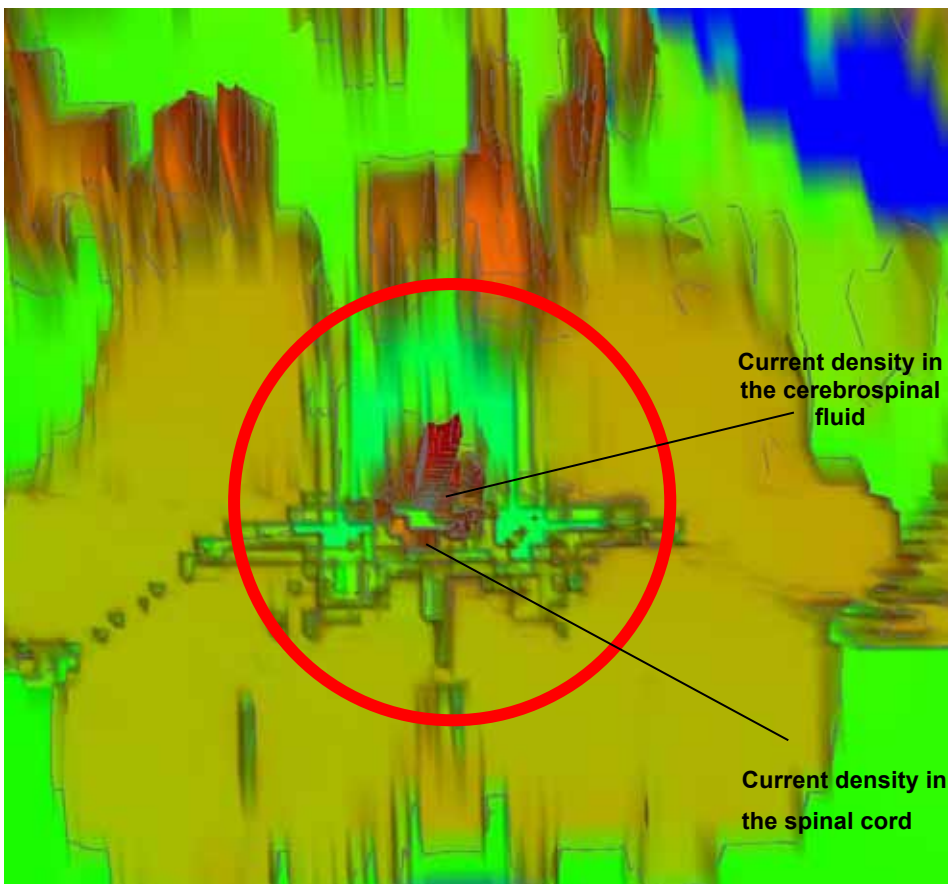
The current density variation in the spinal region, including the spinal cord, is visible in the circled image area. In the middle of the marked area, a region of high current density (shown in red) encircles a region of low current density (shown in green). As

shown by the graduation, the regions of high current density are to be found in the cerebrospinal fluid, those of low current density in the nervous tissue. This becomes clear when the excerpt of the current density is placed over the associated excerpt of the tissue from the body model (Figure 53, page 75).

Figure 53 b confirms the assumption that the current density in the nervous tissue is substantially lower than in the cerebrospinal fluid.

Figure 52:

Excerpt from the distribution of the body current density in a body model with a resolution of 1 mm × 1 mm × 1 mm in the CNS region in the back for the 1200 mm simulation section; distance 0 mm, spot-welding gun with small gun window, body model positioned to the front



Legend

	100.000 mA/m ²		3.162 mA/m ²		100.000 µA/m ²		3.162 µA/m ²
	36.620 mA/m ²		1.000 mA/m ²		31.620 µA/m ²		1.000 µA/m ²
	10.000 mA/m ²		316.200 µA/m ²		10.000 µA/m ²		

In addition, comparison of the current densities in the two tissue types (Figure 52) shows that they differ by a factor of at least 100, consistent with the ratios of their conductivity. For the working positions studied, it follows that the exposure for the CNS lies below the basic values of BGV B11 [1] and the exposure limit values of EU directive 2004/40/EC [4], even for the worst case,

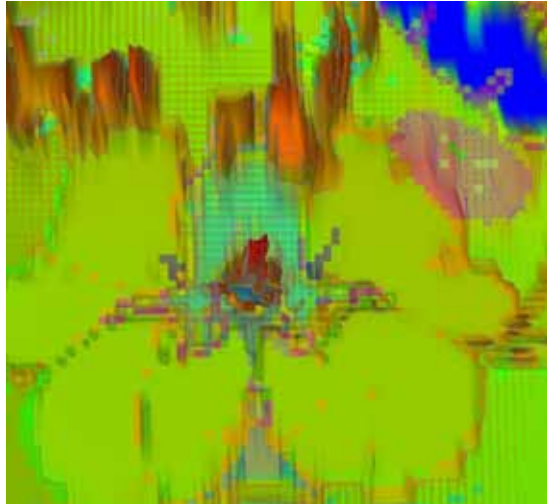
as with cable routing and the spot-welding gun version shown in Table 7. It may therefore be assumed that the exposure for welders and other workers at workplaces with comparable or similar spot-welding guns and working conditions lies below the basic values (body current densities) of BGV B11. No measures are therefore necessary for the protection of these persons.

Figure 53:

Tissue sections of the CNS from Figure 49 c and current density excerpt for the 1200 mm simulation section, overlaid



a) Tissue excerpt from the 1,200 mm simulation plane in Figure 49 c



b) Tissue excerpt from Figure 53 a with current density variation from Figure 52

10 Summary and discussion

The IFA studied the exposure of welders to magnetic fields during welding with hand-held spot-welding guns with separate 50 Hz power supplies. For this purpose, the variation of the magnetic flux density over time was measured at several workplaces equipped with spot-welding guns at one user's site, and the typical working position of the welders was determined. The data obtained show that at the workplaces studied, the welders' exposure to magnetic fields may exceed the permissible „derived values“ of the BGV B11 accident prevention regulation if the distance between the welder and the spot-welding gun is too small. Further measurements were performed in the IFA's laboratory on a spot-welding gun with small and large gun window in order to determine the horizontal and vertical distribution of the magnetic flux density. These measurements also showed that owing to their tasks, welders are not able in practice to observe safety distances, and that exceeding of the permissible values for the magnetic flux density must always be considered. The welders' exposure to magnetic fields was therefore assessed with reference to the body current densities („basic values“ as defined in BGV B11). The body current densities were calculated using the EMPIRE field simulation program in an internationally recognized body model used by the Air Force Research Laboratory (AFRL).

For the purpose of calculation, the field distributions determined in the laboratory on the spot-welding guns with small and large gun window were simulated. The current density was calculated in the body model in five different sections (head, neck, trunk and genitals) for typical working positions (five different positions of the spot-welding gun and of the body model, and four different cable routings). Inhomogeneous current density distributions were found to arise in the body model owing to differences in tissue properties and structures. Depending upon the distance from the spot-welding gun, the current density values in the different tissues may lie above the basic values of BGV B11. Only approximately 10% to 20% of the internationally recognized limit value of 10 mA/m² is however exploited in the central nervous system (brain and spinal cord) during typical work scenarios and cable routings.

The low degree of exploitation of the limit value permits the conclusion that in similar real-case work scenarios on comparable spot-welding guns, the welders' exposure also lies below the basic values stated in BGV B11. No particular measures are required for the protection of welders during work on the spot-welding guns studied or on comparable equipment.

11 References

- [1] Berufsgenossenschaftliche Vorschrift für Sicherheit und Gesundheit bei der Arbeit: Elektromagnetische Felder (Unfallverhütungsvorschrift BGV B11). Issue: 6/2001. Published by: Hauptverband der gewerblichen Berufsgenossenschaften (HVBG), Sankt Augustin. Carl Heymanns, Cologne 2001
- [2] Berufsgenossenschaftliche Informationen: Beurteilung magnetischer Felder von Widerstandsschweißeinrichtungen (BGI 5011). Issue 9/2006. Published by: Hauptverband der gewerblichen Berufsgenossenschaften (HVBG), Sankt Augustin. Carl Heymanns, Cologne 2006
- [3] Guidelines for limiting exposure to time-varying electric, magnetic, and electromagnetic fields (up to 300 GHz). Health Phys. 74 (1998), No 4, pp. 494-522. <http://www.icnirp.de/documents/emfgdl.pdf>
- [4] Directive 2004/40/EC of the European Parliament and of the Council of 29 April 2004 on the minimum health and safety requirements regarding the exposure of workers to the risks arising from physical agents (electromagnetic fields) (18th individual Directive within the meaning of Article 16(1) of Directive 89/391/EEC). OJ EU, L 159 of 30 April 2004, pp. 1-26; last amended. OJ EU L 184 of 24 May 2004, pp. 1-9
- More detailed literature:**
- [5] Berufsgenossenschaftliche Regel für Sicherheit und Gesundheit bei der Arbeit: Elektromagnetische Felder (BGR B11). Issue 1/2006. Published by: Hauptverband der gewerblichen Berufsgenossenschaften (HVBG), Sankt Augustin. Carl Heymanns, Cologne 2006
- [6] DIN VDE 0848: Safety in electrical, magnetic and electromagnetic fields – Part 3-1: Protection of persons with active implants in the frequency range 0 Hz to 300 GHz (5/2002). Beuth, Berlin 2002
- [7] Council Recommendation of 12 July 1999 (1999/519/EC) on the limitation of the exposure of the general public to electromagnetic fields (0 Hz to 300 GHz). OJ EU L 199 of 30 July 1999, pp. 59-70
- [8] Grenzwerte und Vorsorgemaßnahmen zum Schutz der Bevölkerung vor elektromagnetischen Feldern. Empfehlungen der Strahlenschutzkommission. Published by: Strahlenschutzkommission, Bonn 2001. <http://www.berlin.de/sen/umwelt/umweltratgeber/de/emf/pdf/ssk174.pdf>
- [9] *Eggert, S.; Siekmann, H.*: Standardization in the field of non-ionizing radiation. KAN Report 9. 2nd ed. Published by: Verein zur Förderung der Arbeitssicherheit in Europa e. V., Sankt Augustin 2000